論文 / 著書情報
Article / Book Information

題目(和文)	高効率・広帯域無線端末用アンテナにおける周波数・指向性可変の研究
Title(English)	Study of Tunability and Steerability in High-Efficiency and Wideband Wireless Terminal Antennas
著者(和文)	桧垣誠
Author(English)	Makoto Higaki
出典(和文)	学位:博士(工学), 学位授与機関:東京工業大学, 報告番号:甲第10635号, 授与年月日:2017年9月20日, 学位の種別:課程博士, 審査員:廣川 二郎,阪口 啓,西方 敦博,青柳 貴洋,庄司 雄哉
Citation(English)	Degree:Doctor (Engineering), Conferring organization: Tokyo Institute of Technology, Report number:甲第10635号, Conferred date:2017/9/20, Degree Type:Course doctor, Examiner:,,,,
学位種別(和文)	博士論文
Type(English)	Doctoral Thesis

Study of Tunability and Steerability in High-Efficiency and Wideband Mobile Wireless Terminal Antennas

Makoto Higaki
supervised by Prof. Jiro Hirokawa

August 11, 2017

Contents

List of Figures

Chapter 1

Introduction

1.1 Background to the need for variable antennas

In these days, many kinds of wireless communication systems are increasing rapidly. For example, not only cellular phone systems but also wireless LAN, Bluetooth, RF-ID, etc. has been already used widely all over the world. As the number of wireless devices increases, the devices are inevitably required to be compact and low-cost in order to be easily attached to anything or carried with a person. On the other hand, needless to say, the number of devices failing to connect would also increase as the total number increases. And each device is required to meet the specs of connection rate, throughput, etc. regardless of the surrounding environment in the vicinity and propagation environment.

Of course, the remarkable progress in digital signal processing and digital/analogue circuit technology support to get rid of the above-mentioned problems. An antenna, however, as the end part of a wireless terminal plays very important role to capture a radio signal, and the signal is largely influenced by the propagation environment and in the vicinity of various object, e.g. a desk, attached wall, a user's hand/head, etc.

In these situations, for wireless terminals

- Downsizing in order to install them anywhere and not to spoil the fine sight of the original appearance
- Increasing internal devices other than wireless devices like sensors, that leads to high-density packaging of terminals

are still been required. Although also built-in antennas of wireless terminals eventually are required to be small, high-efficiency, wideband and robust

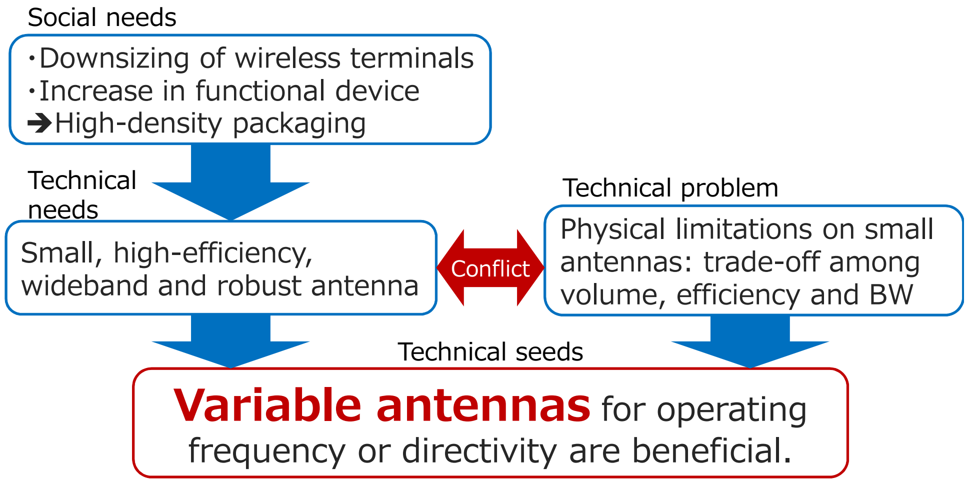

Figure 1.1: The needs and seeds related to variable antennas

performance at the same time, physical limitations on electrically small antennas, or trade-off among the volume, efficiency and bandwidth of the antennas are revealed [1, 2]. Therefore, variable antennas for operating frequency or directivity are supposed to be beneficial to break through this conflicting requirements. These relationships are shown in Fig. 1.1.

As shown in [3], once the volume for an antenna and other scatterers around them are determined, the physical limitations can be calculated. Therefore, tunable and steerable antennas are expected to enhance this limitations in real time as Fig. 1.2 shows the ultimate target image of the variable antennas.

1.2 Conventional studies of variable antennas

There are many conventional studies of variable antennas especially for operating frequency, a so-called tunable antenna [14–16, 19–22]. However, the problem is they did not fully cover wideband cellular systems from 704 MHz to 2690 MHz, with relatively small sized antenna and high-efficiency. In addition, a tunable antenna is thoroughly optimized with some special method to accelerate the simulation and finally its advantage over non-tunable antenna has been confirmed by comparing with the physical limitations [2]. In addition, tunability in real time is required in actual situations. A cellphones

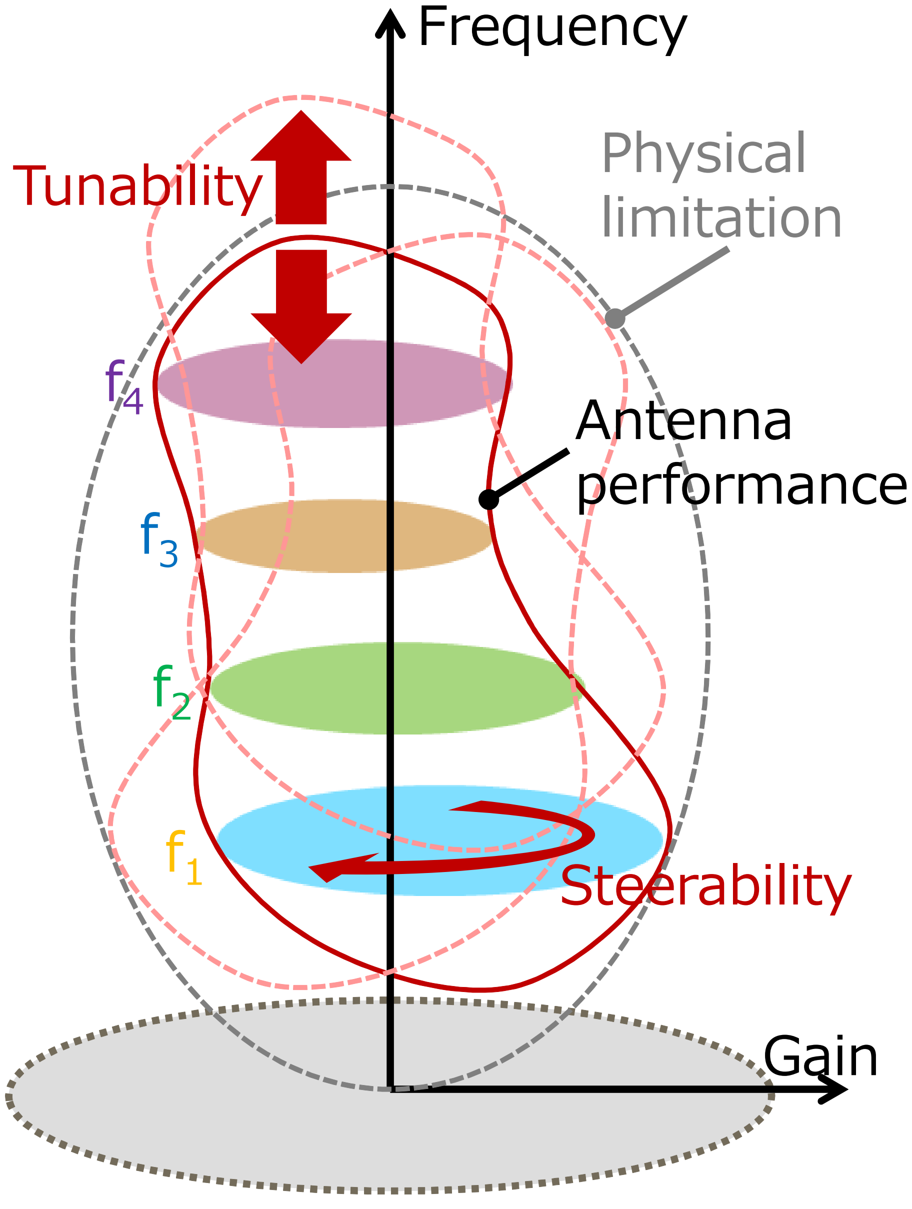

Figure 1.2: The ultimate target image of variable antennas

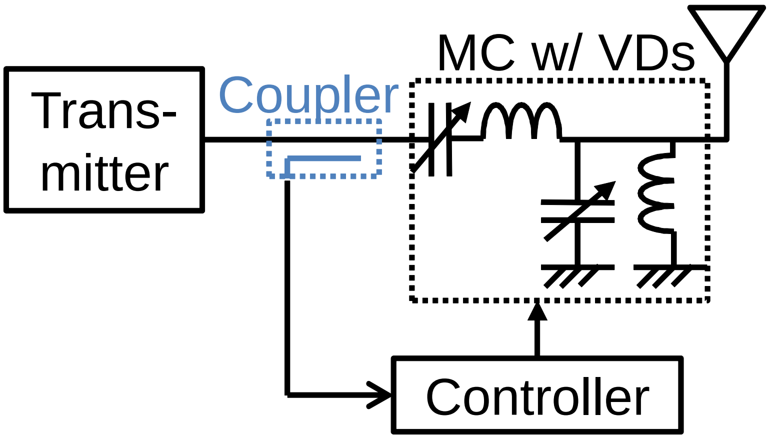

Figure 1.3: The schematic diagram of a conventional automatic tunable antenna using a directional coupler

can be used in the vicinity of various objects, e.g. a user's hand/head, desk, etc. So for them an automatic tunable antenna has been studied in this paper. Although there are some automatic ones among papers about tunable antennas [21,22], and as shown in Fig. 1.3 they solely uses a directional coupler which causes some general problems: an insertion loss, low input SNR of a detector, and especially narrower the operation bandwidth of the total system. Therefore a novel auto-tuning system containing a probe which is located near the tip of an antenna has been proposed and demonstrated in this paper.

There are also conventional study of variable antennas for directivity, or steerable antennas [34–36]. Here, an antenna array the system taking advantage of that, e.g. a phased array, a MIMO system can be also regarded as a kind of steerable. Then, in this paper a small-sized steerable antenna for MIMO system has been studied. The schematic of a MIMO system with steerable antennas The whole structure is small enough as a built-in antenna for a mobile terminal, and the simple combination of a MIMO system with a conventional steerable antenna for each branch would not be able to achieve that size. And also the advantage of the MIMO system with steerable antennas over that with non-steerable antennas would be confirmed.

The motivation to undertake steerable antennas with MIMO is that it is supposed to be beneficial in some situation as shown in Fig. 1.5. The

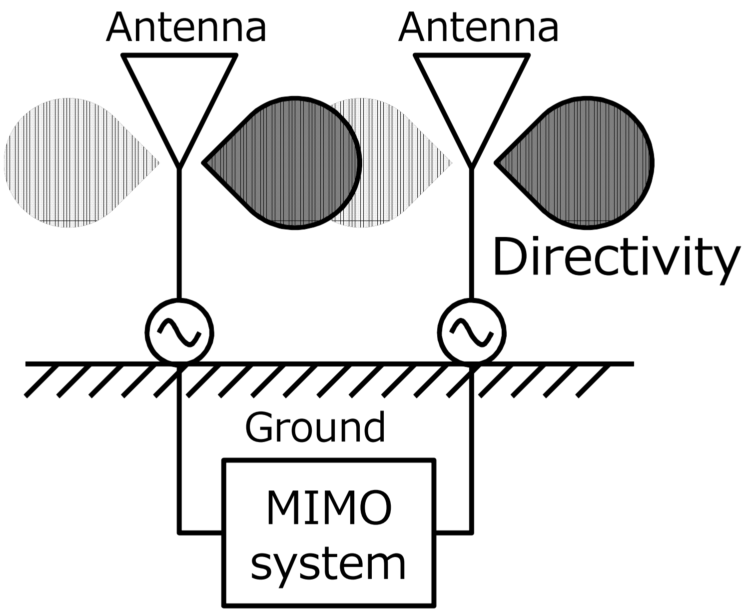

Figure 1.4: The schematic of the MIMO system with steerable antennas

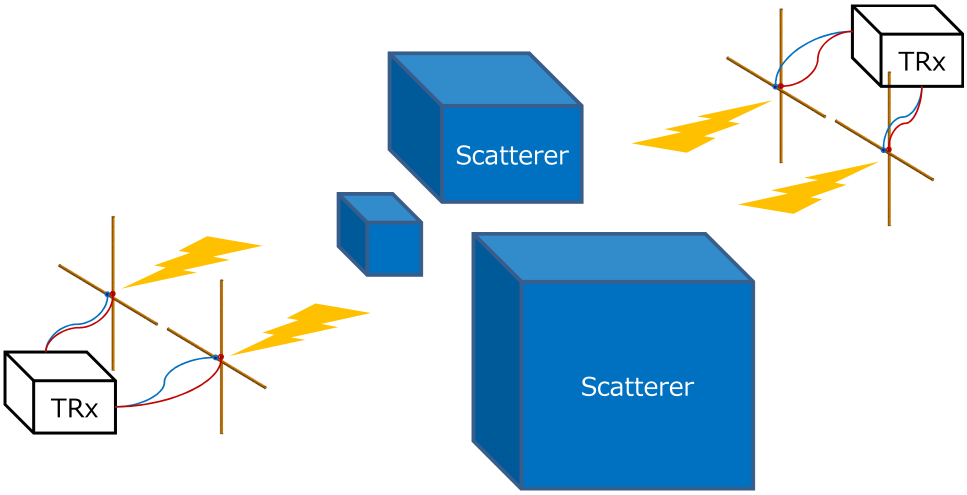

Figure 1.5: Beneficial situation of a MIMO system with steerable antennas

figure shows the two branches of vertically crossed dipole antennas both for the transmitting and receiving end. Supposing both sides can adaptively select the polarization depending on the propagation environment, obviously this system improve the channel capacity more than without the switching because this system completely includes the system without steerability. Although the steerability is focused on polarization, there are other degree of freedom on radiation, i.e. directivity and phase. The general mathematical discussion is done in Chapter 5.

1.3 The difficulty of variable antenna design as a multi-objective problem

The design of variable antennas are usually multi-objective problems, and heuristic algorithms, e.g. Genetic Algorithm (GA), Particle Swarm Optimization (PSO), Annealing method, etc. are suitable to solve it because of their pseudo thorough searching performance. However, there is still a trade-off between the degree of freedom in a design and computation time, or number of iteration. In order to accomplish these works, some special method to design variable antennas has been applied. Figure 1.6 summarize the above.

They are commonly taken advantage of to design both a tunable an-

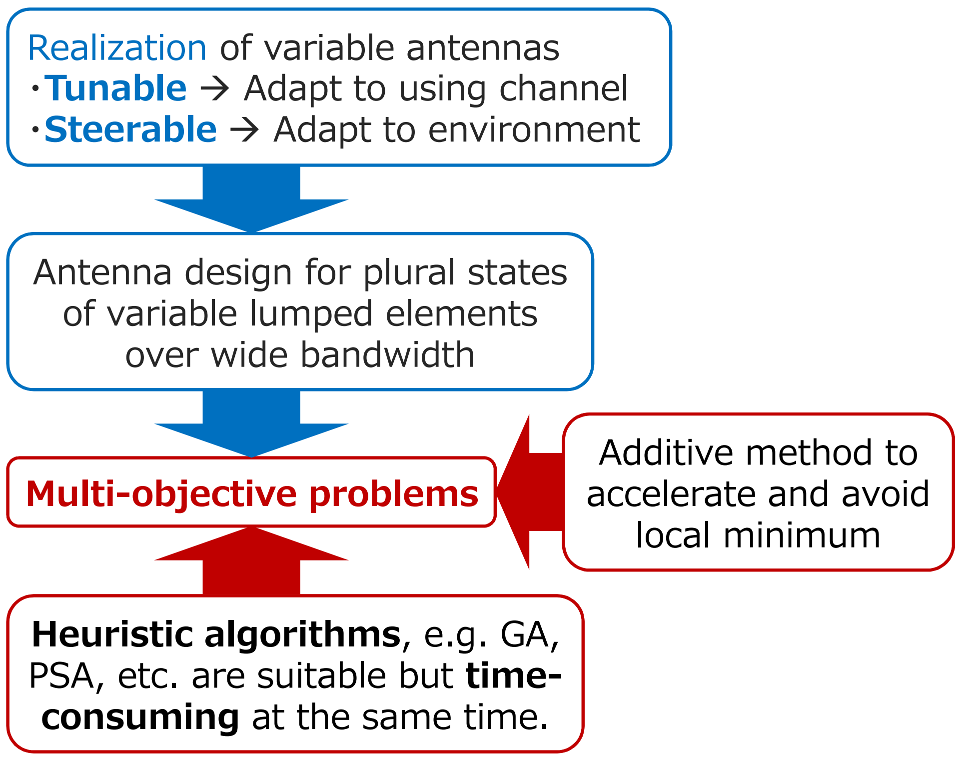

Figure 1.6: Multi-objective problems arising from variable antennas and the approach for it

tenna and steerable antenna for MIMO. GA on which the method based on can perform a global search for the topology of an antenna. On the other hand, its repetitive procedure consumes long time and the design is possibly trapped around local minimum. For those reasons, some acceleration techniques for linear algebra in an electromagnetic calculation and an appropriate function to avoid local minimum has been proposed and applied in the optimization.

1.4 Composition of this dissertation

Lastly, the composition of this dissertation is as stated below and also see Fig. 1.7. The commonly used design method for a tunable antenna and steerable antenna is introduced in Chapter 2. Chapter 3 and 4 are related to a tunable antenna. A normal tunable antenna without a control block is introduced and discussed in Chapter 3, and an automatic one with a feedback control system is in Chapter 4. Chapter 5 and 6 are about a steerable antenna for MIMO system. The design and fundamental features of the antenna are noted in Chapter 5. The mechanism of the steerability and the performance of the antenna as a part of MIMO system are discussed in Chapter 6. Chapter 7 concludes this study.

1.5 Summary

Tunable/steerable antennas can be a solution for built-in antennas of small wireless terminals because there is a conflict between the need for downsizing and physical limitations.

Target of this study is specified: the design and confirmation of

- Small and wideband tunable antenna for cellular systems and
- Small steerable antenna to enhance MIMO channel capacity.

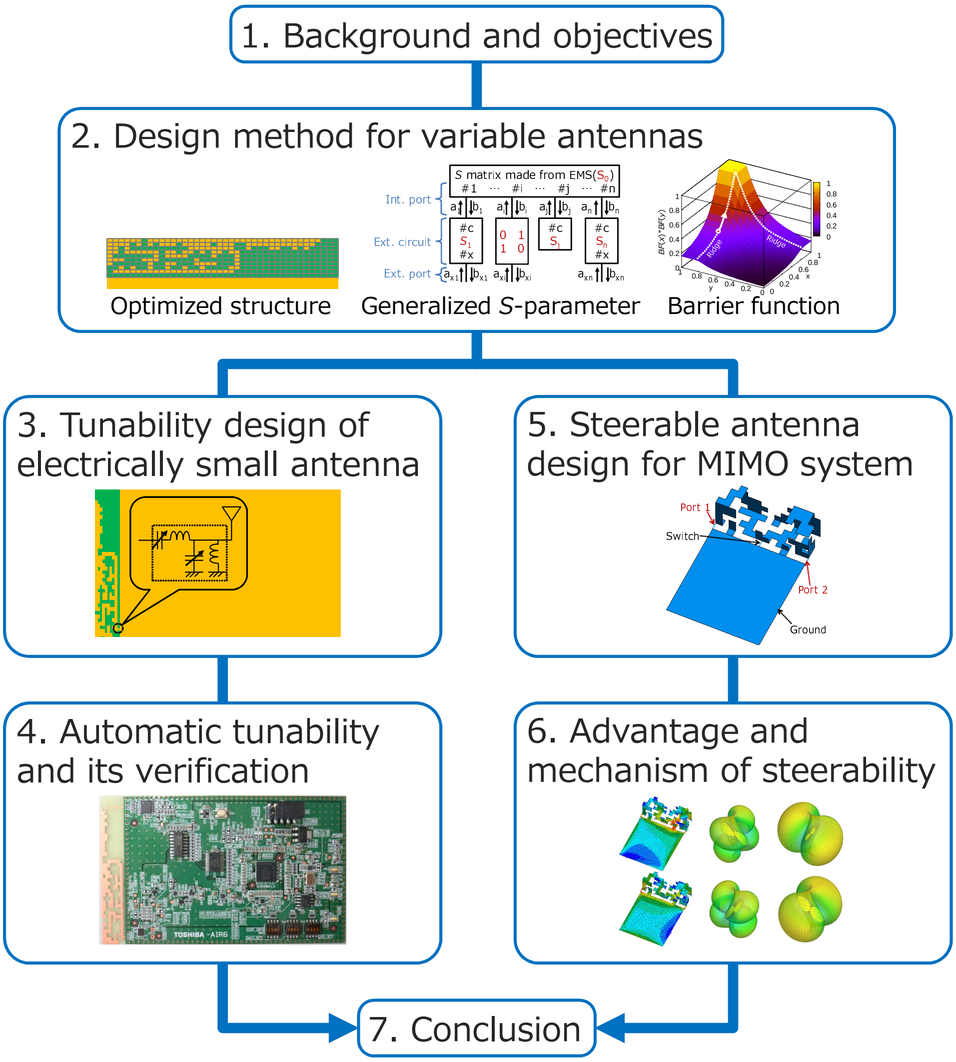

Figure 1.7: Composition of this dissertation

Chapter 2

Design method for variable antennas

2.1 Introductory remarks

Figure 2.1 shows the schematic outline of variable antenna design consistently used in this paper. The process is based on genetic algorithm, or GA as a whole. For applying GA to an antenna design, the area where antenna will be formed is modeled with small metal patches at first. The structure filled up with all patches is called a 'raw structure'. The randomly determined structure that is a set of small patches is computed by electromagnetic simulator and the S-parameters are extracted. The S-parameters and external variable circuits are connected and calculated with a circuit simulator. Finally, the each cost function in terms of some antenna characteristics for each design is calculated and GA updates the bits corresponding to a set of antenna patches for next generation, based on selection, crossover, mutation, etc.

Although many conventional studies have already worked through the above-mentioned method [70–72], there are some issues to be solved:

- Long simulation time
  - Repetitive EM simulations for generation, frequencies, the states of variable lumped elements, etc.
  - The number of possible configurations is so enormous that useless designs frequently arise.
- Local minimum

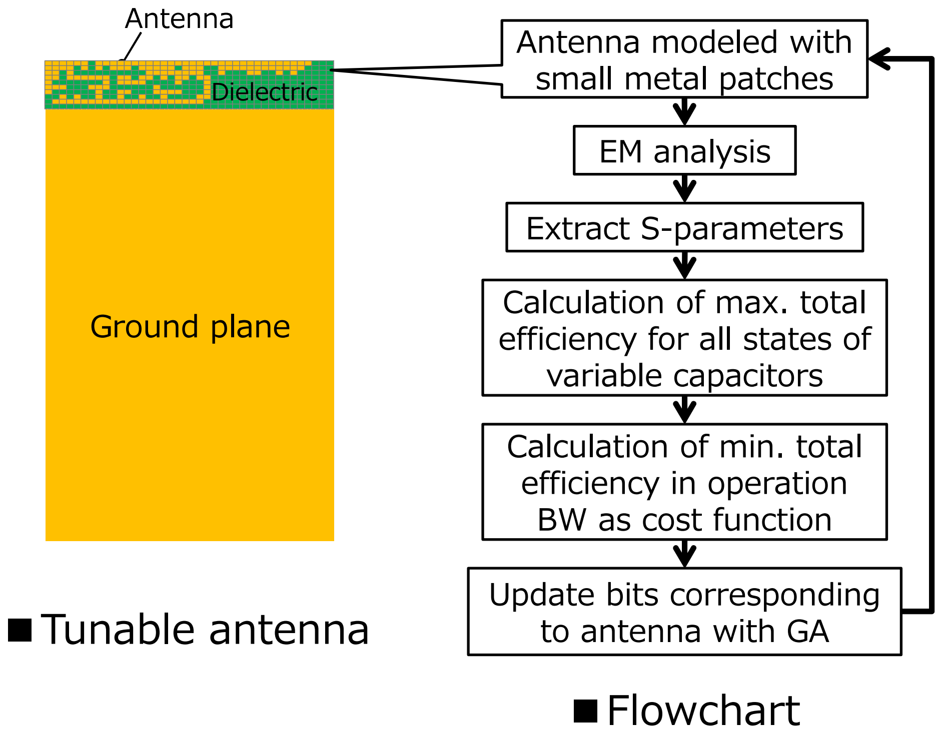

Figure 2.1: Schematic outline of variable antenna design

- The weights for multiple objectives should appropriately be set to avoid local minimum.

- Singular structural point
  - Two patches connected at the corner each other are illegal in the EM simulation.

For each problem, some special techniques are applied, i.e.

- Numerical Green's Function (NGF) [73–75] and S-parameter analysis accelerates the electromagnetic simulation.

- Barrier Function (BF) which have a non-linear profile mitigate the problem of local minimum caused by the trade-off among plural characteristics.

- Configuration error avoidance method based on maze solving algorithm supported by geometric matrices for graph theory completely eliminates singular structural points.

2.2 Numerical Green's Function (NGF) for the acceleration of simulation

Before the introduction of NGF, brief explaination of moment methods (MoM) is necessary. Figure 2.2 shows the impedance between discretized parts for moment methods (MoM). In the MoM analysis for antennas of arbitrary shape, the whole structure usually fragmented to small parts and each current and voltage on each part are related by the summation weighted with an impedance determined by the geometry. In the case in Fig. 2.2, the voltage on ith part V_i is induced by currents from all parts, J_j, J_k, etc. and they are weighted with Z_{ij}, Z_{ik}, etc., respectively. i.e.

$$V_i \;=\; \sum_{j=1}^{n} Z_{ij} I_j. \tag{2.1}$$

Thus, a linear simultaneous equations

$$[\boldsymbol{V}] \;=\; [Z][\boldsymbol{J}] \tag{2.2}$$

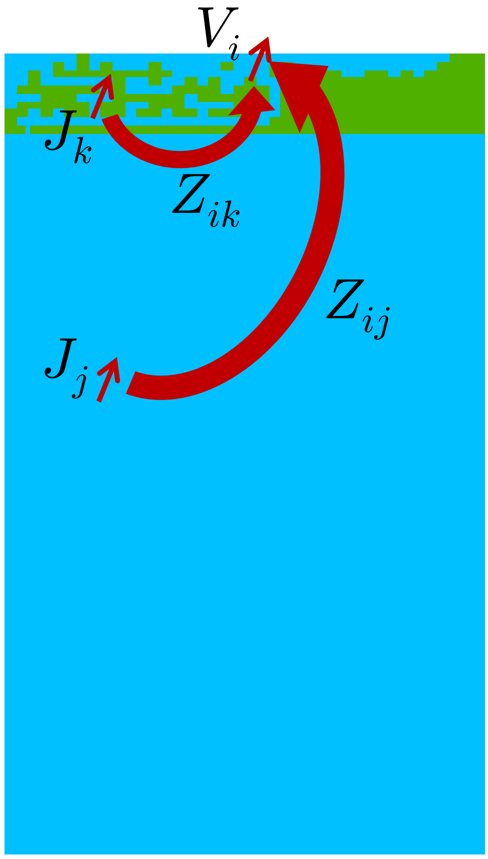

Figure 2.2: The impedance between discretized parts for moment methods (MoM)

or the expression with elements

$$\begin{bmatrix} V_1 \\ \vdots \\ V_n \end{bmatrix} = \begin{bmatrix} Z_{11} & \cdots & Z_{1n} \\ \vdots & \ddots & \vdots \\ Z_{n1} & \cdots & Z_{nn} \end{bmatrix} \begin{bmatrix} J_1 \\ \vdots \\ J_n \end{bmatrix} \tag{2.3}$$

can be obtained. In most cases, the Z matrix is decomposed to the product of L and U matrix because Z is a dense matrix. LU matrix is mathematically expressed as

$$LU = \begin{bmatrix} 1 & & & \mathbf{0} \\ L_{21} & 1 & & \\ \vdots & \ddots & \ddots & \\ L_{n1} & \cdots & L_{n(n-1)} & 1 \end{bmatrix} \begin{bmatrix} U_{11} & U_{12} & \cdots & U_{1n} \\ & U_{22} & \cdots & U_{2n} \\ & & \ddots & \vdots \\ \mathbf{0} & & & U_{nn} \end{bmatrix} \tag{2.4}$$

and the usage of memory in the actual computation is

$$LU = \begin{bmatrix} U_{11} & U_{12} & \cdots & U_{1n} \\ L_{21} & U_{22} & \cdots & U_{2n} \\ \vdots & \vdots & \ddots & \vdots \\ L_{n1} & L_{n2} & \cdots & U_{nn} \end{bmatrix}. \tag{2.5}$$

Hereafter, for simplification, LU matrices have elements as shown in the equation (2.5).

Here, the whole structure can be categorized into two parts:

- fixed part– ground plane, dielectric substrate, etc.
- variable part– antenna,

as the image of categorization shown in Fig. 2.3. Z_{ff}, Z_{fv}, Z_{vf}, Z_{vv} are impedances between both the voltage V and the current J in a fixed part, V in a fixed part and J in a variable part, V in a variable part and J in a fixed part, both V and J in a variable part, respectively.

Then if these parts are separated into the first part and second part, the equations is expressed as

$$\begin{bmatrix} V_f \\ V_v \end{bmatrix} = \begin{bmatrix} Z_{ff} & Z_{fv} \\ Z_{vf} & Z_{vv} \end{bmatrix} \begin{bmatrix} J_f \\ J_v \end{bmatrix}, \tag{2.6}$$

where the suffix ‘f’ denotes the element related to the fixed part and the suffix ‘v’ related to the variable part. In the propose method, a Z matrix

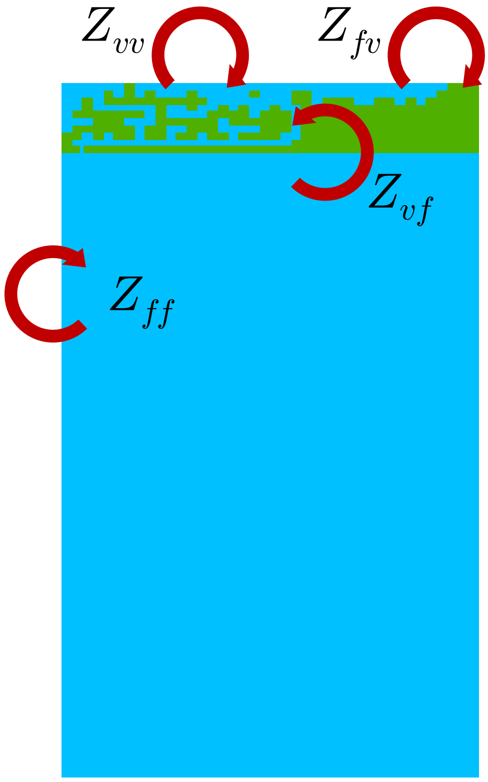

Figure 2.3: The image of the categorization for a fixed part and variable part

is decomposed until the elements related to fixed elements, in other words, the elements which have suffix 'f' are decomposed as

$$LU_{pre} \;=\; \begin{bmatrix} LU_{ff} & U_{fv} \\ L_{vf} & Z_{vv} \end{bmatrix}. \tag{2.7}$$

This matrix is kept in memory while the optimization, and the rest part of the matrix which has not been decomposed for each design is decomposed as

$$LU_{post} \;=\; \begin{bmatrix} LU_{ff} & U'_{fv} \\ L'_{vf} & LU_{vv} \end{bmatrix}. \tag{2.8}$$

2.3 S-parameter analysis to accelerate the calculation for variable antennas

An S-parameter analysis can combine the result of a electromagnetic simulation and non-radiating circuits and calculate them all in a circuit simulation, and then it is beneficial to simulate variable antennas. Figure 2.4 shows the schematic diagram of S-parameter analysis combined with an electromagnetic simulation (EMS). The S matrix S_0 indicated at the upper box in the figure is obtained from an EMS and $\#1, \cdots, \#i, \cdots, \#j, \cdots,$ and $\#n$ are the internal ports of this total system. The four boxes in the lower part in the figure are the external circuits. As is conventionally done [77], incident (a_*) and reflected (b_*) power waves are defined at all internal and external ports and the whole matrix can be obtained from the required condition at each port. Then with external boundary conditions– excitations and loads at the external ports– give the waves at the internal ports.

The way the S-parameter analysis is configured in the case of Fig. 2.4 is as the following. At first, focusing on the internal port 1, the equations there

$$a_1 \;=\; S^1_{22} b_1 + S^1_{21} a_{x1} \tag{2.9}$$

$$b_1 \;=\; \sum_{k=1}^{n} S^0_{1k} a_k \tag{2.10}$$

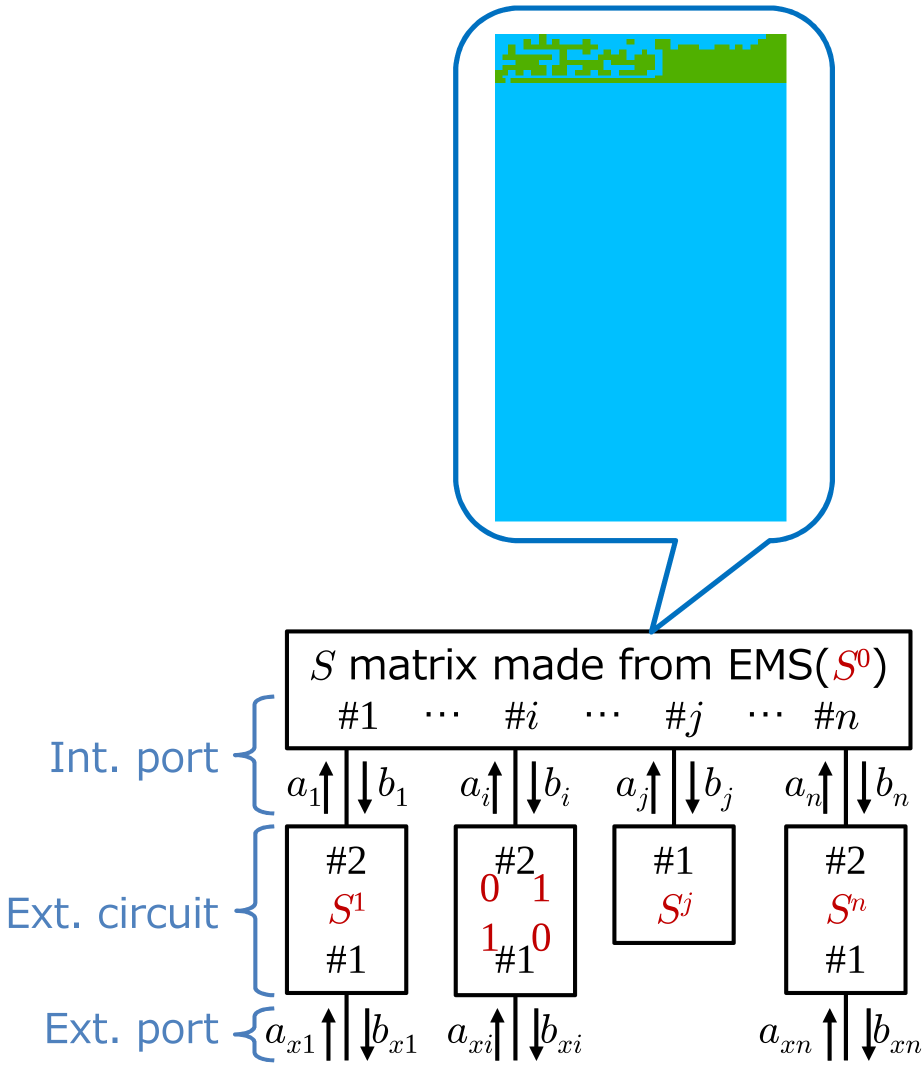

Figure 2.4: Schematic diagram of S-parameter analysis combined with an electromagnetic simulation (EMS)

are obtained. Similarly,

$$\begin{aligned} a_i &= 0 \cdot b_i + 1 \cdot a_{xi} && (2.11)\\ b_i &= \sum_{k=1}^{n} S^0_{ik} a_k && (2.12)\\ &\cdots \\ a_j &= S^j_{11} b_j && (2.13)\\ b_j &= \sum_{k=1}^{n} S^0_{jk} a_k && (2.14)\\ &\cdots \\ a_n &= S^n_{22} b_n + S^n_{21} a_{xn} && (2.15)\\ b_n &= \sum_{k=1}^{n} S^0_{nk} a_k && (2.16) \end{aligned}$$

are obtained. Then a linear simultaneous equations

$$[A][\boldsymbol{x}] = [\boldsymbol{y}] \tag{2.17}$$

is configured, where a total matrix

$$[A] = \begin{bmatrix} -1 & S^1_{22} & \cdots & 0 & 0 & \cdots & 0 & 0 & \cdots & 0 & 0 \\ S^0_{11} & -1 & \cdots & S^0_{1i} & 0 & \cdots & S^0_{1j} & 0 & \cdots & S^0_{1n} & 0 \\ \vdots & \vdots & \ddots & \vdots & \vdots & \ddots & \vdots & \vdots & \ddots & \vdots & \vdots \\ 0 & 0 & \cdots & -1 & 0 & \cdots & 0 & 0 & \cdots & 0 & 0 \\ S^0_{i1} & 0 & \cdots & S^0_{ii} & -1 & \cdots & S^0_{ij} & 0 & \cdots & S^0_{in} & 0 \\ \vdots & \vdots & \ddots & \vdots & \vdots & \ddots & \vdots & \vdots & \ddots & \vdots & \vdots \\ 0 & 0 & \cdots & 0 & 0 & \cdots & -1 & S^j_{11} & \cdots & 0 & 0 \\ S^0_{j1} & 0 & \cdots & S^0_{ji} & -1 & \cdots & S^0_{jj} & -1 & \cdots & S^0_{jn} & 0 \\ \vdots & \vdots & \ddots & \vdots & \vdots & \ddots & \vdots & \vdots & \ddots & \vdots & \vdots \\ 0 & 0 & \cdots & 0 & 0 & \cdots & 0 & 0 & \cdots & -1 & S^n_{22} \\ S^0_{n1} & 0 & \cdots & S^0_{ni} & 0 & \cdots & S^0_{nj} & 0 & \cdots & S^0_{nn} & -1 \end{bmatrix}, \tag{2.18}$$

an unknown signal vector at the internal ports

$$[\boldsymbol{x}] = [a_1,\ b_1,\ \cdots,\ a_i,\ b_i,\ \cdots,\ a_j,\ b_j,\ \cdots,\ a_n,\ b_n]^T, \tag{2.19}$$

and a given excitation vector at the external ports,

$$[\boldsymbol{y}] = [-S^1_{21} a_{x1},\ 0,\ \cdots,\ -a_{xi},\ 0,\ \cdots,\ 0,\ 0,\ \cdots,\ -S^n_{21} a_{xn},\ 0]^T. \tag{2.20}$$

Then, setting $a_{xk} = 1$ and $a_{xm} = 0 (m \neq k)$ gives $S_{pk}(p = 1, 2, \cdots, n)$ of S parameters for the external ports.

The problem of applying an S-parameter analysis to an antenna simulation is that the currents, loss, radiation efficiency, and other antenna characteristics are changed depending on the waves at the internal ports. Therefore, these characteristics should be calculated repeatedly everytime the waves at the internal ports changes. In order to reduce the time, the responce for the unit incident wave at every internal port is kept in memory and the antenna characteristics are calculated with using that data and flowchart as shown in Fig. 2.5. First the internal current when each port is excited step by step, and Y matrix and S matrix for internal ports are serially calculated. Combining the S matrix with the S matrix for external circuits, a total matrix and terminated S matrix are obtained. The terminated S matrix gives the input power, and the internal voltages which reconstruct the actual internal current distribution. Then the loss of an antenna and the radiation efficiency are determined.

Figure 2.6 shows the total flowchart to calculate a cost function. This chart includes the evaluation for a multiple frequencies, ports, and state of circuits analysis. The part lower than blue box in the figure corresponds to Fig. 2.5. After the evaluation for each port excitation with the best combination of ports, the worst evaluation among all excited ports is selected. Similar process is repeated at each frequency, and the worst evaluation among all frequencies is selected. A barrier function is described in the next section.

2.4 Barrier Function (BF)

Barrier function is defined as

$$BF(x, a, t) = \min\left(\frac{2\arctan a(x-t)}{\pi} + 1, 1\right). \tag{2.21}$$

Fig. 2.7 shows some examples of barrier functions with various parameters. Apparently every function sharply drops at a target parameter t, and also is equal where x is greater than t. Therefore, if some performance A corresponding to the above x deteriorates even slightly from the target value t, GA operation tends to reject the design because the cost function sharply drops near the point.

And if another performance B is far from the target value at the same time, the change of B is less sensitive to the cost function than the change

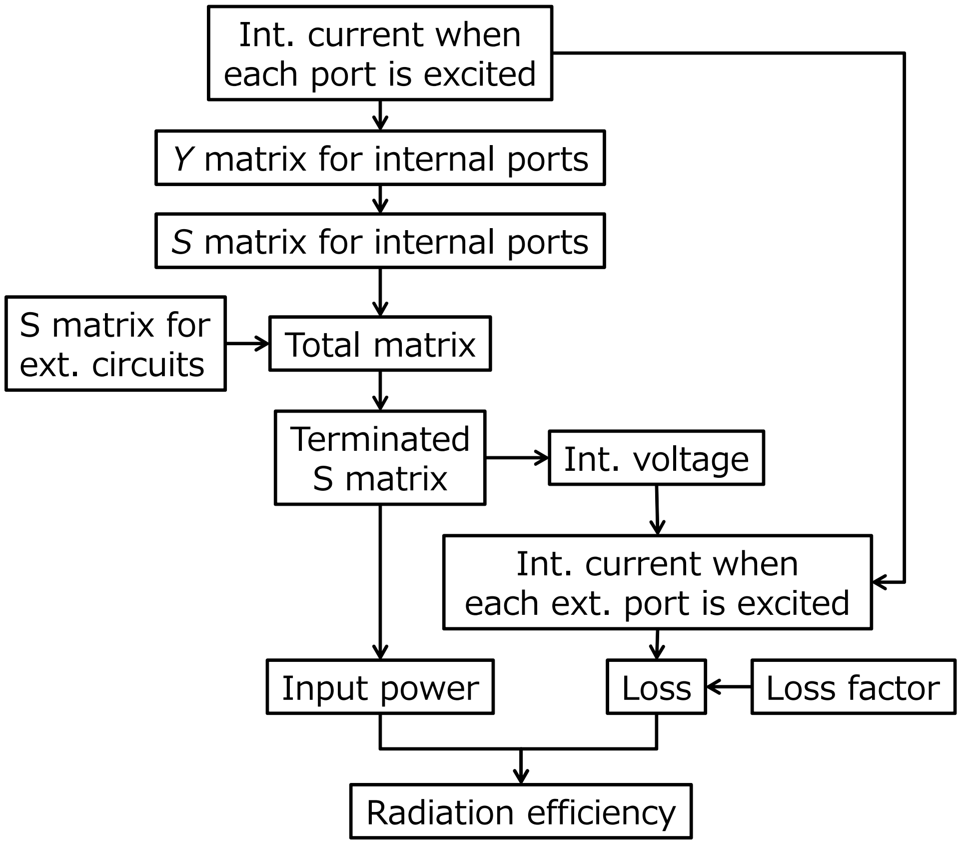

Figure 2.5: Flowchart to calculate antenna characteristics using an S-parameter analysis

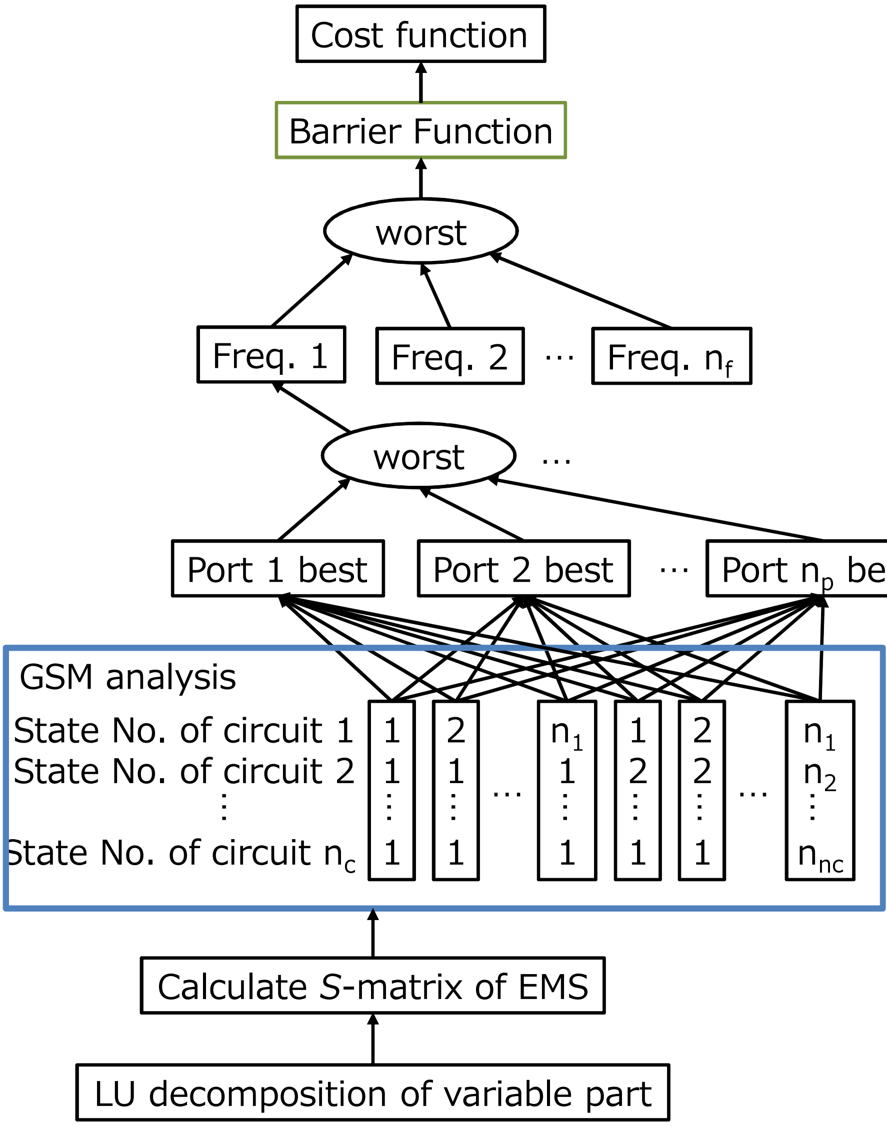

Figure 2.6: Total flowchart to calculate a cost function

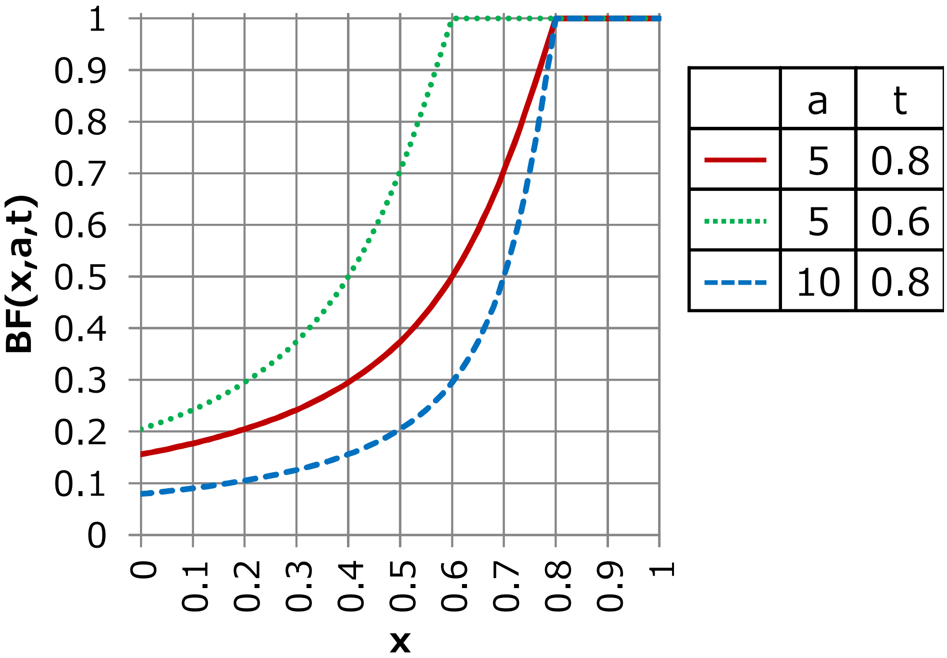

Figure 2.7: Examples of barrier functions with various parameters

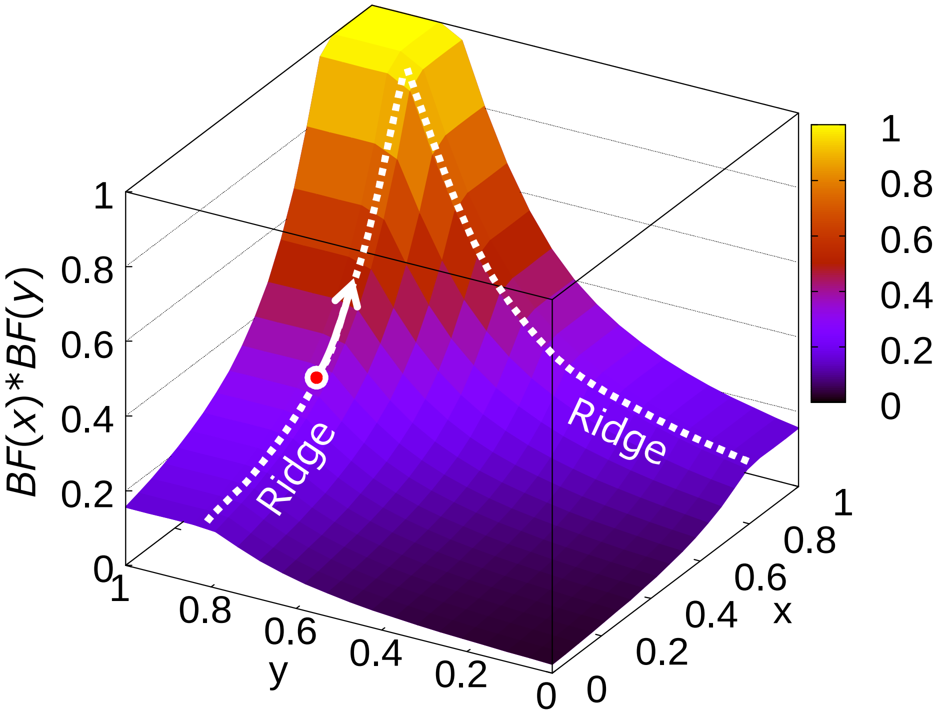

Figure 2.8: Product of two barrier functions

of A. Exactly speaking this is when the cost function is the product of two barrier function as shown in Fig. 2.8. The surface has two ridgelines along a target value, $t = 0.8$ in this case, which keeps satisfied objective value and promote another in a multi-objective optimization.

The value of this function is 1 when both x and y are greater than or equal to the target value t, and sharply decrease in the domain where either of x or y is slightly less than t, and the steepness is proportional to a.

2.5 Configuration error avoidance method

In this section, the method to eliminate the illegal patches causing error in electromagnetic simulation and trivial patches that are less likely to improve an antenna performance. The patches of interest are

- corner-touching patches– which cause an error in electromagnetic sim-

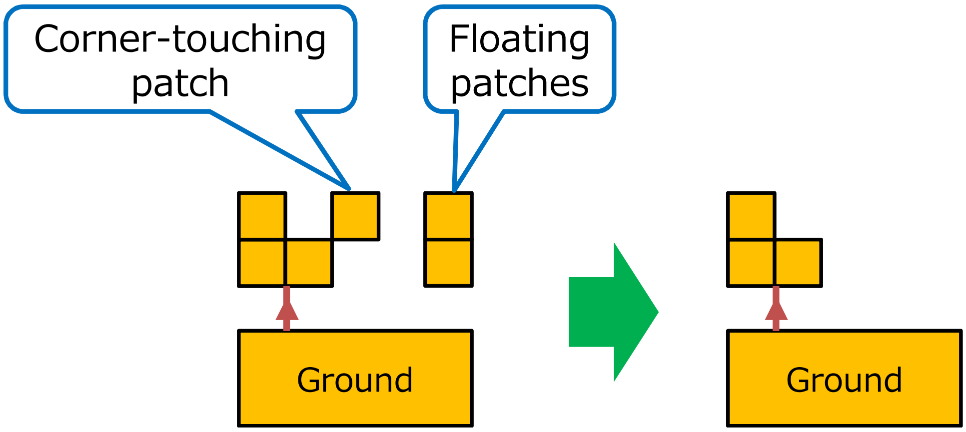

Figure 2.9: corner-touching patches and floating patches, and their elimination

ulations, and

- floating patches– which are not directly connected to a ground or signal line and probably useless because they must grow to about half wavelength to resonate and occupy a wide area

as shown in Fig. 2.9.

At first, each patch has a numbering in sequential order for GA as shown in Fig. 2.10. Then the geometrical relation between each patch and others can be expressed as in a graph theory manner.

For example, the adjacency on the edges and the connectivity at the corners between each patch and another are expressed with an 'adjacent

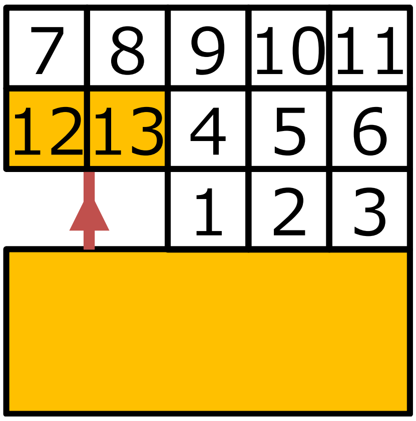

Figure 2.10: Numbering of patches for GA

matrix':

$$A = \begin{bmatrix}
F & T & F & T & F & F & F & F & F & F & F & F & F \\
T & F & T & F & T & F & F & F & F & F & F & F & F \\
F & T & F & F & F & T & F & F & F & F & F & F & F \\
T & F & F & F & T & F & F & F & T & F & F & F & T \\
F & T & F & T & F & T & F & F & F & T & F & F & F \\
F & F & T & F & T & F & F & F & F & F & T & F & F \\
F & F & F & F & F & F & F & T & F & F & F & T & F \\
F & F & F & F & F & F & T & F & T & F & F & F & T \\
F & F & F & T & F & F & F & T & F & T & F & F & F \\
F & F & F & F & T & F & F & F & T & F & T & F & F \\
F & F & F & F & F & T & F & F & F & T & F & F & F \\
F & F & F & F & F & F & T & F & F & F & F & F & T \\
F & F & F & T & F & F & F & T & F & F & F & T & F
\end{bmatrix} \tag{2.22}$$

and a ‘corner-connectivity matrix’:

$$C = \begin{bmatrix} F & F & F & F & T & F & F & F & F & F & F & F & T \\ F & F & F & T & F & T & F & F & F & F & F & F & F \\ F & F & F & F & T & F & F & F & F & F & F & F & F \\ F & T & F & F & F & F & F & T & F & T & F & F & F \\ T & F & T & F & F & F & F & F & T & F & T & F & F \\ F & T & F & F & F & F & F & F & F & T & F & F & F \\ F & F & F & F & F & F & F & F & F & F & F & F & T \\ F & F & F & T & F & F & F & F & F & F & F & T & F \\ F & F & F & F & T & F & F & F & F & F & F & F & T \\ F & F & F & T & F & T & F & F & F & F & F & F & F \\ F & F & F & F & T & F & F & F & F & F & F & F & F \\ F & F & F & F & F & F & F & T & F & F & F & F & F \\ T & F & F & F & F & F & T & F & T & F & F & F & F \end{bmatrix}, \quad (2.23)$$

respectively, where T denotes true and F denotes false. Then, some process to find geometrical relation becomes briefly coded, e.g.

- The matrix A^n denotes an indirect connectivity with n-th steps.
- Two matrices show the connectivity of patches for easy reference, e.g.
  - The matrix C shows the patch 4 and 10 are corner-touching.
  - The matrix A shows the deletion of either depends on the existence of patch 5 or 9 that are adjacent to both the patch 4 and 10.

These trimming process can avoid geometrical errors and accelerate the computation at the same time. On the other hand, that can decrease the number of patches rapidly. In order to avoid this problem geno and pheno type chromosomes are used in GA operation. Althoug geno-type chromosomes are inherited down the next generation, for the evaluation pheno-type ones are used. This way, it helps to avoid an error by hiding corner-touching patches and to accelerate the calculation by hiding floating patches. In fact, it was confirmed that optimized structures without the process of hiding floating patches have never had useful floating patches, e.g. the characteristics of the structure without the floating patches is almost the same with the floating patches. Lastly, the bits for the patches directly connected to a port are added to simplify the coding. This thing has already been shown in Fig. 2.10 and Fig. 2.11.

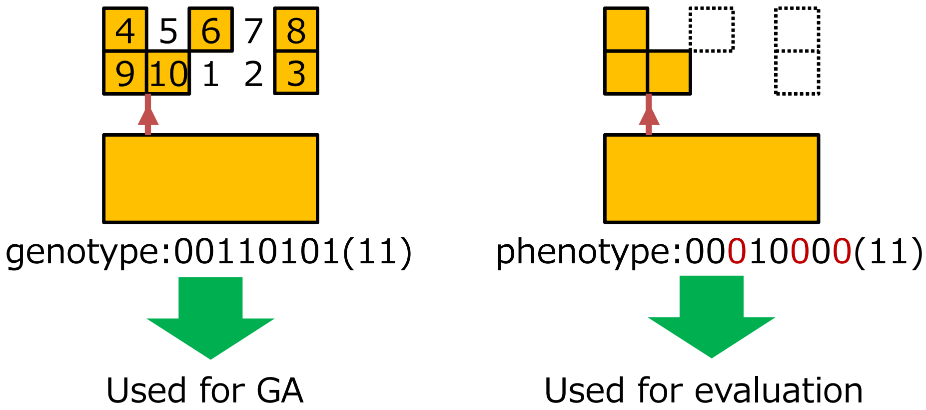

Figure 2.11: Example of geno and pheno type chromosomes

2.6 Summary

GA has been applied to designs of tunable/steerable antennas as multi-objective optimization problems. And 4 techniques to solve three problems in the optimization:

- NGF and S-parameter analysis for acceleration of simulation
- Barrier functions for the avoidance of local minima
- Maze searching, etc. for configuration error avoidance

have been introduced.

Chapter 3

Tunability design of electrically small antenna

3.1 Introductory remarks

Built-in antennas of mobile terminals are required to be smaller and to cover more frequency bands than ever before as the number of available wireless systems has burgeoned recently. On the other hand, in principle, small antennas have a trade-off between size and performance [1, 2]. Therefore, utilizing tunability [14–16, 19–22] is expected to be one of the solutions to enhance the performance of small antennas.

This chapter proposes a multi-band tunable antenna as one of the solutions for the above-mentioned problems. The antenna has been designed with GA based algorithm introduced in chapter 2. At first the idea of matchable impedance is discussed beforehand to choose the topology of a matching circuit. Next, an antenna has been designed with a selected matching circuit. Finally, the designed tunable antenna performance has been evaluated and compared with some conventional studies of a tunable antenna.

3.2 Matchable impedance

In order to choose a topology of a matching circuit in advance of antenna design, a matchable impedance was studied. Figure 3.1 shows the explanatory diagram related to matchable impedance. Z_a is an input impedance of an antenna, F, Z are 2-port matrix of a matching circuit, and Z_{in} is an input impedance of the antenna with the matching circuit. The matchable impedance of this diagram is the range of Z_a where Z_{in} can realize the

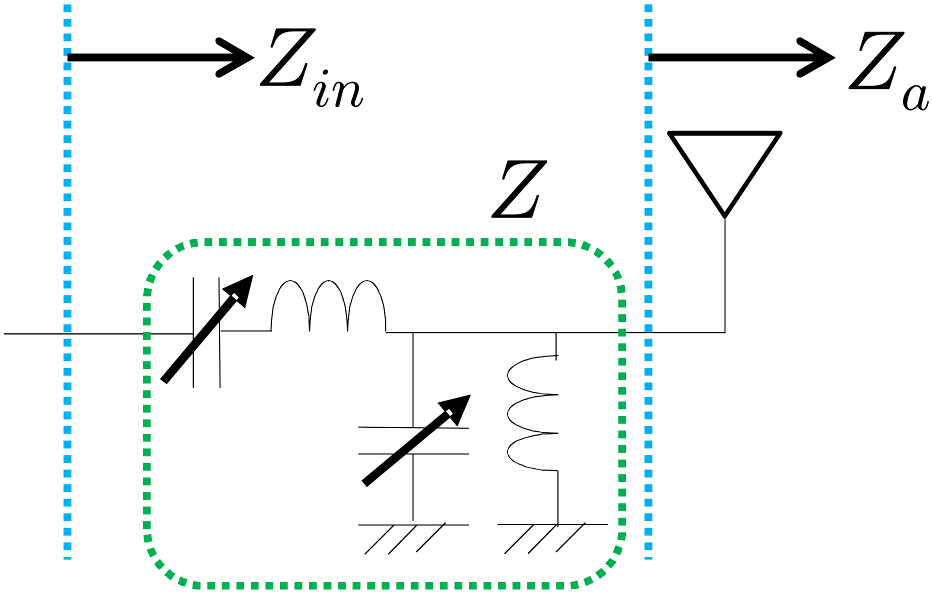

Figure 3.1: Explanatory diagram related to matchable impedance

VSWR less than a certain value with all variations of variable capacitances. The detailed calculation is introduces in the appendix A.

Figure 3.2 shows the matchable impedance of three matching circuits with 2, 3, and 4 lumped elements including 2 variable capacitances. The target VSWR is 3 and all inductances are 4 nH. The charts in the leftmost, middle and rightmost columns indicate the matchable impedance of matching circuits with 2, 3, and 4 lumped elements as shown in the top row in the figure, respectively. Judging from the charts, the range of matchable impedance with 4 lumped elements is larger than others and include the original matching range indicated with blue circles. The reason is easily found because capacitances change the matchable region in one direction, that is minus in reactance or susceptance.

Then the matching circuit with 4 lumped elements covers have a large area of matchable impedance and also intuitively that is supposed to make an antenna design easier compared with the original matching range.

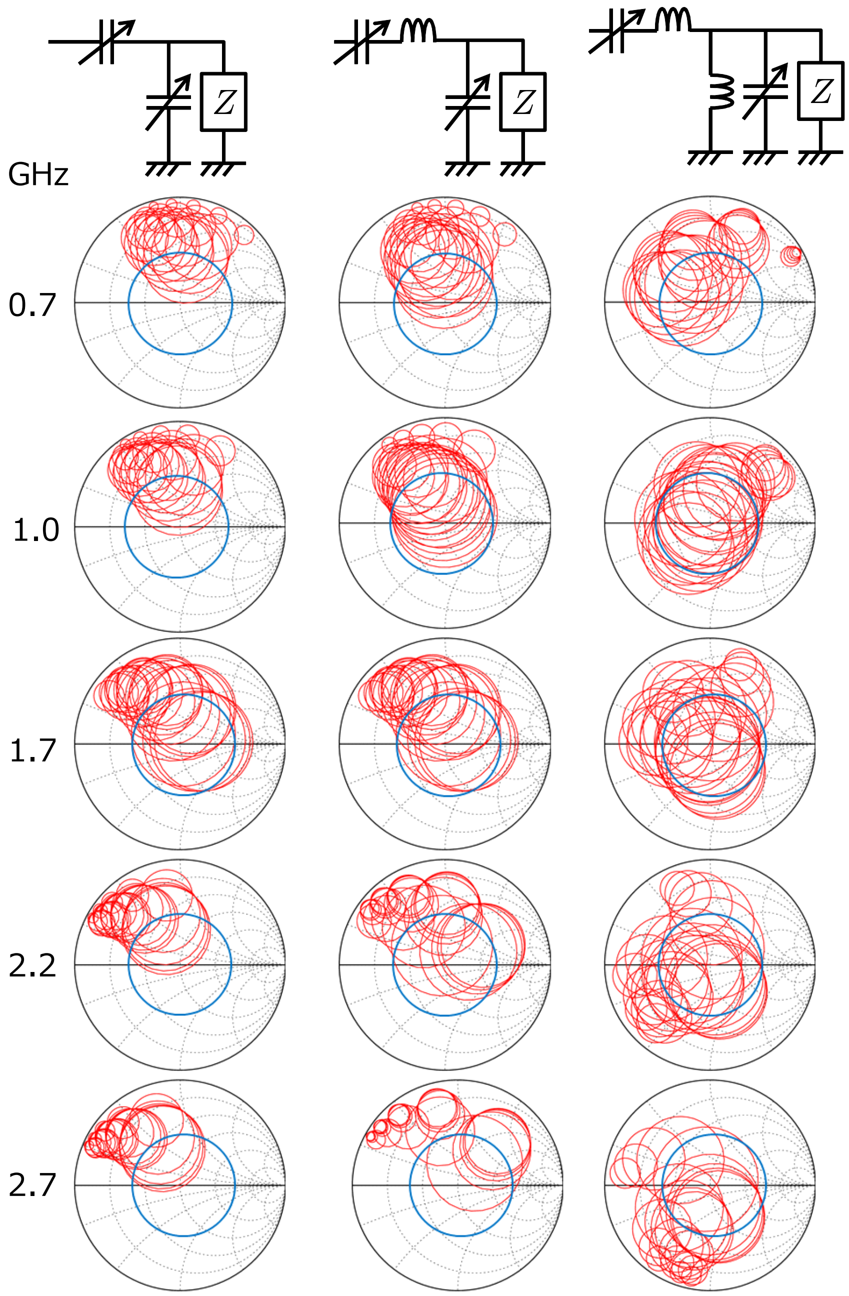

Figure 3.2: Matchable impedance of three matching circuits with 2, 3, and 4 lumped elements including 2 variable capacitances.

3.3 Antenna design and the performance

Figure 3.3 shows the optimized tunable antenna with the matching circuit including 4 lumped elements shown in Fig. 3.2. The multiband antenna design without a matching circuit [25] was used as an initial model to make the input impedance go through the matchable impedance shown in the rightmost column in Fig. 3.2.

The calculated VSWR, radiation efficiency of the designed tunable antenna are shown in Fig. 3.4. Light- and dark-colored lines show the characteristics with all variations of varicap diodes and the optimum envelope, respectively. Blue and red lines indicate VSWR and total efficiency, respectively. In this paper, total efficiency is defined as radiated-to-incident power ratio, which is equal to the product of transmission coefficient and radiation efficiency [69]. The red dotted lines indicate the radiation efficiency regardless of the lossless matching circuit. The VSWR is lower than 3 and the total efficiency is higher than -4 dB over the five frequency bands of typical wireless communication systems, i.e. LTE, GSM, DCS, PCS and UMTS indicated with bidirectional arrows, except for a part of lower LTE band around 0.7 GHz and UMTS around 2.1 GHz. The radiation efficiency indicates the potential total efficiency that is achieved with the perfect matching of the antenna, and could not be improved with a matching circuit. It is deteriorated by the ohmic loss on the antenna and the ground plane, and dielectric loss. Therefore, the improvement depends on the design and the material of the antenna structure.

3.4 Benchmarking of tunable antennas

Although the antenna has been designed only in a small area of 60 mm $\times$ 10 mm and covers the wideband for LTE, GSM, DCS, PCS and UMTS as shown in the previous section, the absolute figure of merit is unclear. So in this section the designed tunable antenna is compared with the physical limitations on (non-tunable) antennas and conventional studies.

At first, to confirm the accuracy of the physical limitations and the antenna optimization by GA, the performances obtained with these two method are compared. Figure 3.5 shows the comparison between the designed tunable antenna shown in Fig. 3.3 and physical limitations [2] for the parameter L. The figure of merit is $G/(k_0^2a^2Q)$, where G is a realizable maximum gain, k_0 is a wavenumber, a is the radius of the smallest circumscribing sphere of the whole structure, and Q is a quality factor. Obviously,

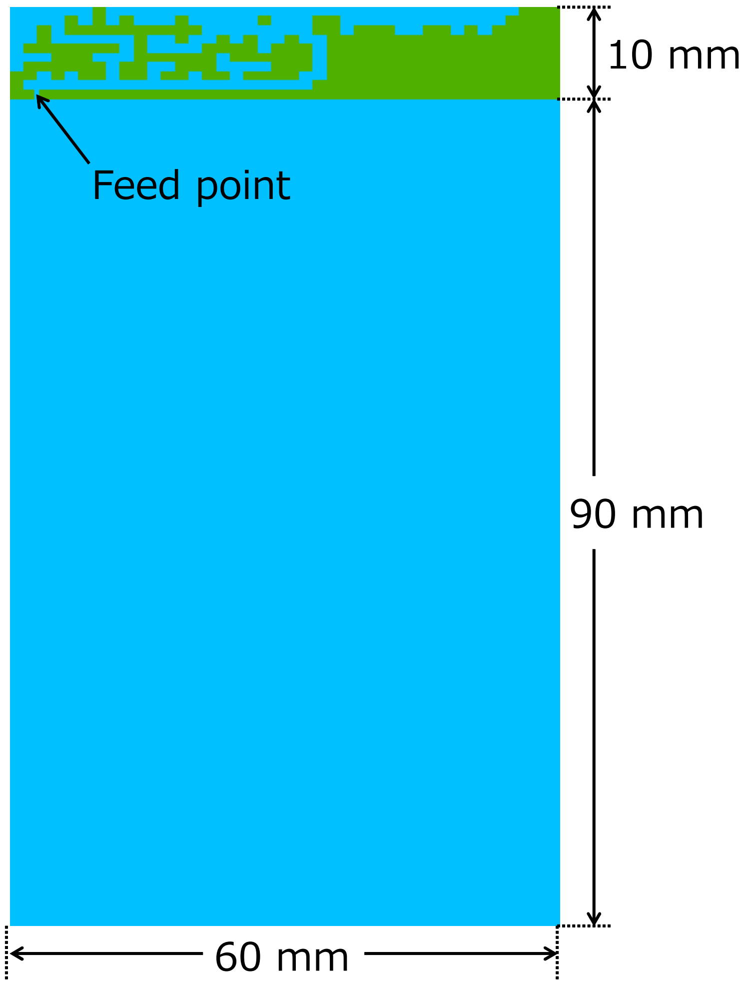

Figure 3.3: Optimized tunable antenna with the matching circuit including 4 lumped elements shown in Fig. 3.2

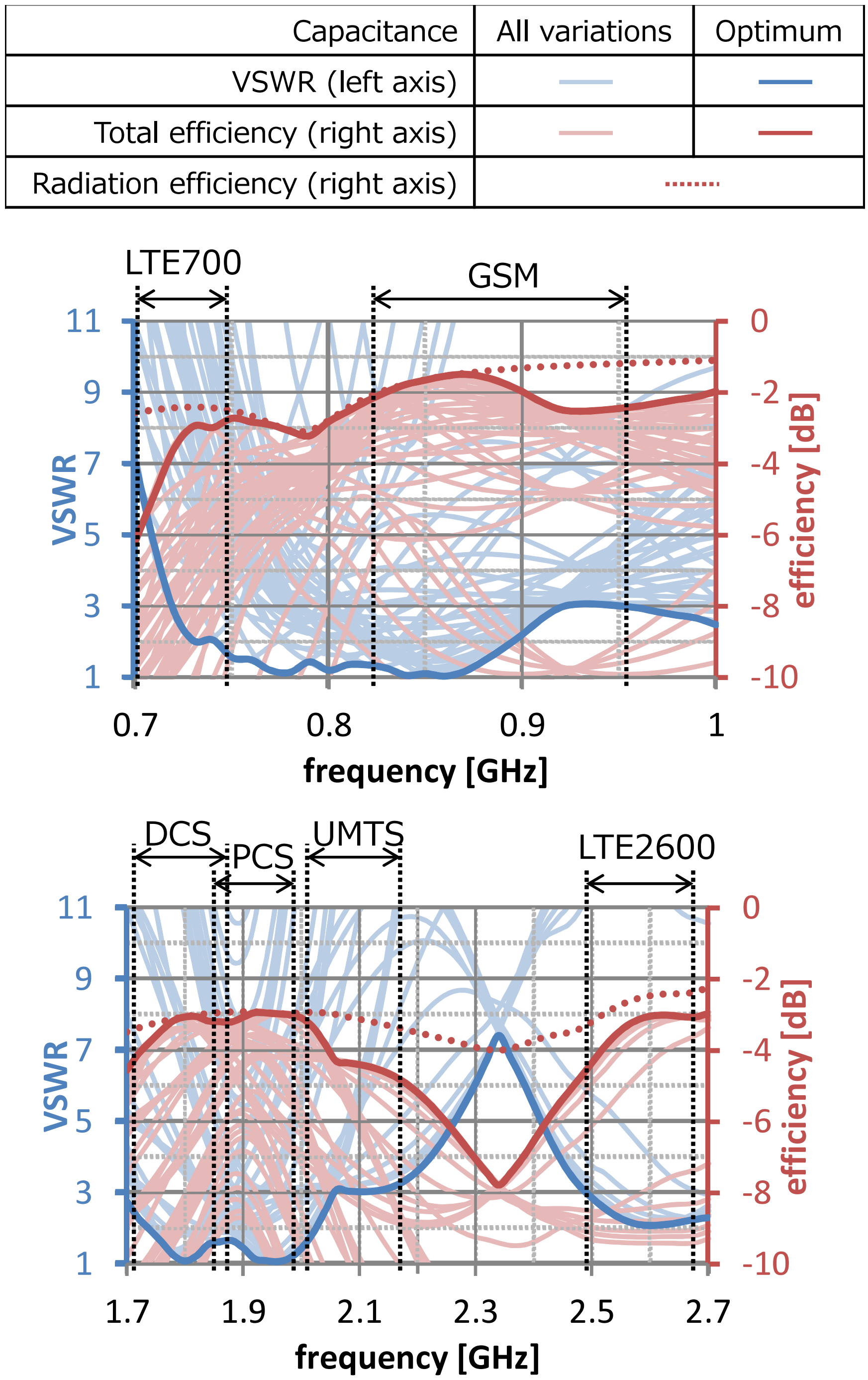

Figure 3.4: Calculated VSWR, radiation efficiency of the designed tunable antenna shown in Fig. 3.3

Table 3.1: Benchmark of tunable antenna

		Tunability					
Wireless System		LTE700 EGSM	DCS PCS UMTS	LTE2600	Size (W × L × T) [mm]		Radiation Efficiency (%)
Band (MHz)	f_{min}	704	1710	2500	Antenna	Ground	
	f_{max}	960	2170	2690			
This work		✓ 749 MHz—	✓	✓	60 × 10 × 1	60 × 90 × 1	> 40
Takemura[14]		✓		✓	50 × 10 × 1	50 × 90 × 1	> 40
Liu[15]		823 MHz—	✓		38 × 10 × 6	40 × 90 × 1	—
Chen[16]		✓	✓	✓	64 × 11 × 6	64 × 129 × 1.5	> 30
Xia[17]		✓	✓	✓	45 × 6 × 6	45 × 110 × 1	> 50
Ramachandran[18]		✓		✓	45 × 12 × 6	66 × 110 × 1	> 35

they denote the same tendency for L and the antenna designed with GA provide comparable performance with that of the physical limitation.

Next, the absolute bandwidth of the designed tunable antenna shown in Fig. 3.3 and the physical limitations for the parameter H are compared each other as shown in Fig. 3.6. This comparison only focus on the lower frequency band less than 1 GHz. The designed tunable antenna has a three times wider bandwidth of the physical limit.

Lastly, the designed tunable antenna is benchmarked with conventional studies on tunable antennas as shown in Table 3.1. The conventional studies in the table except for [16] does not cover all cellular wireless systems. Although [17] appears to cover all, in the paper LTE700 and EGSM is obtained by physical switching the line in a matching circuit. [16] covers all, however the size of the antenna is a little larger than this work and the radiation efficiency is also a little worse than this work.

To confirm that the designed tunable antenna is on the frontier in the trade-off among the size, bandwidth and efficiency of an antenna, a bubble chart of efficiency on the size-bandwidth map is shown in Fig. 3.7. The size is determined without a ground plane in the upper chart, and with a ground plane in the lower one. The size of bubbles denotes the efficiency and the center is located on the size-bandwidth map. Since the result marked Xia is obtained physically shorted wire, and the result marked Liu does not clarify the efficiency in the paper, it is valid that this work on the frontier in the trade-off among the size, bandwidth and efficiency of an antenna.

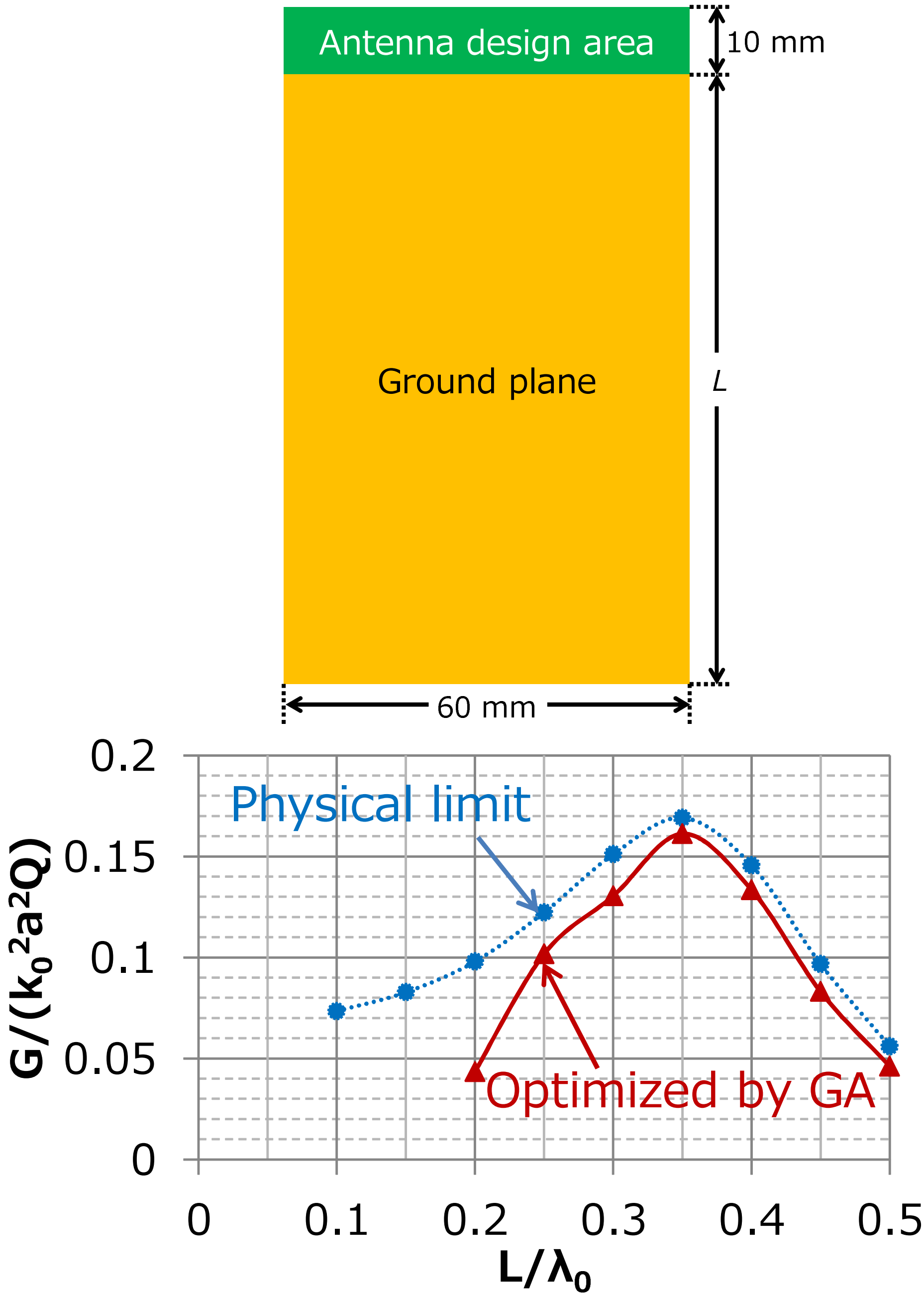

Figure 3.5: Comparison between the designed tunable antenna shown in Fig. 3.3 and physical limitations [2] for the parameter L

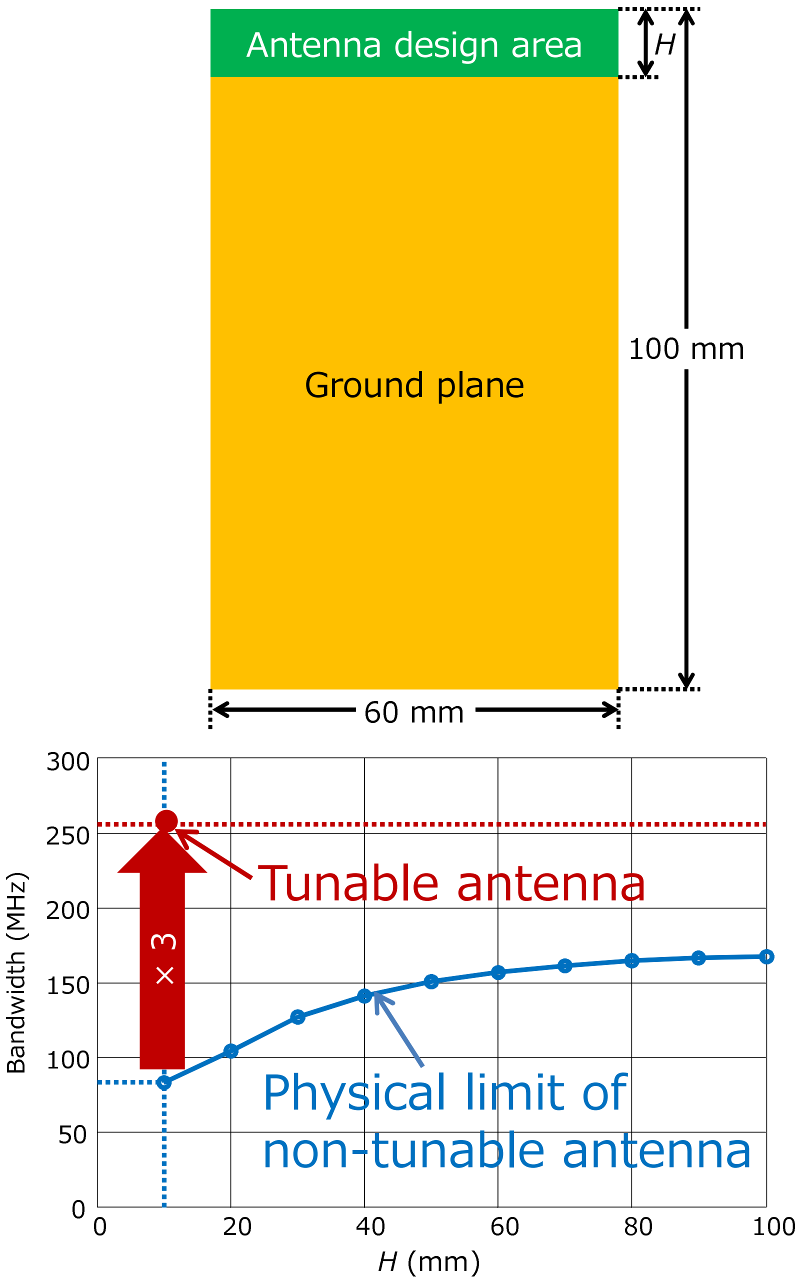

Figure 3.6: Comparison between the designed tunable antenna shown in Fig. 3.3 and physical limitations [2] for the parameter H

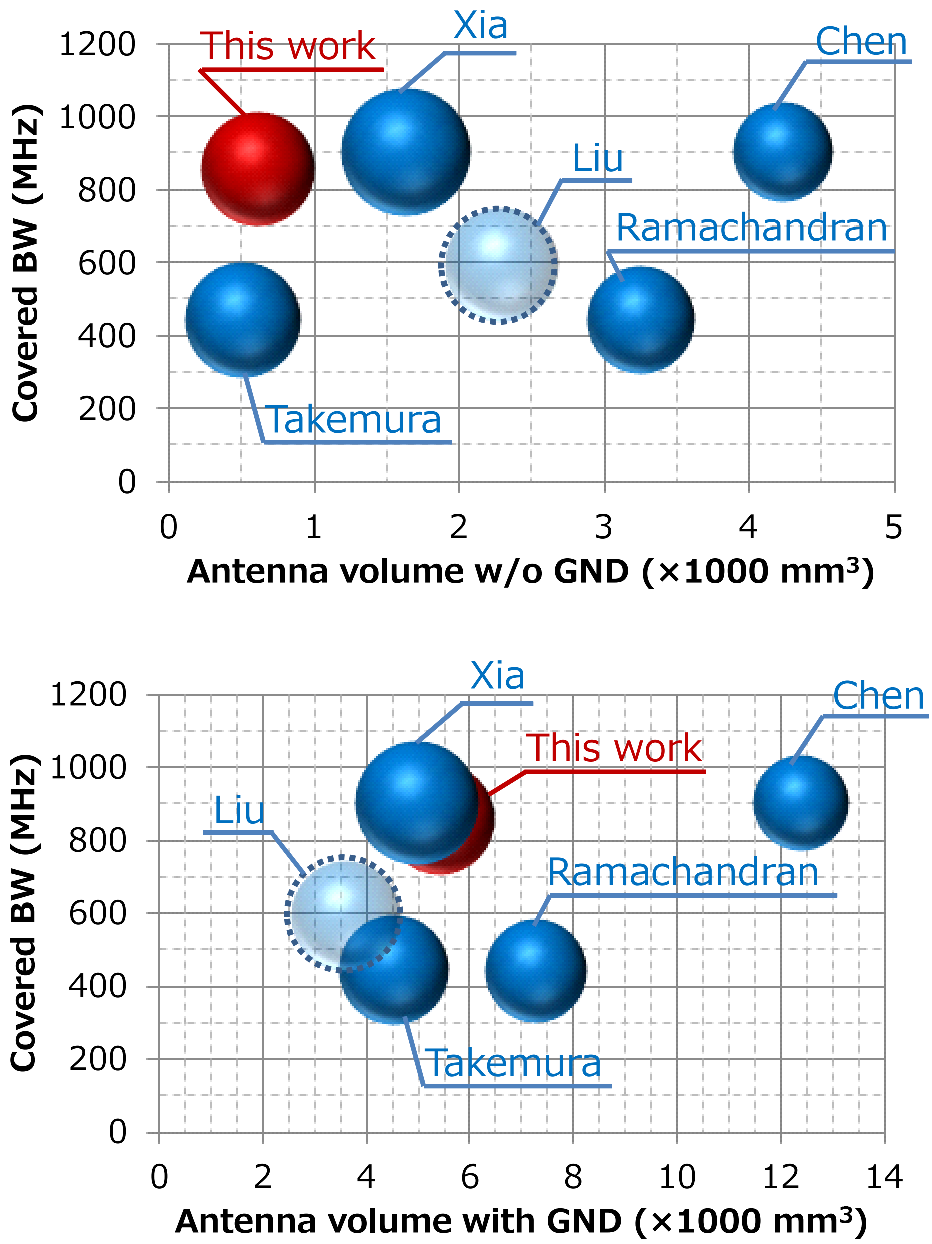

Figure 3.7: Bubble chart of efficiency on the size-bandwidth map

3.5 Summary

Based on matchable impedance, 4-element matching circuit was adopted. It is confirmed that the designed tunable antenna achieves wideband operation with a small size:

- 3 times wider bandwidth than physical limitation, and
- on the frontier in terms of tunability and the size of an antenna compared with conventional studies.

Chapter 4

Automatic tunability and its verification

4.1 Introductory remarks

This chapter proposes a multi-band automatic tunable antenna system for wide frequency bands of 704–2690 MHz for cellular wireless communication systems. The proposed system controls variable capacitors connected between the antenna and a transmitter based on the received power of a probe. Locating the probe near the tip of the antenna enables frequency-a operation. The antenna is a multi-band two-arm monopole antenna printed on a 60 mm×10 mm area of a 60 mm×100 mm FR-4 printed circuit board (PCB). The probe is a small dipole antenna capacitively coupled with the antenna. Fine-tuning based on simple hill-climbing optimization compensates the mismatch due to the surroundings, e.g., a user's hand/head or desk assuming channel-informed rough-tuning beforehand. A prototype consisting of varicap diodes and some other devices demonstrates automatic tunability.

Built-in antennas of mobile terminals are required to be smaller and to cover more frequency bands than ever before as the number of available wireless systems has burgeoned recently. On the other hand, in principle, small antennas have a trade-off between size and performance [1, 2]. Therefore, utilizing tunability [19–21] is expected to be one of the solutions to enhance the performance of small antennas.

However, narrower frequency bandwidth in each state of variable elements while downsizing the antenna tends to cause a mismatch due to the surroundings, e.g., a user's hand/head or desk. Therefore, the problem could be severer than in the case of a larger passive (non-tunable) antenna, and automatic tuning [22] is useful for a small built-in tunable antenna.

This paper proposes a multiband automatic tunable antenna system as one of the solutions for the above-mentioned problems. The proposed system includes a probe located near the tip of an antenna to detect transmission power, and a field-programmable gate array (FPGA) that controls varicap diodes based on the received power of the probe. The proposed system is advantageous in terms of the operational bandwidth, the loss caused by additional blocks, and high input signal-to-noise ratio (SNR) of a detector for low reflection of the antenna, compared with a conventional system using a directional coupler to detect the reflection from an antenna.

In this chapter, the proposed system is introduced in Sect.2. The design approach for an antenna and a control part of the system is described in Sect.3. The calculated and measured results are shown in Sect.4 and 5, respectively. Following a discussion of the operating mechanism of the proposed antenna in Sect.6, the final section is devoted to a conclusion.

4.2 Proposed system

Figure 4.1 shows the conventional method and the proposed automatic tuning method. An automatic tuning system requires information about the input impedance matching of the antenna. The conventional method uses a directional coupler connected between a matching circuit and a transmitter. The proposed method uses a probe capacitively connected with an antenna instead of a coupler.

Whereas the conventional system is based on the reflected signal from the antenna via the matching circuit to control the matching circuit, the proposed system is based on the received power of the probe. This difference results in the advantages of the proposed system listed in Table 4.1.

- Although the operational bandwidth is limited by the isolation of the directional coupler in the conventional system, the proposed system is frequency-independent because a small probe is located near the tip of the antenna (see the discussion section).

- Although the directional coupler has substantial insertion loss [23, 24], if the ratio of the received power of the probe to the input power is less than −20 dB, that corresponds to less than 0.1 dB loss, for example.

- Whereas the low reflection from the matching circuit directly gives low input SNR of the detector in the conventional system, the opposite

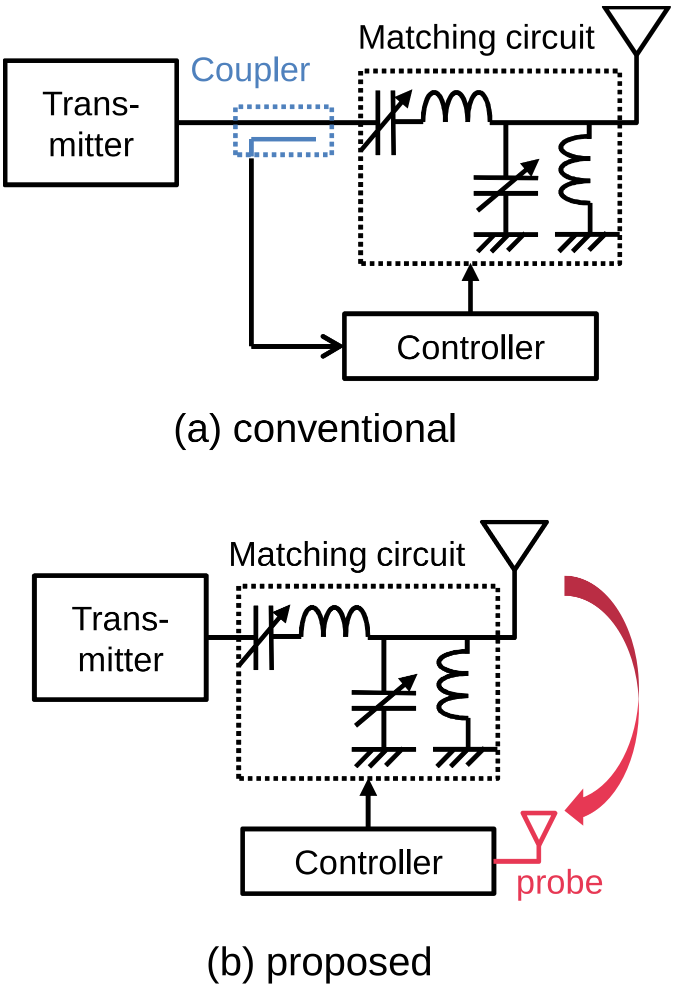

Figure 4.1: Conventional and proposed automatic tuning method

relation applies in the proposed system. E.g. when $S_{11} = -10$ dB, the coupling of a directional coupler in the conventional system is -20 dB, and the coupling between an antenna and a probe in the proposed system is also -20 dB, input SNR of the detector is approximately 10 dB higher in the proposed system than in the conventional system.

Table 4.1: The feature of the conventional and proposed method

Performance	Conventional	Proposed
Bandwidth	Limited by isolation of directional coupler	Frequency independent
Loss	Typ. 0.3–1 dB	<0.1 dB
Input SNR of detector	Low reflection gives low SNR	Low reflection gives high SNR

4.3 Design approach for antenna and control

Figure 4.2 shows the matchable impedance region with the matching circuit shown in Fig. 4.1 at each frequency. The circuit consists of two inductances and two variable capacitances. Both inductances are 4 nH. Both variable capacitances can be 1, 2, 3, 4, 5 and 6 pF. The impedance is easily calculated from the F parameters of the matching circuit (see appendix A). The union of the area enclosed with multiple red circles is the matchable impedance region. If the input impedance of an antenna is in this region, the matching circuit can decrease the voltage standing wave ration (VSWR) to less than 3 indicated with a blue circle. As shown in Fig. 4.2, the matchable impedance region is obviously advantageous to match the VSWR of an antenna without a matching circuit. Although the matchable impedance region does not cover the original VSWR<3 area only at 0.7 GHz, the antenna design is easier in the external region of the smith chart than near the center because the input impedance changes more slowly as the frequency changes.

We modified the original multiband antenna designed without a matching circuit [25] as an initial model to make the input impedance go through the matchable impedance shown in Fig. 4.2. Figure 4.3 shows the configuration of the antenna and the probe to be incorporated into the proposed automatic tunable antenna system shown in Fig. 4.1(b). The antenna is printed in a 60 mm×10 mm area on a 60 mm×100 mm FR-4 ($\varepsilon_r = 4.4$,

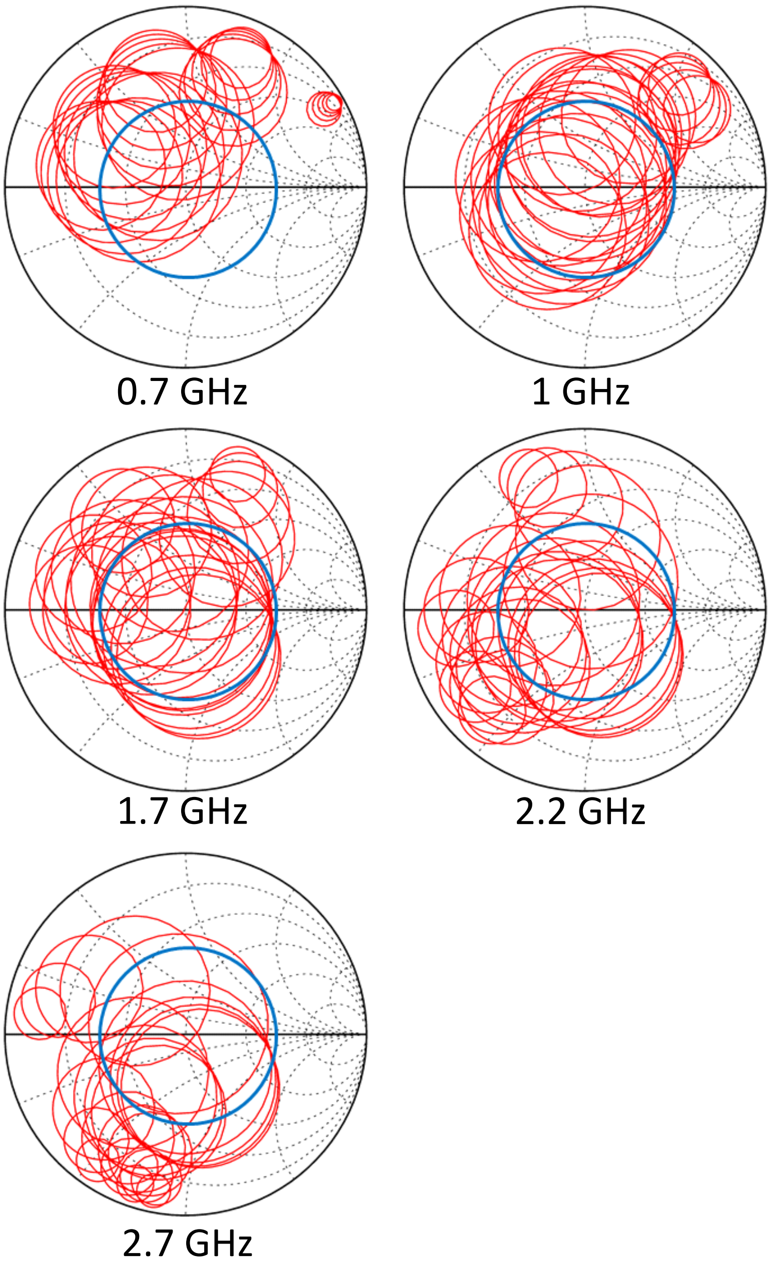

Figure 4.2: Matchable impedances at each frequency with the matching circuit shown in Fig. 4.1

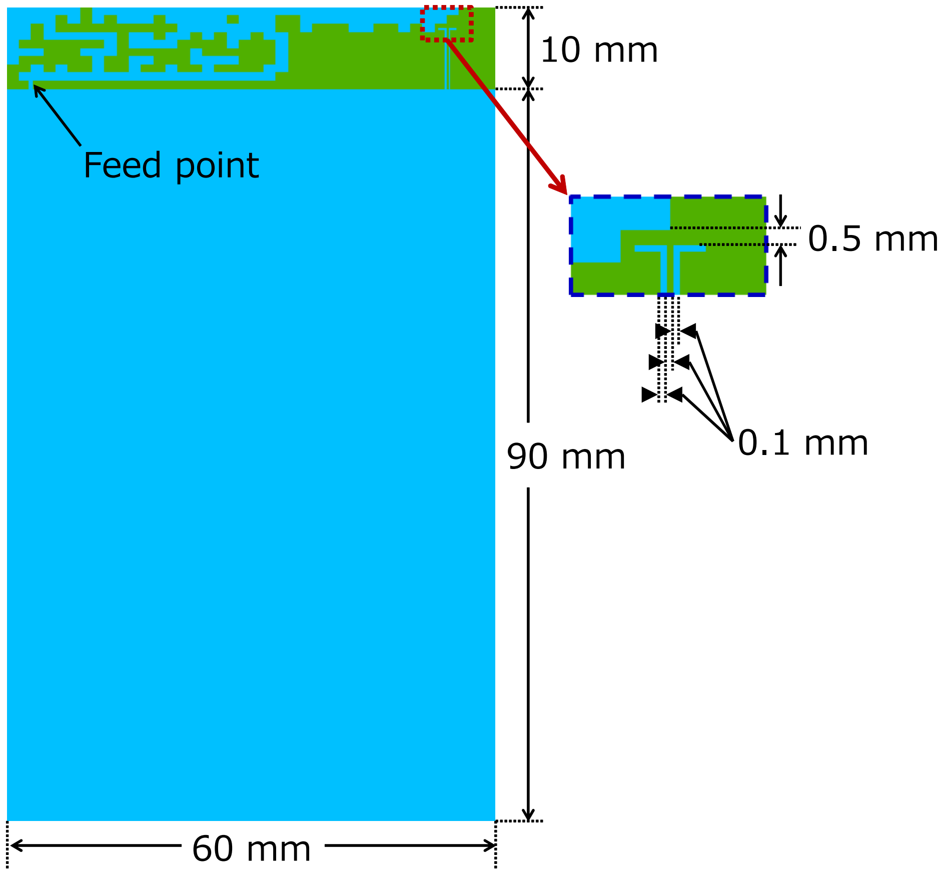

Figure 4.3: Configuration of the antenna and the probe

$\tan\delta = 0.02$) PCB. The probe is printed near the tip of the antenna and its length of 4 mm is substantially shorter than that of the antenna. The antenna and the probe are coupled capacitively. Assigning the feeding points of the antenna and the probe to port #1 and #2, respectively, S_{21} indicates the coupling between them.

Figure 4.4 is a schematic diagram of the original idea of applying hill-climbing optimization to the antenna system. The received power of a probe P_{det} converted from an RF signal received by a probe via a power detector is converted to 8-bit binary data via an Analog-to-Digital Converter (ADC). The comparator indicated as CMP compares a previous binary data $P_{\mathrm{det}}(t-\Delta t)$ with the current one $P_{\mathrm{det}}(t)$, and the result determines whether the two sets of 8-bit binary data are counted up or down for the bias V_1 and V_2 to varicap diodes via Digital-to-Analog Converters (DACs) indicated as DAC1 and DAC2. Two varicap diodes are alternately controlled. Eventually, the block enclosed with dotted line is realized in an FPGA in the prototype. In addition, it is possible to integrate the control section, a power detector, an ADC, two DACs and two variable capacitors into a small IC, e.g., with a footprint of a few square millimeters.

4.4 Calculated results

Figure 4.5 shows the VSWR, radiation efficiency and total efficiency of the proposed antenna in free space shown in Fig. 4.3. Light- and dark-colored lines show the characteristics with all variations of varicap diodes and the optimum envelope, respectively. Blue and red lines indicate VSWR and total efficiency η_{tot}, respectively. In this paper, total efficiency is defined as radiated-to-incident power ratio, which is equal to the product of transmission coefficient and radiation efficiency η_{rad}. The red dotted lines indicate the radiation efficiency regardless of the lossless matching circuit. The value when S_{21} is at the maximum value agrees with the optimum value at every frequency. This means at least the matching circuit is optimized when the controller can maximize the received power of the probe. The VSWR is lower than 3 and the total efficiency is higher than -4 dB over the five frequency bands of typical wireless communication systems, i.e. LTE, GSM, DCS, PCS and UMTS indicated with bidirectional arrows, except for a part of lower LTE band around 0.7 GHz and UMTS around 2.1 GHz. The radiation efficiency indicates the potential total efficiency that is achieved with the perfect matching of the antenna, and could not be improved with a matching circuit. It is deteriorated by the ohmic loss on the antenna and the ground plane, and dielectric loss. Therefore, the improvement depends on the design and the material of the antenna structure.

Figure 4.6 shows the model of the proposed antenna in the vicinity of a hand. The hand is modeled with a dielectric block that has the same area as a PCB and is 10 mm in thickness. The dielectric constant $\varepsilon_r = 50$ and the conductivity $\sigma = 1$ S/m are determined with reference to the values of human muscle at around 1 GHz shown in [26]. The proposed antenna PCB model shown in Fig. 4.3 is located right above the hand model with 8 mm gap. A chassis surrounding a PCB and supporting the gap in practical use is not modeled.

Figure 4.7 shows the VSWR, radiation efficiency and total efficiency of

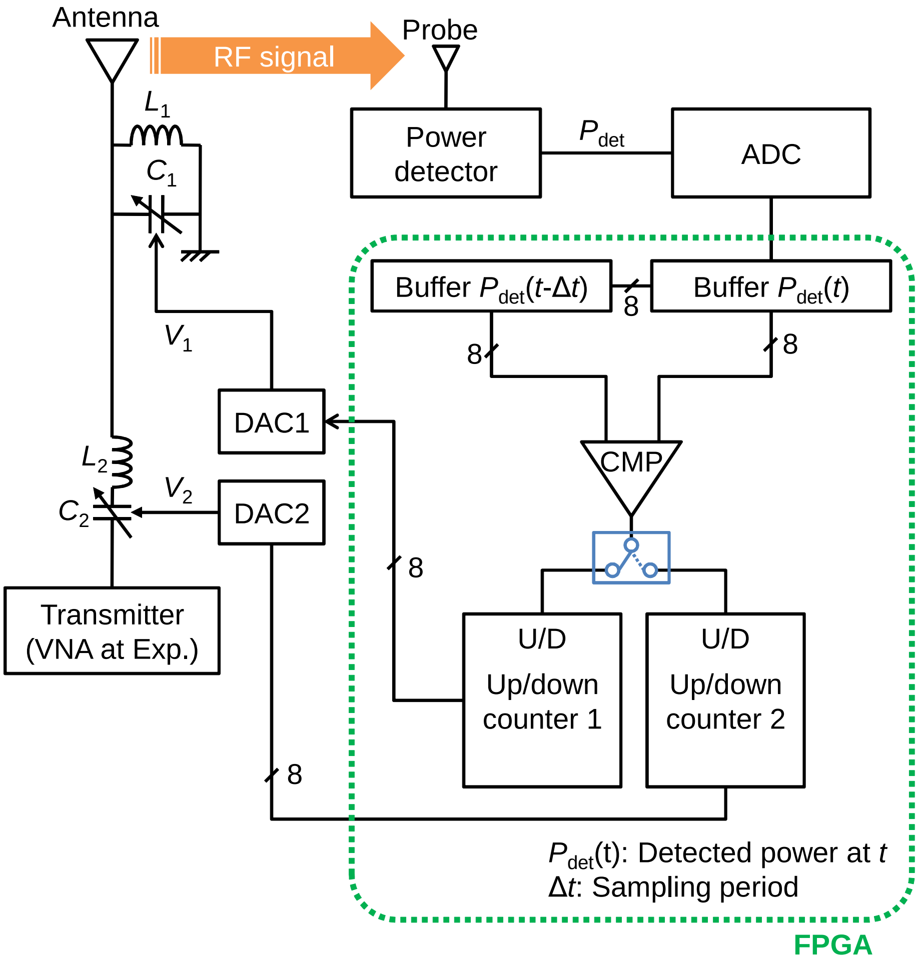

Figure 4.4: Schematic diagram of the original idea to realize hill-climbing optimization applying to the antenna system

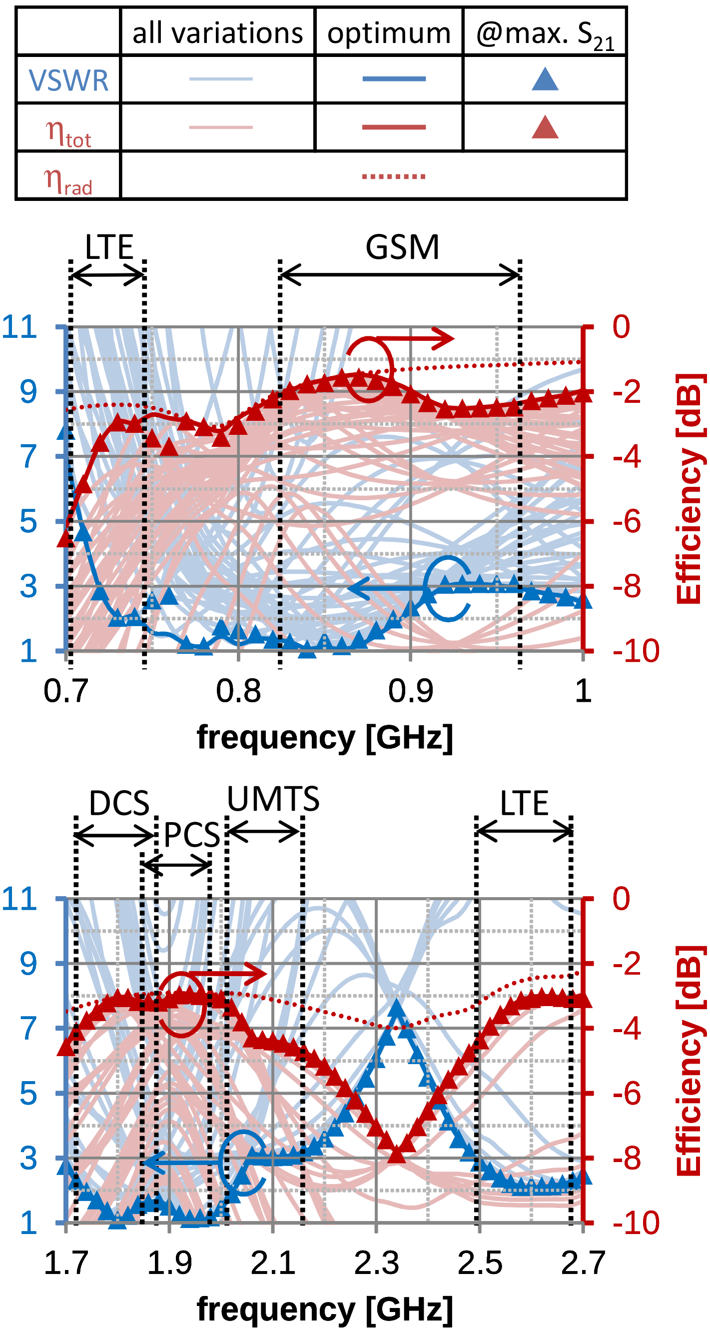

Figure 4.5: The VSWR, radiation efficiency and total efficiency of the proposed antenna in free space shown in Fig. 4.3

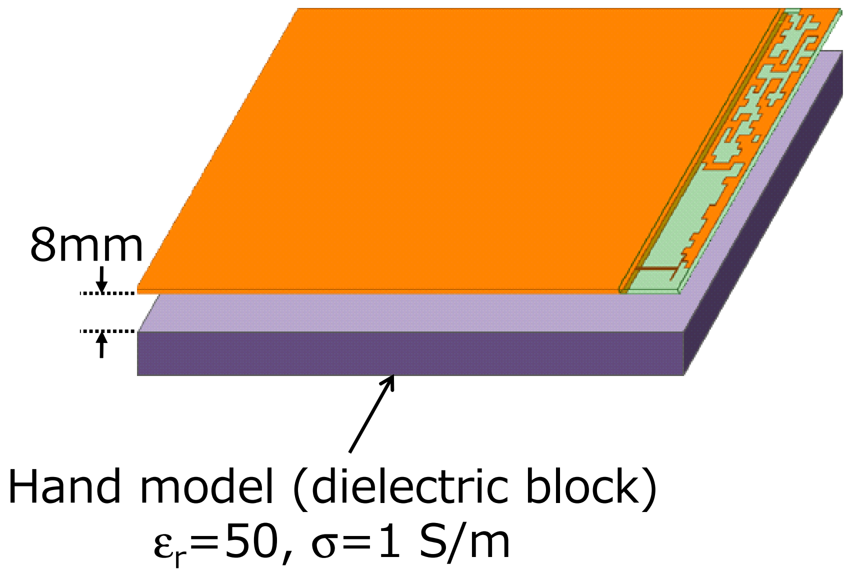

Figure 4.6: The model of the proposed antenna in the vicinity of a hand

the proposed antenna in the vicinity of a hand shown in Fig. 4.6. The legend and the meaning of each plot or line are identical to those in Fig. 4.5. Although the total efficiency averagely decreases over all frequencies, the VSWR and the total efficiency when S_{21} is at the maximum value agree with the optimum values at every frequency, respectively. Therefore, the VSWR and the total efficiency is optimized if the received power of the probe were maximized as is the case in free space.

4.5 Measured results

Figure 4.8 shows the prototype of the proposed antenna system. A vector network analyzer (VNA) feeds an RF signal into the antenna printed on an FR-4 PCB via the matching circuit that includes two varicap diodes and two inductors. A power detector converts the received power of the probe to DC voltage, and an ADC converts the DC voltage to 8-bit binary signal. An FPGA controls the varicap diodes based on the 8-bit binary signal via DAC1 and DAC2 to bias the diodes with DC voltage. Then the voltage can be in 256 steps from 1 V to 10 V, and the corresponding capacitance is from around 1 pF to around 6 pF. The hill-climbing optimization is realized in

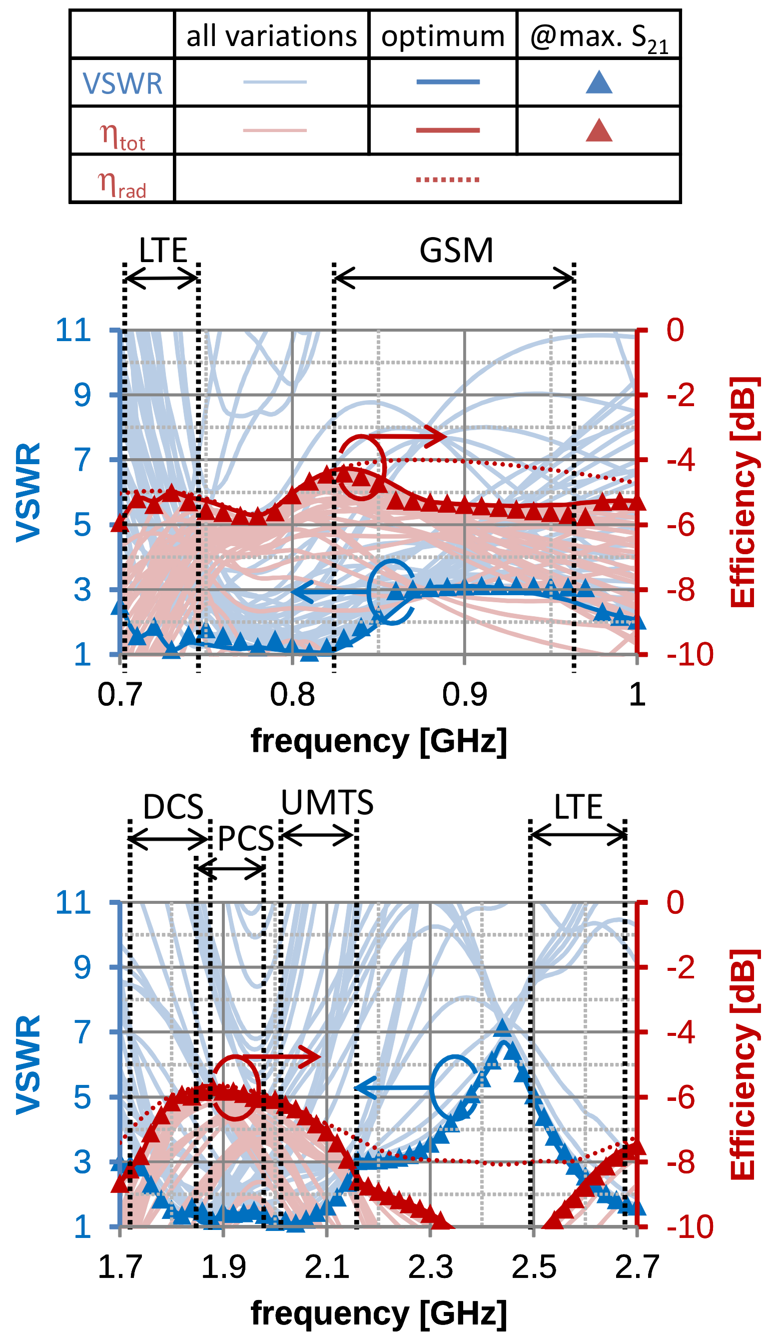

Figure 4.7: The VSWR, radiation efficiency and total efficiency of the proposed antenna in the vicinity of a hand shown in Fig. 4.6

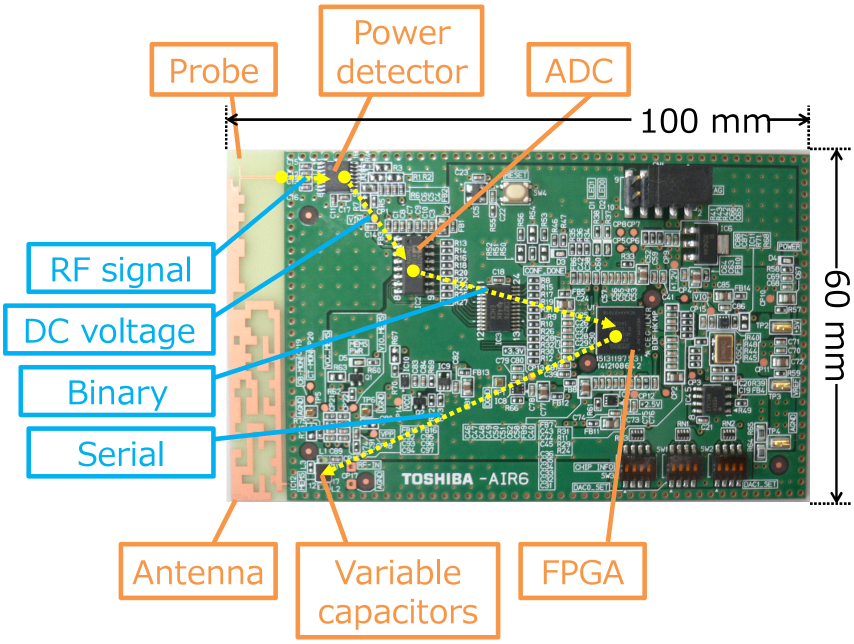

Figure 4.8: Prototype of the proposed antenna system

the FPGA.

The measured VSWR and impedance of the prototype are shown in Fig. 4.9. The VNA sweeps a 20 MHz span for each center frequency (700, 750, ... MHz) and the VSWRs converge to low values around 3 over a wide frequency range approximately from 700 MHz to 950 MHz. Apparently the impedance of the prototype for each frequency range is scattered around the center of the Smith chart and the distribution is unlikely to be realized without variable elements in such a small antenna design.

Figure 4.10 shows the change in the VSWR of the prototype when the impact of the proximity of a hand is included. The red line indicates the value when the varicap diodes are NOT controlled after convergence is achieved in free space, and the blue line is the re-converged VSWR. The converged VSWRs at 700 MHz and 800 MHz in free space (See also Fig. 4.9) are significantly deteriorated and improved again from around 2.5 to less than 1.5. This performance leads to power savings of around 20%.

The above results are for lower frequency band of less than 1 GHz. On the other hand, for higher frequency band of more than 1.7 GHz, the VSWR

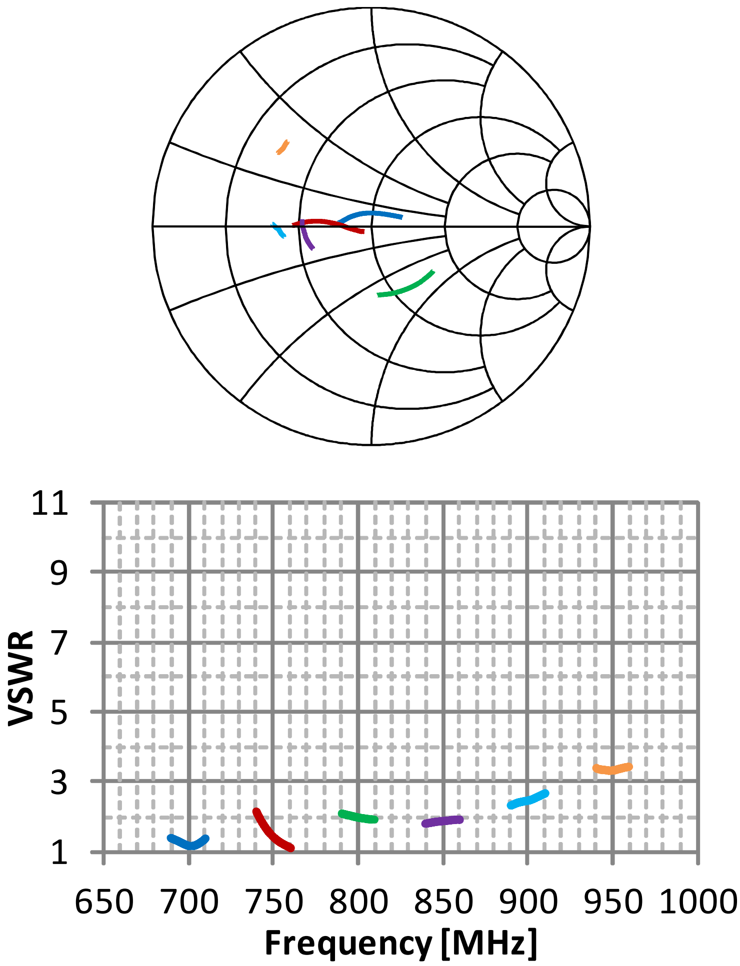

Figure 4.9: Measured VSWR and input impedance of the prototype shown in Fig. 4.8

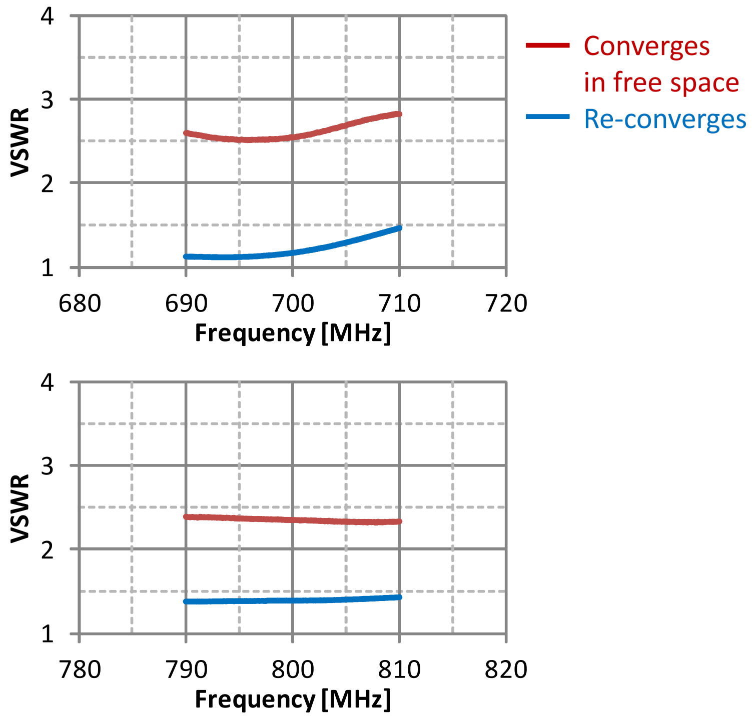

Figure 4.10: The change in the VSWR of the prototype when the impact of the proximity of a hand is included

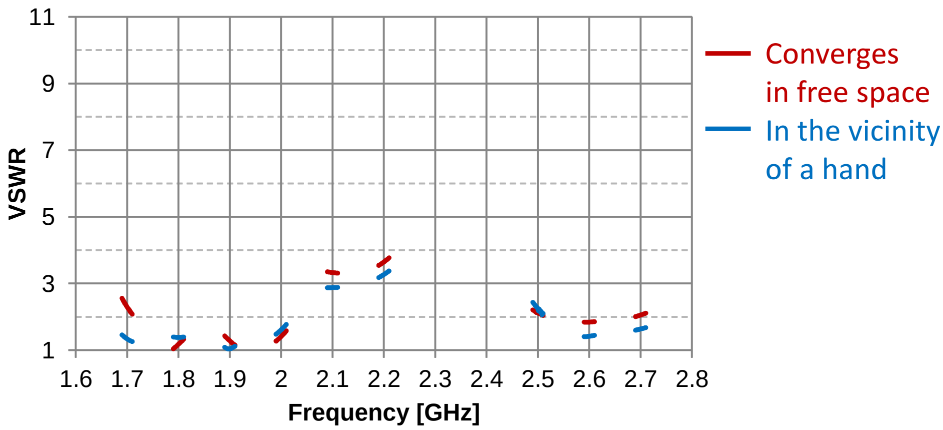

Figure 4.11: The VSWR of the prototype in free space and in the vicinity of a hand

of the prototype in the vicinity of a hand indicated with blue lines in Fig. 4.11 changes only slightly and can even be improved from the state in free space indicated with red lines in Fig. 4.11. It is thought that the coupling between the antenna and a hand in higher band is less than in lower band because of the distance between them in wavelength. Therefore, the tuning system is important for lower band but not for higher band.

4.6 Discussion

In this section, referring to the calculated results, the relation between the received power of the probe and the matching of the antenna in the proposed antenna system is discussed. The calculated results shown in Fig. 4.5 and Fig. 4.7 ensure the best matching state at least when S_{21} is at the maximum. In order to ascertain the behavior in the course of the optimization, we confirmed the correlation between S_{21} and VSWR of the proposed antenna system in free space as shown in Fig. 4.12. S_{21} and VSWR have strong negative correlation and most of the plots are aligned in a curve at every frequency. Hence, the VSWR decreases as S_{21} increases regardless of frequencies. The range of S_{21} is 33 dB from -52 to -19 dB. This is easily covered by a usual power detector. In addition, if the system can receive the information of the frequency of a transmitted signal, the required dynamic range of a power detector can be limited to a much higher part.

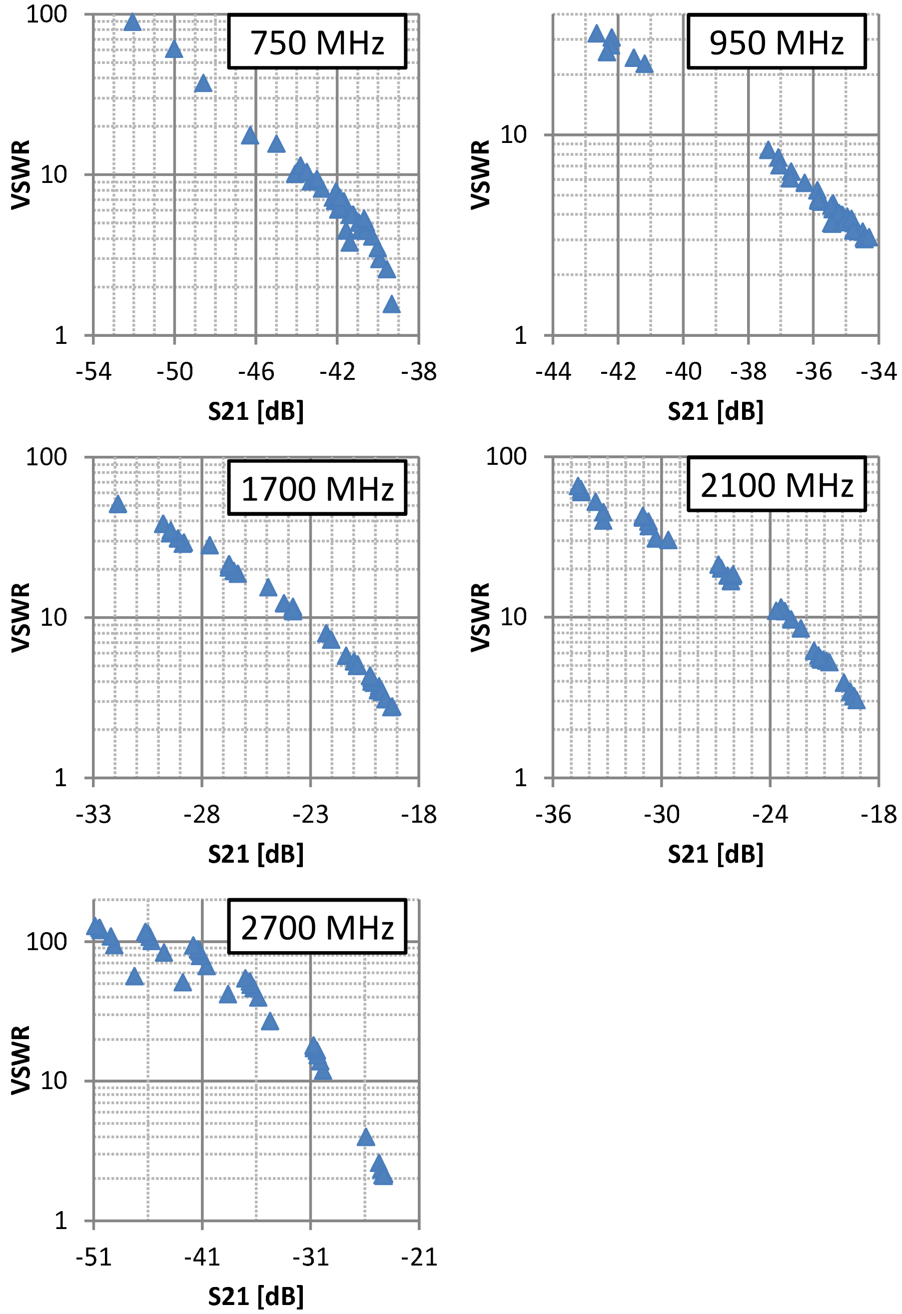

Figure 4.12: Correlation between S_{21} and VSWR of the proposed antenna system in free space (calculation)

Figure 4.13 shows the correlation between S_{21} and VSWR of the proposed antenna system in the vicinity of a hand. The correlation is sustained when the antenna is in the vicinity of a hand as shown in Fig. 4.6 as well. Although the correlation is a little weak at 750 MHz, it does not substantially matter because the plots out of a curve are localized around where the VSWR is lower than 3. The slight increase of S_{21} is thought to be due to the reflection and intensified field caused by a hand. Hence, the required dynamic range is narrower than that in free space.

Figure 4.14 shows the distribution of S_{21} and VSWR for the shunt (C_1) and series (C_2) capacitances shown in Fig. 4.1. The left-hand and right-hand graphs show S_{21} and VSWR at each frequency captioned just below the two graphs, and a red x-mark in each graph indicates the maximum S_{21} and the minimum VSWR. The locations of the red x-marks are identical at each frequency. Both S_{21} and VSWR have the unimodal distribution for the variation of two varicap diodes and are complementary. This permit the proposed system to control capacitances with the hill-climbing optimization for the received power of the probe.

The proposed antenna system can be matched independently of frequency, due to the strong negative correlation shown in Fig. 4.12. And it seems that depends on locating the probe near the tip of the antenna because the better the matching, the greater the charge density regardless of the frequency. To confirm this, we offset the probe nearer to the feed point and further from the tip of the antenna as shown in Fig. 4.15. The distance between the center line of the feeder of the antenna and the probe is 8 mm. The correlation between S_{21} and VSWR is supposed to be lower than the model shown in Fig. 4.3 because the charge density and the electrostatic coupling vary with frequency. Therefore, a probe is required to be located near the tip of an antenna as in Fig. 4.3 for frequency-independent operation, i.e. the impedance matching is obtained as long as the received power of the probe is increased at every frequency.

Figure 4.16 shows the calculated result of the probe-offset model shown in Fig. 4.15. The explanation of this chart is the same as that for Fig. 4.5. The figure shows that the difference between the characteristics when S_{21} is at the maximum and at the optimum is greater at lower frequencies.

The probe-offset model also lowers the correlation between S_{21} and VSWR. Figure 4.17 shows the correlation between S_{21} and VSWR of the probe-offset model shown in Fig. 4.15. The plots are distributed not in a curve as shown in Fig. 4.12 and Fig. 4.13 but in the band with the significant width at every frequency. At lower frequencies, S_{21} and VSWR are uncorrelated.

Figure 4.18 indicates the tunability for each wireless communication system that is widely available in the world. The proposed system is assumed to use a transmitted signal from a mobile terminal. Therefore, after a matching circuit has been tuned to Tx band, the antenna performance at Rx band might be a problem. Each curve shows the best performance matched to Tx band, and the lines parallel to the abscissa show the Tx/Rx band of each wireless communication system and the boundary of the target performance (VSWR$\leq$3 and total efficiency $\eta_{\rm tot} \geq -4$ dB). Although the VSWR and the total efficiency achieve the target value both in Tx and Rx band in the cases of GSM850, DCS, PCS and LTE2500, they do not in other cases: LTE700, EGSM and UMTS. However, the antenna performance in Tx band is more important than in Rx band in terms of the battery life of a mobile terminal in many actual situations.

Now, although we should consider the possibility of malfunction when a hand gets closer to the proposed antenna, that has not happened in the prototype. One of the reasons is that the distance between the probe and the tip of the antenna is quite close. Therefore, the radiated power is more absorbed and the input impedance is much easier to match when a hand gets closer. In fact, the radiation efficiency is deteriorated much as shown in Fig. 4.7, and the number of matching state is greater in the vicinity of a hand than in free space as shown in Fig. 4.19.

4.7 Summary

A novel multiband automatic tunable antenna system was proposed and demonstrated. Based on the received power of a probe located near the tip of a multiband antenna, frequency-independent operation is realized. The proposed system using a probe is advantageous also in terms of the input SNR of a detector compared with the conventional system that detects the reflected signal from an antenna.

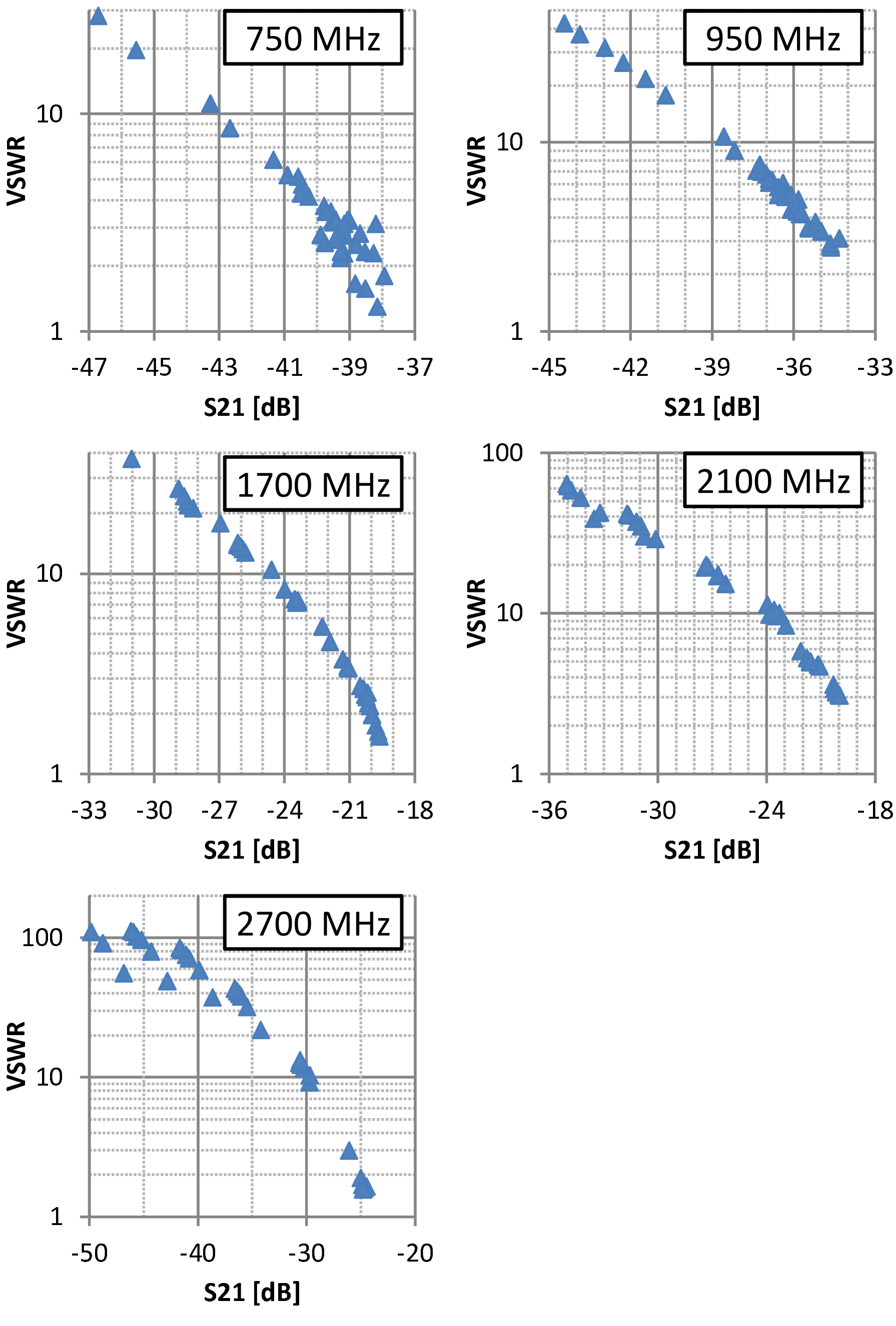

Figure 4.13: Correlation between S_{21} and VSWR of the proposed antenna system in the vicinity of a hand (calculation)

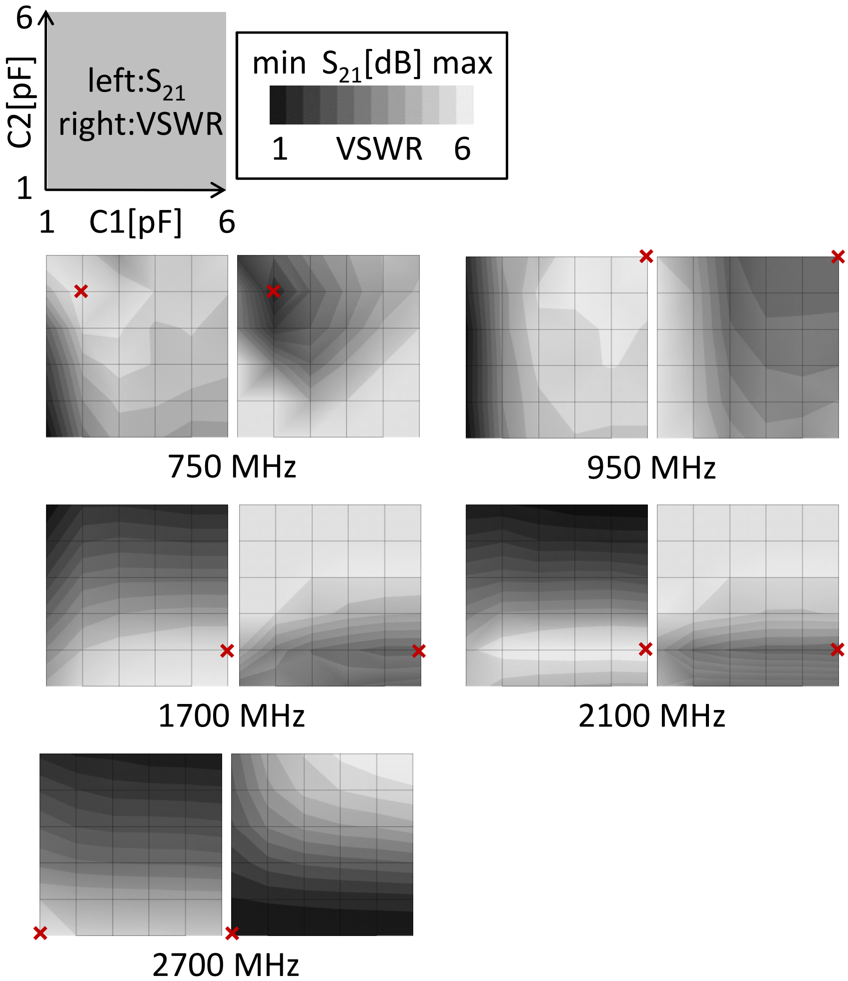

Figure 4.14: Distribution of S_{21} and VSWR for the shunt (C_1) and series (C_2) capacitances shown in Fig. 4.1

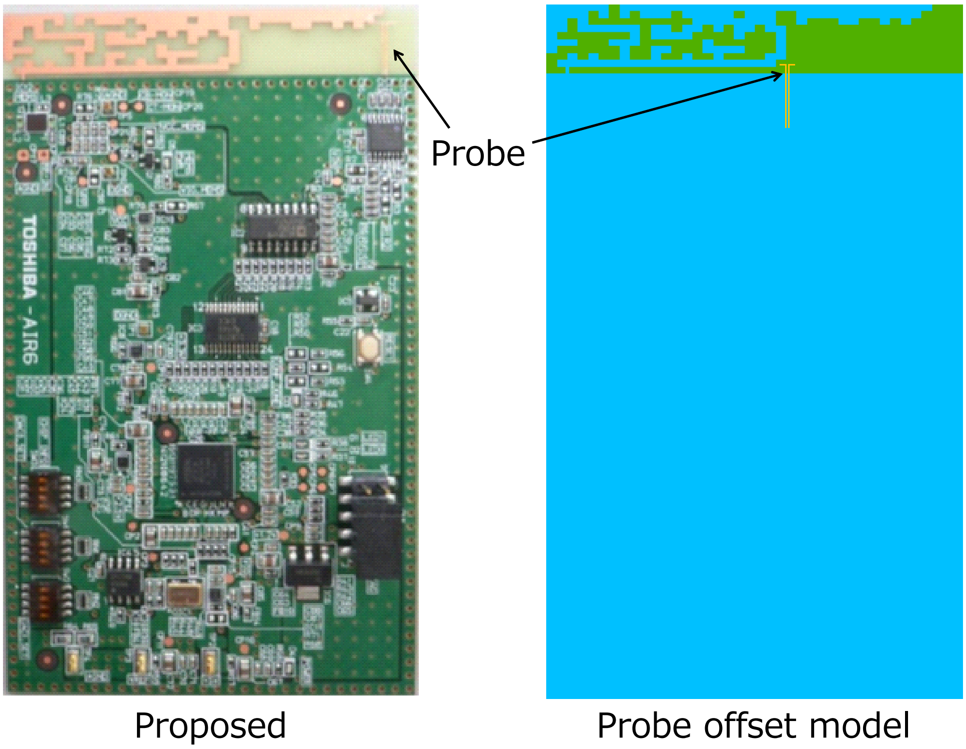

Figure 4.15: Probe-offset model

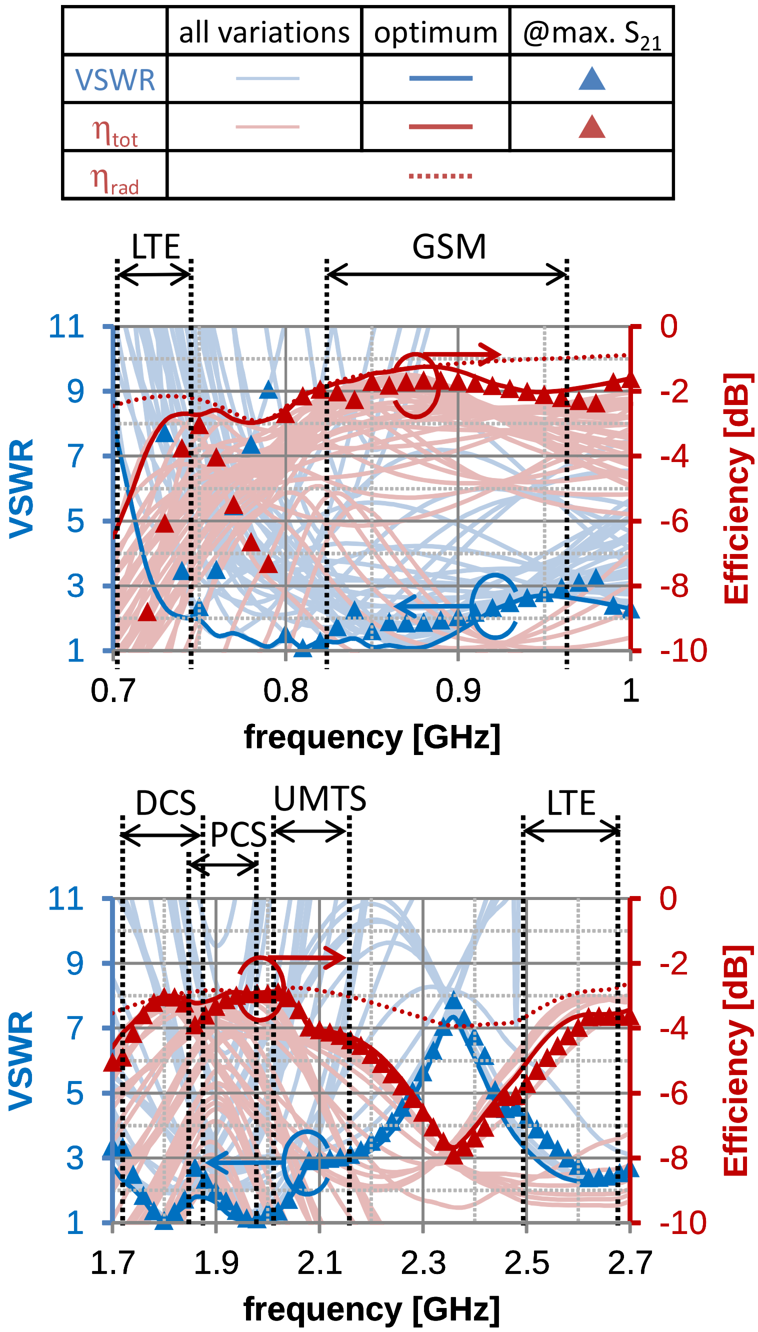

Figure 4.16: Calculated result of the probe-offset model shown in Fig. 4.15

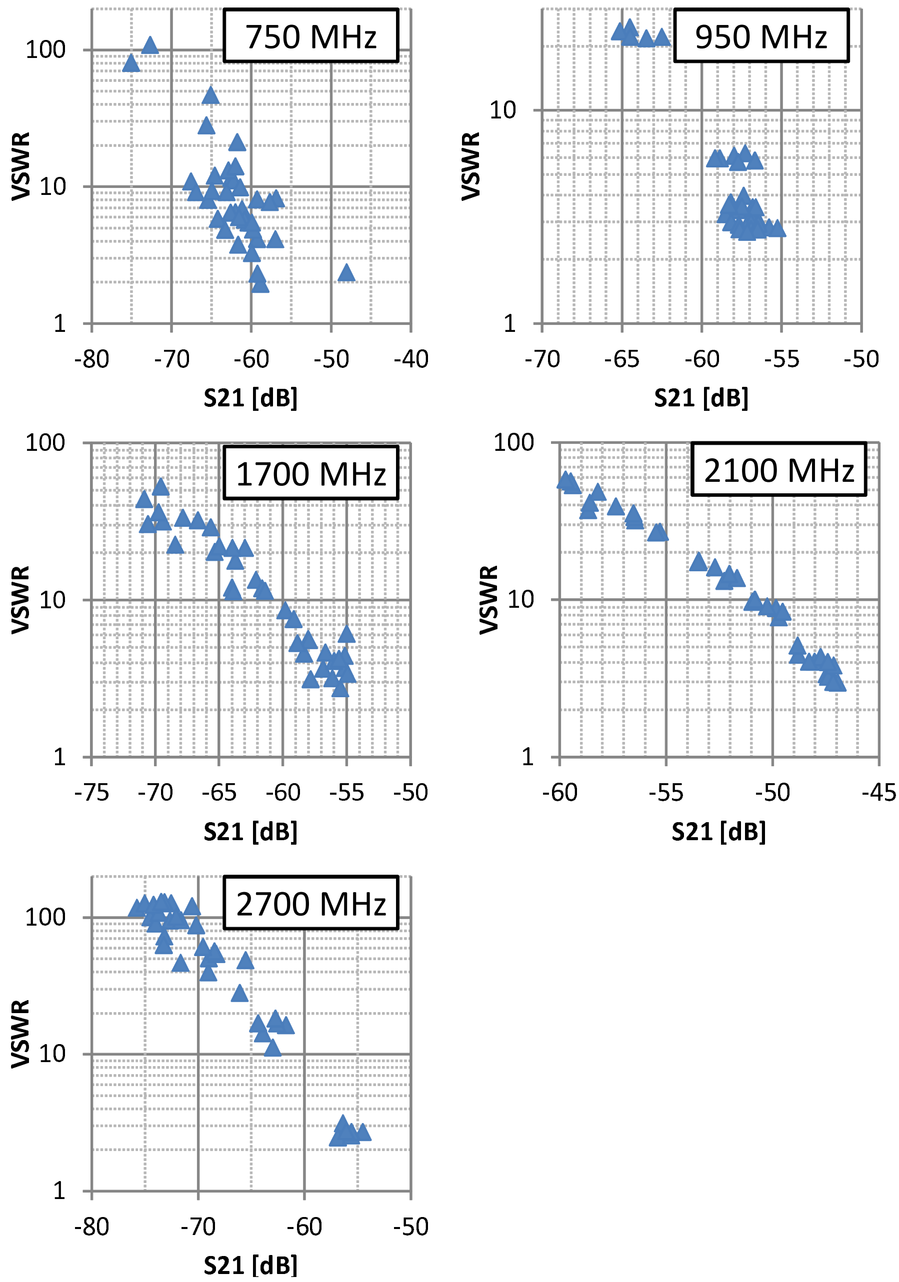

Figure 4.17: Correlation between S_{21} and VSWR of the probe-offset model shown in Fig. 4.15

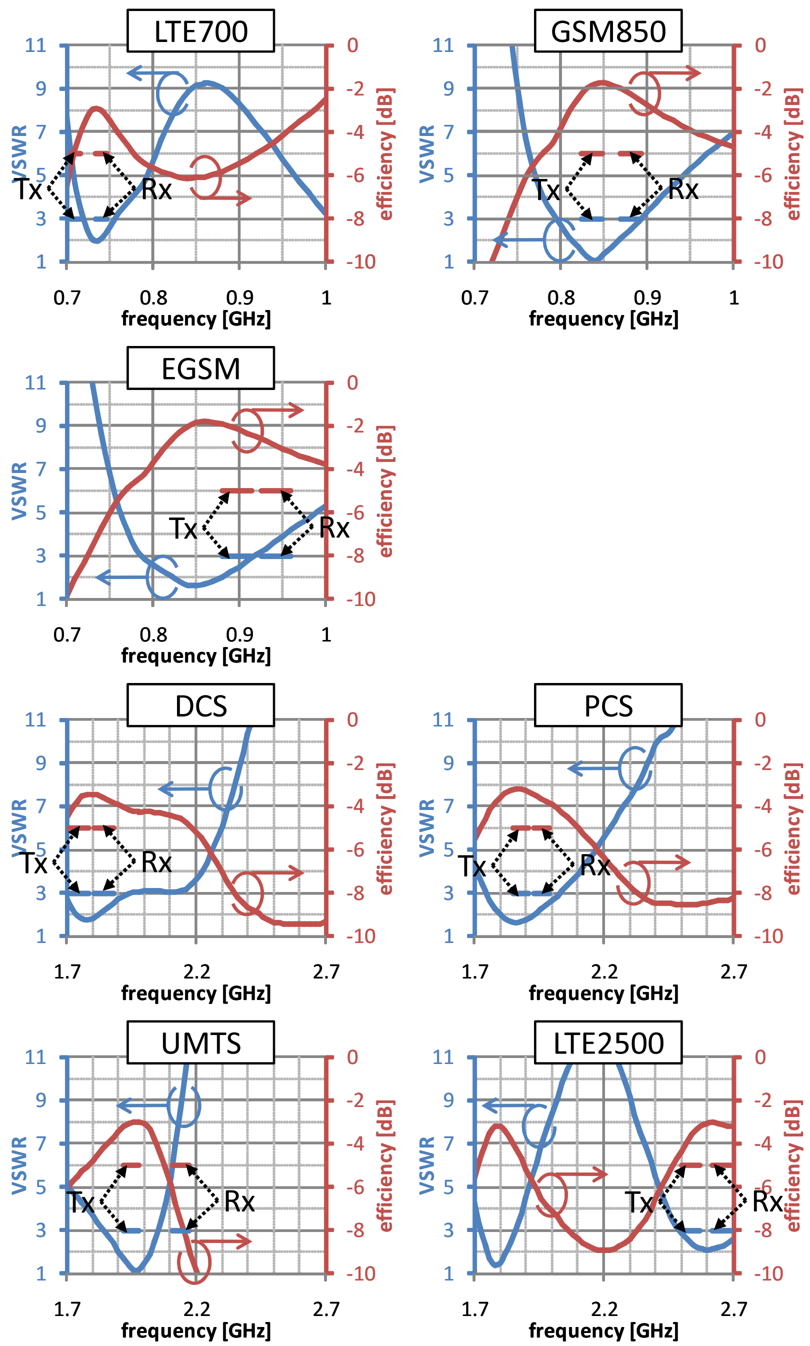

Figure 4.18: Tunability for each wireless communication system

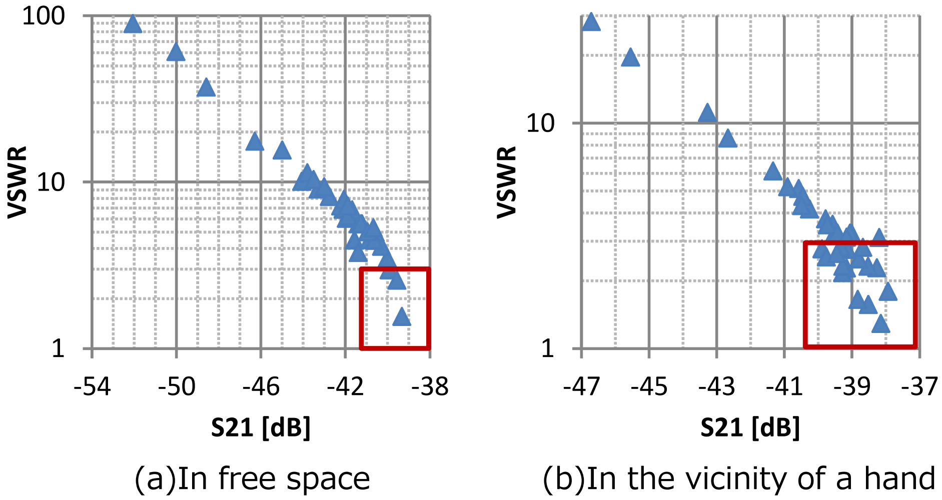

Figure 4.19: The matching state of the proposed antenna in free space and in the vicinity of a hand shown in Fig. 4.6

Chapter 5

Steerable antenna design for MIMO system

5.1 Introductory remarks

For maintaining and raising channel capacity or connection probability in wireless communications, we have proposed a low-cost, simple directivity-switching antenna. The antenna consists of two-branch diversity antenna and a parasitic element between the branches connected to a ground through a switch. The shape is optimized with genetic algorithm to obtain a high efficiency, well-matched and low correlation antenna. A characteristic mode analysis reveals that depends on the change of the power distribution to each mode. The channel capacity calculated with Rayleigh distribution of the proposed antenna is higher than that of lossless two dipoles with a probability of 65 percent.

As cellular phone system, wireless LAN, Bluetooth, etc. are gaining in popularity, many amount and kinds of wireless devices are connected to those wireless systems these days. Hereafter, it is estimated that the number explosively keeps increasing with the penetrating of IoT: Internet of Things and M2M: Machine-to-Machine. How to accomplish this scenario is up to the maintenance or enhancement of connection probability and channel capacity of each terminal. On the other hand, enormous number of terminals are required to be simple and low-cost at the same time. Therefore, the authors are thinking of apply an antenna array with steerable elements for each to intermediate concentrators to solve this problem.

Steerable antennas [34–36] or diversity antennas [48–52] have been studied and taken advantage of as one of the technologies to improve connection probability, and MIMO to enhance channel capacity in the past, respectively. Our exploration, however, the study of the combination of these has been stayed within the simple arrangement of conventional steerable antennas as an array for MIMO system. [60] combine sector-beam antennas with MIMO, for example. Thus, conventional studies have focused on propagation channel and channel capacity rather than antennas themselves. Then this study emphasize on the downsizing of the antenna array to be incorporated in a few-centimeter small-sized terminal, the two-branch composition with a single switch to change the directivity simultaneously for the simplicity, and the confirmation of the advantage over the conventional MIMO without steerability for each branch.

ESPAR (Electrically Steerable Passive Array Radiator) antenna is well-known as a conventional study of the simple and low-cost antenna to realize steerability [34,35]. By the appropriate control of the rotation-symmetrically arranged parasitic elements, the directivity of beam and null is changed toward required directions and also the input impedance can keep matching in a certain operation bandwidth [36]. However, an ESPAR antenna occupies the space in the order of the wavelength for the operation frequency. Therefore, it must be difficult to install that in such as a smartphone which is small and operates microwaves, and it is supposed for ESPAR antennas to be used in higher frequency like millimeter wave, or considerably large apparatus such as, base stations, intermediate repeaters, and gap-fillers.

There are also various diversity antennas [48–51], which are suitable for small terminals, improve the communication performance within a simple and low-cost mounting. Especially, there are some remarkable studies: polarization diversity for MIMO to obtain low correlation even in a small terminal [48, 49], including estimation of the channel capacity with the consideration of propagation channel models [50, 51].

Moreover, following the recent paper theoretically deriving the equivalence between S-parameters and correlation of directivity [61], the decoupling circuits between antenna branches are actively studied [62–64]. However, decoupling circuits include transmission lines with a certain length in the order of wavelength or a considerably large inductance, and their actual size will be comparable with an antenna. Therefore the application of decoupling circuits to small terminals is supposed to be difficult for now. Then in this paper, a two-branch directivity-switching antenna using a single switch for 2.4 GHz band, which has a size of a quarter wavelength on a size and is simple and low cost, has been proposed.

The contents of this chapter is as below. From the concept to the actual design of the proposed directivity-switching antenna are described in sec-

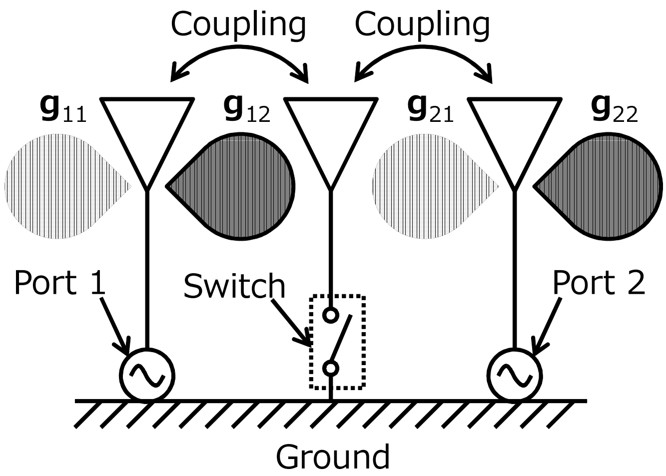

Figure 5.1: Conceptual model of the proposed directivity-switching antenna

tion 2. Section 3 shows the fundamental characteristics and the remarkable features seen from them. Further constructive analysis would be discussed in the next chapter.

5.2 Proposed directivity-switching antenna

Figure 5.1 shows the schematic showing the concept of the directivity-switching antenna proposed in this chapter. There is a common finite ground plane, two branches of antenna elements excited on the ground plane at port 1 and port 2, and a parasitic element between the two antennas connected to the ground via switch.

Both two antennas are supposed to be capacitively connected with the parasitic element, therefore also to be changed the current distributions and the directivity by the state of the switch. The vector $\boldsymbol{g}_{ij}$ denotes the gain distribution when the port i ($i = 1, 2$) is excited and the state of the switch j (j = 1:open and j = 2:short), where $\boldsymbol{g}_{ij}$ is a vector consists of the gain corresponding to electric fields E_θ and E_ϕ radiating toward (θ, ϕ) discretized over all solid angle Ω on a spherical coordinate system.

$$
\begin{aligned}
\boldsymbol{g}_{ij} \;=\; & \left[g_{ij}^{\theta}\left(\frac{\pi}{m}, \frac{2\pi}{n}\right), g_{ij}^{\theta}\left(\frac{\pi}{m}, \frac{4\pi}{n}\right), \cdots, g_{ij}^{\theta}\left(\frac{\pi}{m}, 2\pi\right), \right. \\
& g_{ij}^{\theta}\left(\frac{2\pi}{m}, \frac{2\pi}{n}\right), g_{ij}^{\theta}\left(\frac{2\pi}{m}, \frac{4\pi}{n}\right), \cdots, g_{ij}^{\theta}\left(\frac{2\pi}{m}, 2\pi\right), \\
& \cdots \\
& g_{ij}^{\theta}\left(\pi, \frac{2\pi}{n}\right), g_{ij}^{\theta}\left(\pi, \frac{4\pi}{n}\right), \cdots, g_{ij}^{\theta}(\pi, 2\pi), \\
& g_{ij}^{\phi}\left(\frac{\pi}{m}, \frac{2\pi}{n}\right), g_{ij}^{\phi}\left(\frac{\pi}{m}, \frac{4\pi}{n}\right), \cdots, g_{ij}^{\phi}\left(\frac{\pi}{m}, 2\pi\right), \\
& g_{ij}^{\phi}\left(\frac{2\pi}{m}, \frac{2\pi}{n}\right), g_{ij}^{\phi}\left(\frac{2\pi}{m}, \frac{4\pi}{n}\right), \cdots, g_{ij}^{\phi}\left(\frac{2\pi}{m}, 2\pi\right), \\
& \cdots \\
& \left. g_{ij}^{\phi}\left(\pi, \frac{2\pi}{n}\right), g_{ij}^{\phi}\left(\pi, \frac{4\pi}{n}\right), \cdots, g_{ij}^{\phi}(\pi, 2\pi), \right]^{T}, \qquad (5.1)
\end{aligned}
$$

where $g_{ij}^{\theta}(\theta, \phi)$ and $g_{ij}^{\phi}(\theta, \phi)$ are the gains corresponding to the electric field radiating toward (θ, ϕ) on a spherical coordinate (θ, ϕ) when the port i is excited and the state of the switch is j, respectively. All the combinations of the two ports and the two states of the switch makes totally four kinds of gain distributions $\boldsymbol{g}_{ij}$ ($i = 1, 2$ and $j = 1, 2$). So for them, if the switch is set to the state which gives higher signal-to-noise ratio or channel capacity, the combined antenna system of the conventional directivity diversity and array antenna for MIMO is realized. Hence, in a actual propagation environment, defining the vector of incoming wave distribution $\boldsymbol{p}$ which has the components toward the same directions as $\boldsymbol{g}_{ij}$, the received signal

$$
\oint_{\Omega} \mathrm{d}\Omega \; \boldsymbol{g}_{ij}^{H} \boldsymbol{p} \sin\theta \qquad (5.2)
$$

is supposed to change in various ways. Where $*^{H}$ denotes the Hermitian transpose. The following actually designed proposed antenna would be confirmed whether it can increase the channel capacity by the switching by simulations in the next chapter.

Figure 5.2 illustrates the raw structure of the proposed antenna. The coordinate shown at the lower left in the figure indicates the width along X axis, the length along Y axis, and the height along Z axis. The left figure is the whole structure and the right one shows the only antenna part to be designed. A rectangular finite ground plane has the width of 28 mm $\times$ the length of 30 mm. Port 1 and port 2 assumed to excite two antennas with the characteristic impedance of 50 Ω are on the two corners adjacent each other on the ground plane. There is a switch just midpoint between the port 1 and port 2 connecting between the midpoint on a edge of the ground plane and antenna design region. The ports and the switch are modeled with wires with the radius of 0.1 mm. A surface of a cuboid with the width of 28 mm $\times$ the length of 8 mm $\times$ the height of 10 mm as an antenna design region which is spaced at a distance of 2 mm from the ground plane. The parts of this 2-mm gap between the cuboid and the ground plane apart from the wires by 2 mm are also used as a part of the antenna design region. The whole structure is a conductor with the conductivity of 5.8×10^7 S/m. The antenna design region consists of the pieces of the squared patches with the area of 2 mm $\times$ 2 mm, and the shape of antenna, or the combination of the patches can be optimized by mapping them to the chromosomes in genetic algorithm.

In addition, if there is much space for the design, although two antennas usually designed with the constraint of symmetry in order to obtain the same performance of each antenna, at this time the space is small and both antennas are connected to the common ground plane in the near point each other. Therefore no limitation of the symmetry are applied in order to suppress the coupling and to diversify the directivity for low correlation between two antennas. As shown in the next section, actually the antenna has an asymmetric design.

Although the antennas for MIMO without steerability can be downsized as mentioned in chapter 1, this study focus on the confirmation of the advantage of the MIMO system with steerable antennas. As the result of feasibility study of the size, it is found that the antenna requires the size shown in Fig. 5.2 to keep the input impedance matching and low correlation of directivity for the change of the state of the switch. The study of downsizing the antennas for MIMO with steerable antennas is a future work. Additionally the mesh size of the antenna design area is set to 2 mm because it is small enough and less than a sixtieth of a wavelength at the lowest frequency 2.4 GHz in the operational bandwidth, and in the light of the trade-off between the degree of freedom in the shape of the antenna and the computation time.

At this moment of this raw structure shown in Fig. 5.2, the boundary between each antenna directly connected to port1 and another to port 2 and between each of them and a parasitic element are not determined, and the freedom of the design especially in the connection relation remains. The total size of the proposed antenna system, the width of 28 mm $\times$ the length

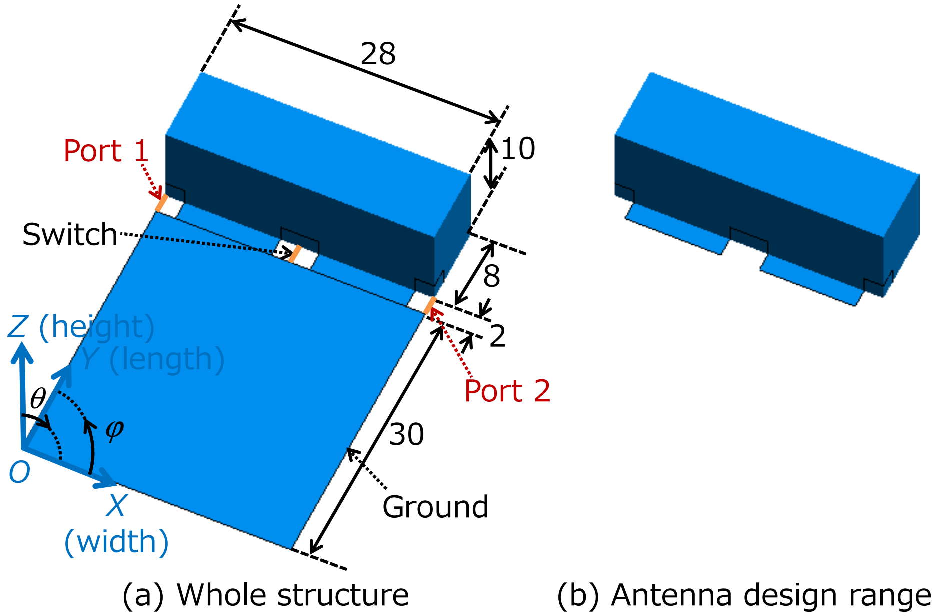

Figure 5.2: Raw structure of the proposed antenna (Dimensions unit: mm)

of 40 mm × the height of 10 mm, corresponding to $0.224\lambda \times 0.32\lambda \times 0.08\lambda$ where λ is the wavelength at the lowest frequency 2.4 GHz in the operational bandwidth, is fairly small and suitable to be mounted in a small terminal. It had been found to be difficult for the antenna to lower the correlation of directivity with the height of less than 10 mm in the preliminary study with genetic algorithm. It is supposed that this is because the longest dimension of the total size of the antenna including the ground plane is about a quarter wavelength, and the different polarization along Z axis is expected to obtain lower correlation of directivity with the height of 10 mm.

The cost function to evaluate and optimize the antenna should include the degree of impedance matching, e.g. $|S_1 1|$ or VSWR when each port is excited, the radiation efficiency as well, the correlation of directivity between the states of the switch at each port and between two ports at each state of the switch. As is the case in the gain $\boldsymbol{g}_{ij}$, T_{ij}, Γ_{ij}, η^r_{ij} and η^t_{ij} are the power transmission coefficient, reflection coefficient, radiation efficiency and total efficiency when the port i ($i = 1, 2$) is excited and the state of the switch is open ($j = 1$) or short ($j = 2$), respectively, where the total efficiency defined in [69]:

$$\eta^t_{ij} = T_{ij}\eta^r_{ij} = (1 - |\Gamma_{ij}|^2)\eta^r_{ij} \tag{5.3}$$

is the antenna efficiency including the loss by mismatch. For the balanced optimization and without biased improvement, the cost function is

$$\begin{aligned} f = & \prod_{\substack{i=1,2\\j=1,2}} BF(T_{ij}, a_T, t_T) BF(\eta^r_{ij}, a_\eta, t_\eta) \\ \times \quad & BF\left[\prod_{i=1,2}\left\{1 - \left\| \oint_\Omega \mathrm{d}\Omega\ \hat{\boldsymbol{g}}^H_{i1}\hat{\boldsymbol{g}}_{i2}\sin\theta \right\|^2\right\}\right. \\ & \left.\prod_{j=1,2}\left\{1 - \left\| \oint_\Omega \mathrm{d}\Omega\ \hat{\boldsymbol{g}}^H_{1j}\hat{\boldsymbol{g}}_{2j}\sin\theta \right\|^2\right\}, a_c, t_c\right], \end{aligned} \tag{5.4}$$

where BF is a barrier function to avoid the biased optimization and is defined as

$$BF(x, a, t) = \min\left(\frac{2\arctan a(x - t)}{\pi} + 1, 1\right). \tag{5.5}$$

Figure 5.3 shows some examples of barrier functions with various parameters. Apparently every function sharply drops at a target parameter t, and also is equal where x is greater than t.

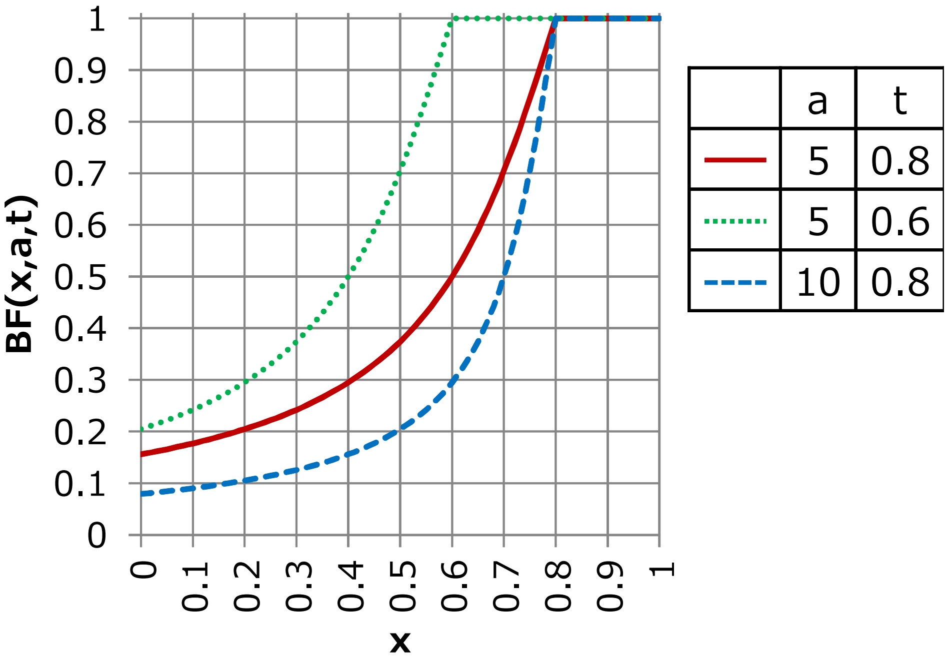

Figure 5.3: Examples of barrier functions with various parameters

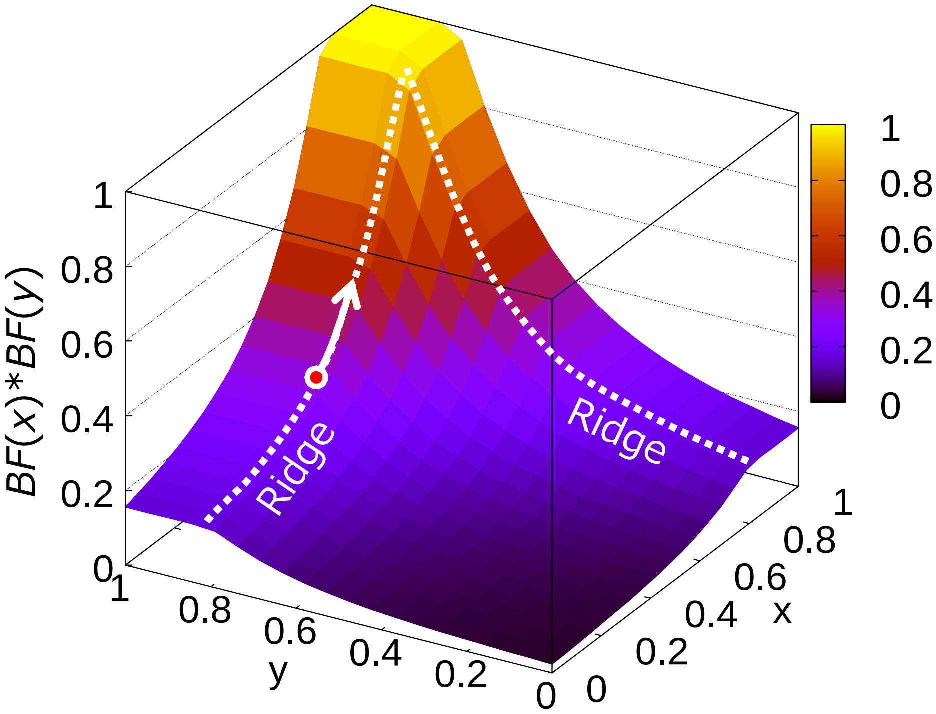

Figure 5.4: Product of two barrier functions

Figure 5.4 shows the product of two barrier functions. The surface has two ridgelines along a target value, $t = 0.8$ in this case, which keeps satisfied objective value and promote another in a multi-objective optimization.

The value of this function is 1 when x is greater than or equal to the target value t, and sharply decrease in the domain where x is slightly less than t, and the steepness is proportional to a. In the actual optimization, $a_T = a_\eta = a_c = 10$, $t_T = 0.75$ corresponding to the VSWR of 3, $t_\eta = 0.8$ aiming at the total efficiency of 0.6 ($= 0.75 \times 0.8$), and $t_c = 0.0625 = 0.5^4$ aiming at all the four correlation of directivity of 0.5.

The value of the first product $\prod$ in the cost function (5.4) becomes larger as the four power transmission coefficients T_{ij} and the four radiation efficiencies η^r_{ij} increases. The value of the second and third product increase and approach to 1 as the correlation of directivity decreases and decrease and approach to 0 as the correlation of directivity increases. The second product is the evaluation of the correlation of directivity between the state of the switch at each port, and the third product is the one between the ports at each state of the switch. Every evaluation term mentioned above is in each barrier function and each barrier function expressed in the product, then the optimization always proceed to Pareto optimal region. In addition, even if just one characteristic deteriorates, the cost function rapidly drops owing to barrier functions, and on the contrary there is no order of merit between the characteristics over the target. For those reasons, a balanced optimization with the degree of freedom can be expected. This cost function f is calculated at 2.4 GHz and 2.5 GHz and the worse value is set to a individual evaluation in GA. Besides, note that since gain includes radiation efficiency, in order to avoid doubling that, gain is normalized as $\hat{\boldsymbol{g}} = \boldsymbol{g}/|\boldsymbol{g}|$.

5.3 Calculated results

Figure 5.6 shows the VSWRs and total efficiencies of the proposed antenna shown in Fig. 5.5. As mentioned in the explanation of cost function in the previous section, total efficiency is the product of power transmission and radiation efficiency. The figure in the upper and lower row is the results when the port 1 is excited and when the port 2 is excited, respectively. In each figure, broken lines and solid lines indicate the results when the switch is open ($j = 1$) and short ($j = 2$), respectively. VSWR of blue lines and the total efficiency of red lines refer the left and right axis, respectively. The VSWR is around 3 and the total efficiency is around 0.6, or 60% within the operation bandwidth from 2.4 GHz to 2.5 GHz. Judging from the curves when the switch is short indicated with solid lines, the antenna seems to match around the center frequency of a single resonance. On the contrary, the curves when the switch is open indicated with broken lines implicit that the antenna is in the intermediate state of a double resonance. This thing is reconfirmed in the next chapter.

Figure 5.7 shows the current distribution and gain patterns of the proposed antenna at 2.45 GHz when the port 1 is excited and the switch is open ($j = 1$). The left, center and right figures show the current distributions, the gain with the electric field of E_θ component, and the gain with the electric field of E_ϕ component, respectively. The viewpoints of all perspective figures are the same. The intensity of the current and gain are indicated on the top row with color bars. Note, however, that since the moment method which deal with incident voltages as a boundary condition was used, the absolute value of currents depending on the input impedance of an antenna is not important, and the distribution showing relative intensity are taken notice.

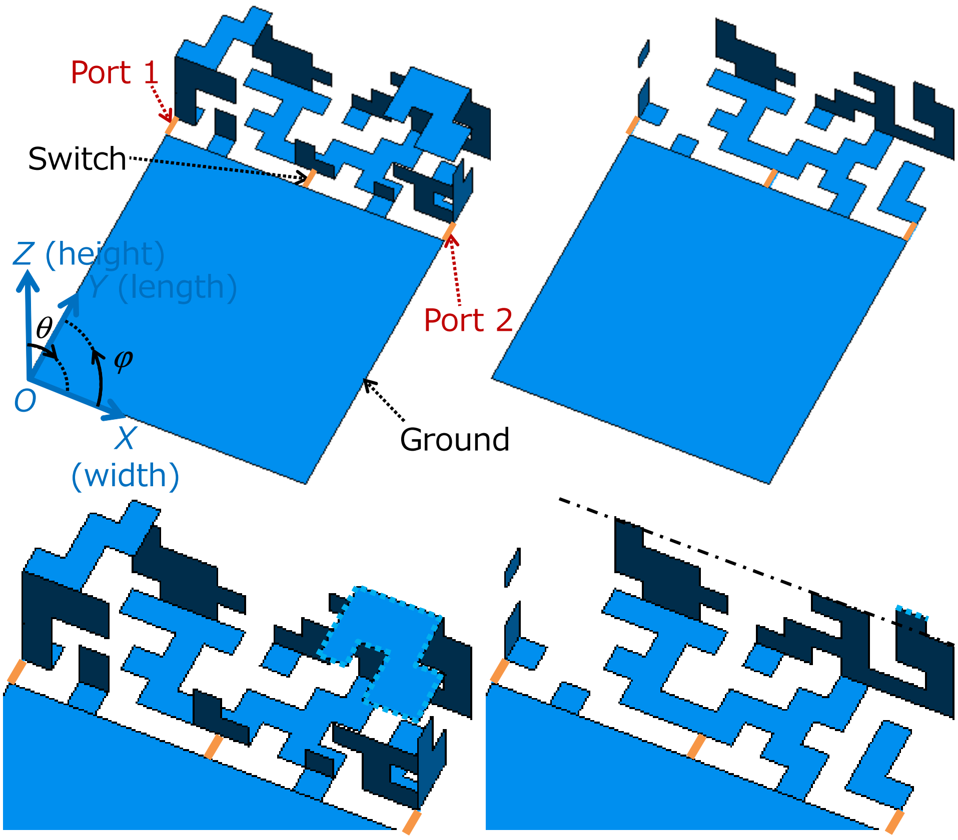

Figure 5.5: The proposed antenna optimized with genetic algorithm (Dimension unit: mm. The front faces are invisible in the right figure to see the back faces. Lower two figures are extended ones for the antenna.)

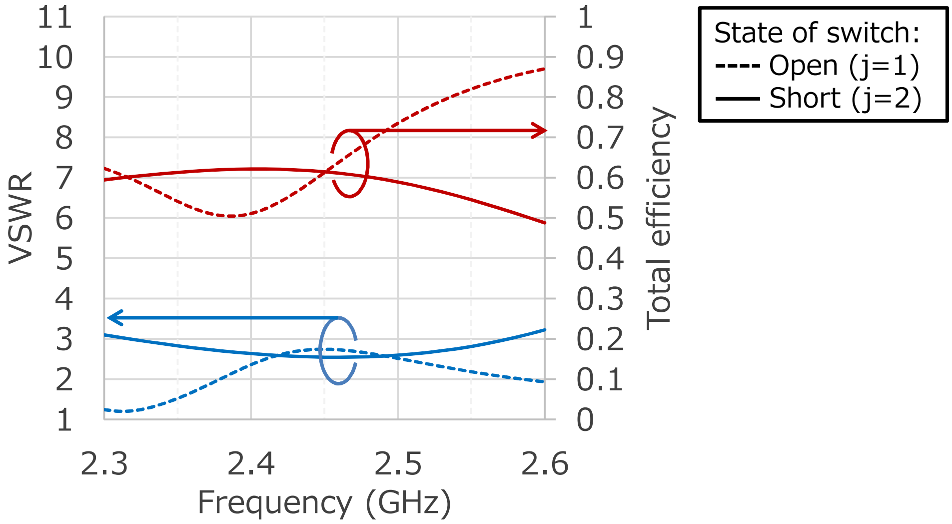

(a) Port 1 excitation

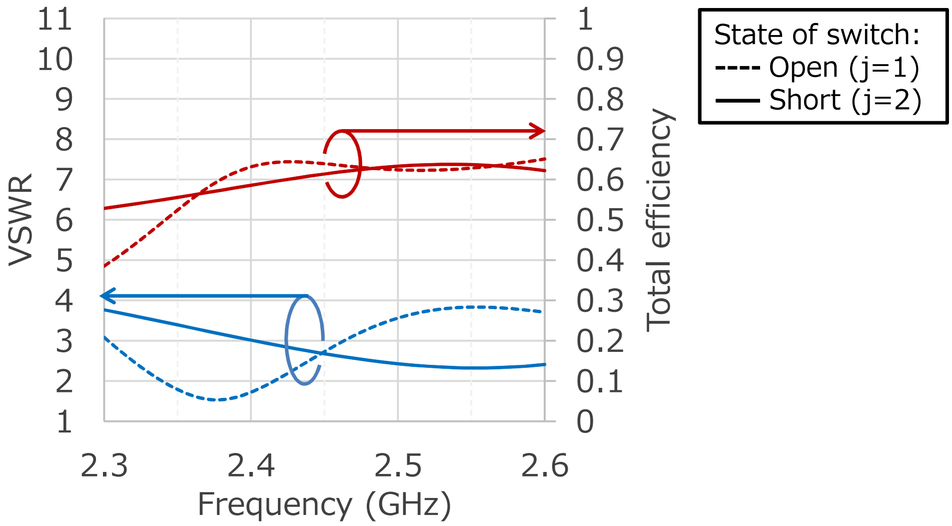

(b) Port 2 excitation

Figure 5.6: The VSWRs and total efficiencies of the proposed antenna shown in Fig. 5.5

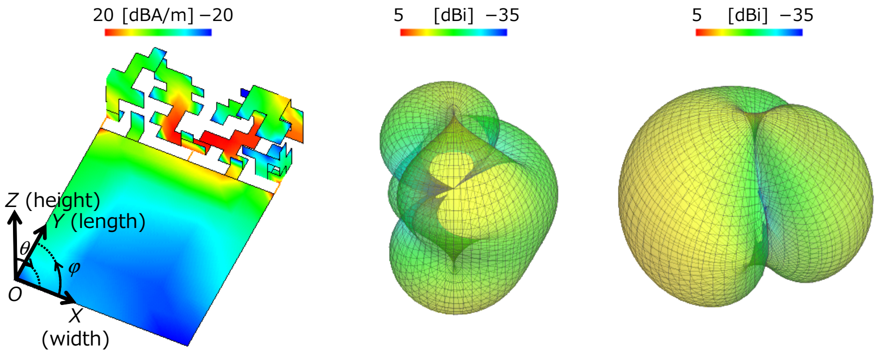

Figure 5.7: The current distribution and gain patterns of the proposed antenna at 2.45 GHz when the port 1 is excited and the switch is open ($j = 1$)

Therefore the dynamic range is fixed 40 dB here and hereafter. Similar to Fig. 5.7, the antenna characteristics when the switch is short ($j = 2$) are shown in Fig. 5.8. Comparing Fig. 5.8 with Fig. 5.7, the gain with the electric field of E_θ toward the direction parallel to the ground plane increases, and this is supposed to be caused by the current on the part perpendicular to the ground plane. Also the gain with the electric field of E_ϕ is rotated a little around Z axis, and also the directions of the main radiation are different toward left and right on the paper. This is supposed to be caused by the current on the edge of the ground plane near the antenna.

Similar to Fig. 5.7 and Fig. 5.8, Fig. 5.9 and Fig. 5.10 shows the current distribution (left) and gain patterns (center, right) of the proposed antenna at 2.45 GHz when the port 2 is excited and the switch is open ($j = 1$) and short ($j = 2$), respectively. The way to see these figures are identical with Fig. 5.7 and Fig. 5.8. The figures show both the current and gain distributions are similar to them when the port 1 is excited. However, the change of the gain distribution for the state of the switch seems to be less than that when the port 1 is excited. In order to quantitatively evaluate this actually, the correlation of directivity is calculated as shown in Table 5.1. The correlation of directivity between ports– $\boldsymbol{g}_{1j}$ and $\boldsymbol{g}_{2j}$–, is greater than the one between the state of the switch– $\boldsymbol{g}_{i1}$ and $\boldsymbol{g}_{i2}$. The correlations of directivity influencing the effectiveness of diversity are the one between $\boldsymbol{g}_{11} - \boldsymbol{g}_{21}$ of 0.11 and the one between $\boldsymbol{g}_{12} - \boldsymbol{g}_{22}$ of 0.07. On the other hand, the correlations of directivity the state of the switch are 0.5 and 0.83 at port 1 and 2, respectively, and the switch changes the both

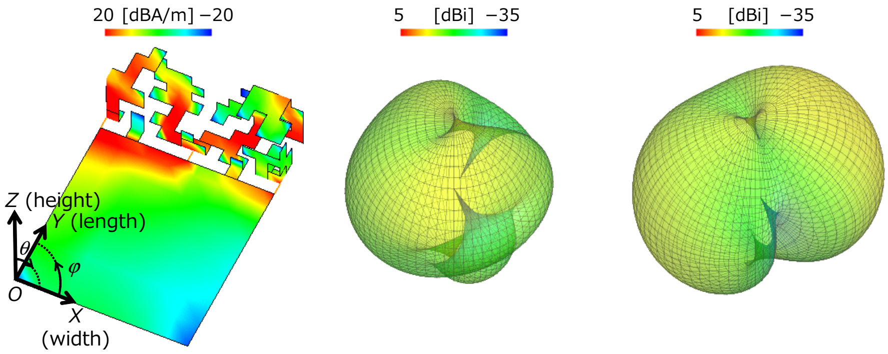

Figure 5.8: The current distribution and gain patterns of the proposed antenna at 2.45 GHz when the port 1 is excited and the switch is short ($j = 2$)

Table 5.1: The correlation of directivity of the proposed antenna

	$\boldsymbol{g}_{11}$	$\boldsymbol{g}_{12}$	$\boldsymbol{g}_{21}$	$\boldsymbol{g}_{22}$
$\boldsymbol{g}_{11}$	1.00	0.50	0.11	—
$\boldsymbol{g}_{12}$		1.00	—	0.07
$\boldsymbol{g}_{21}$			1.00	0.83
$\boldsymbol{g}_{22}$				1.00

directivity to some extent, at port 2, however, seems to be not enough. Then the enhancement of the effectiveness of diversity with switching remains. Therefore, the improvement of MIMO channel capacity is verified in the next chapter.

5.4 Summary

Compact two-branch directivity-switching antenna using a single switch for 2.4 GHz band has been proposed. The raw structure shown in Fig. 5.2 as an embodiment of the concept model shown in Fig. 5.1 was optimized to obtain the matching, high-efficiency, low correlation among 4 set of directivity, for both 2 ports, at both states of the switch. In order to accomplish this, an appropriate cost-function including barrier functions and those characteristics as their terms has been applied. Successfully VSWR is around 3 and total efficiency is around 60 percent at every situation, and also low

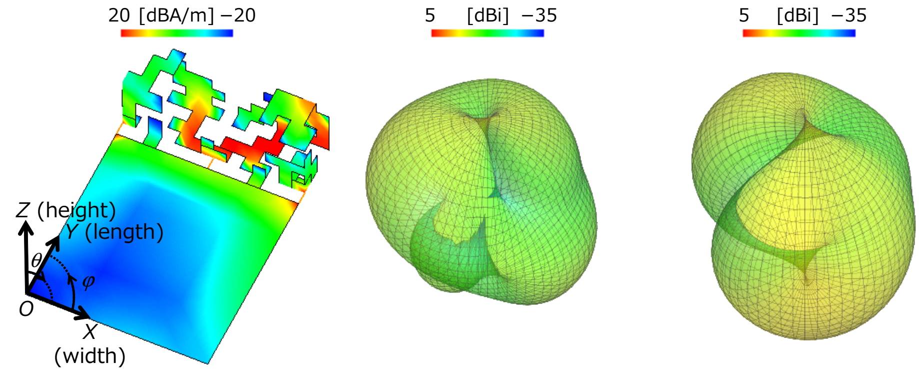

Figure 5.9: The current distribution and gain patterns of the proposed antenna at 2.45 GHz when the port 2 is excited and the switch is open ($j = 1$)

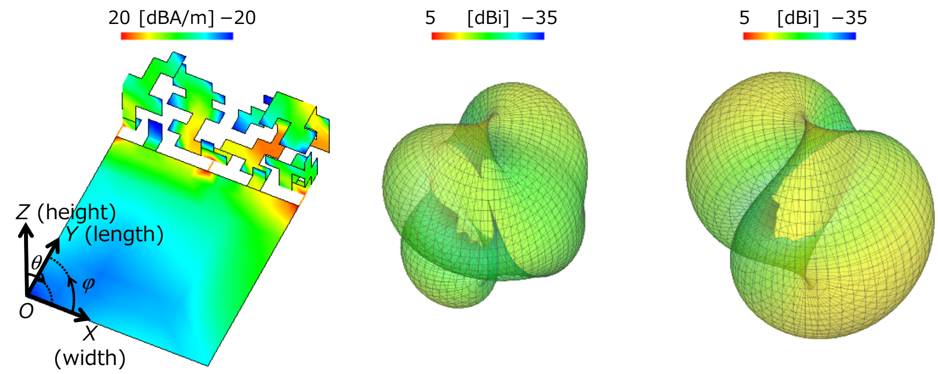

Figure 5.10: The current distribution and gain patterns of the proposed antenna at 2.45 GHz when the port 2 is excited and the switch is short ($j = 2$)

correlations of directivity are also obtained. At least, it is supposed that the less-than-one correlation between the state of the switch improves the communication performance.

Chapter 6

Advantage and mechanism of steerability

6.1 Introductory remarks

In the previous chapter, successfully two-branch directivity-switching antenna using a single switch for 2.4 GHz band has been designed, and the less-than-one correlation between the state of the switch seems to improve the communication performance, at least, however the quantitative evaluation has not been confirmed. Before that, since the antenna has been designed based on genetic algorithm, the shape is too complicated as shown in Fig. 5.5 to understand the operating principle. Therefore, in this chapter, by applying the characteristic mode analsis [68] to the proposed antenna, the mechanism is attempted to clarify.

6.2 Analysis of operational mechanism

Figure 6.1 shows some current distributions and directivity of modes when the switch is open. Although the current distributions on the antenna element appear complicated, judging from the series of corresponding directivity, the mode 1 is the electric dipole along Y-axis (or length dimension), the mode 2 is the electric dipole along X-axis (or width dimension), the mode 3 is the magnetic dipole along Z-axis (or height direction), and the mode 4 is the magnetic dipole along Z-axis (or height direction), respectively. These concise properties are graspable from the directivity but not from the current distribution. On the other hand, focusing only on the current distribution on the ground plate, those are alike their corresponding dipole's current, then the unrelated currents for example the current near the antenna on the ground plane along X-axis (or width direction) in the mode 1 is almost canceled out with the current on the antenna element. However, unfortunately the every mode hardly resembles the current distribution and directivity when the state of the switch is open and each port is actually excited shown in Fig. 5.7 and Fig. 5.9, the actual operation is difficult to be explained with a specific mode.

Therefore, by projecting the current distribution $\boldsymbol{J}$ when each port is excited onto the mode current distributions $\boldsymbol{J}_n$ $(n = 1, 2, 3, \cdots)$, the power distribution ratio of modes were calculated. Figure 6.2 shows the cumulative power distribution by mode current when each port is excited and the switch is open. The curves show the cumulative line chart from mode 1 to 4, and both when port 1 is excited and when port 2 is excited, the mode 4 accounts for grater rate than other mode 1 to 3. The reason why the correlation of directivity between ports regardless of the slight change in the power ratio of modes is thought to be the phase difference for incoming waves by the displacement of the port, i.e. space diversity effect. In addition, although the dominant mode could not be found from their appearance of the current distributions and directivity and actually the sum of these 4 modes reaches into 50 to 60 percent, computationally the mode 4 occupies near the half of the total radiated power.

Next, the current distribution and radiation pattern of four modes when the switch is short are shown in Fig. 6.3. The figure shows that although the current distributions are slightly different from the ones when the state of the switch is open shown in Fig. 6.1, the series of directivity are almost the same. Especially, the current near the antenna on the ground flows straight from one corner to another when when the state of the switch is open, on the other hand, it is interrupted at the center when the state of the switch is short. Therefore the reason why the similar directivity is formed regardless of that is the current on the antenna especially the component along x-axis (or width direction) is supposed to contribute.

Next, the cumulative power distribution by mode current when each port is excited and the switch is short are shown in Fig. 6.4. Similar to those when the state of the switch is open shown in Fig. 6.2, there is no large difference in the power distribution ratio of modes between ports. Therefore it is supposed that the spatial correlation mainly contributes to the correlation of directivity between ports. On the other hand, comparing Fig. 6.2 and Fig. 6.4, apparently the power distribution ratio of modes changes between them, and it is found that the coupled mode at each port is changed by the state of the switch. That is, the operation principle on the

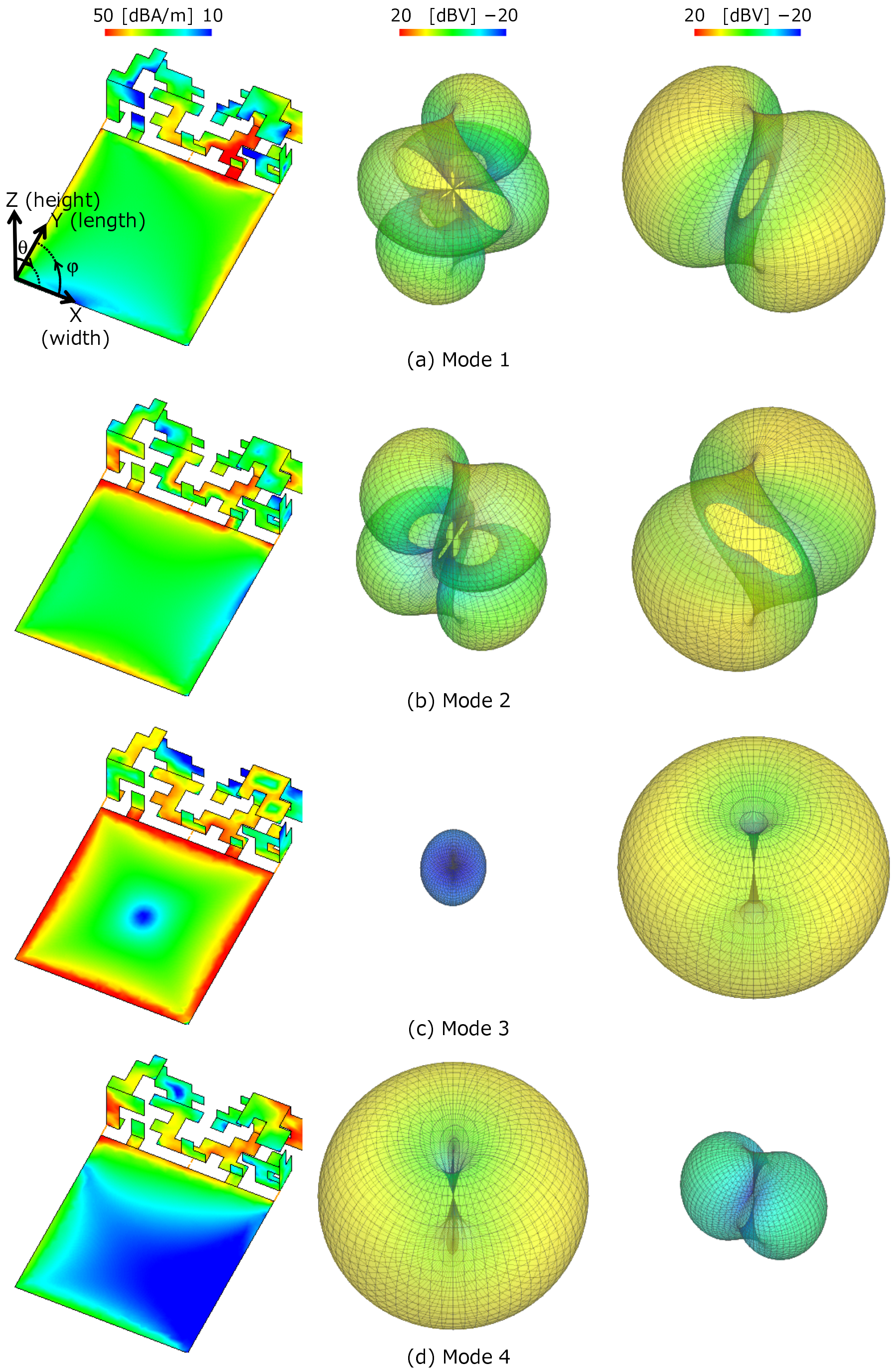

Figure 6.1: The current distribution and radiation pattern of four modes when the switch is open

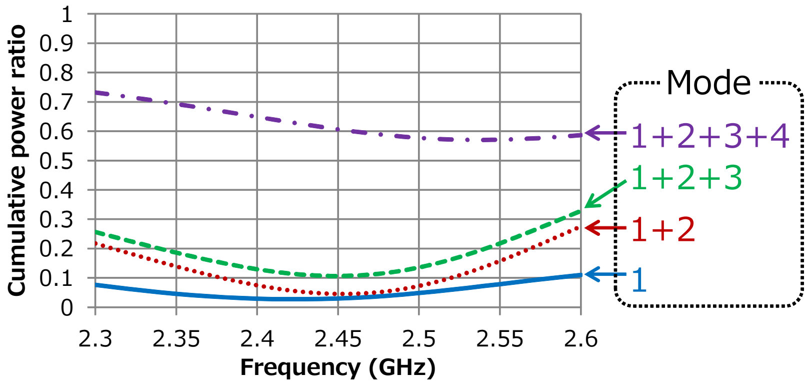

(a) Port 1 excitation

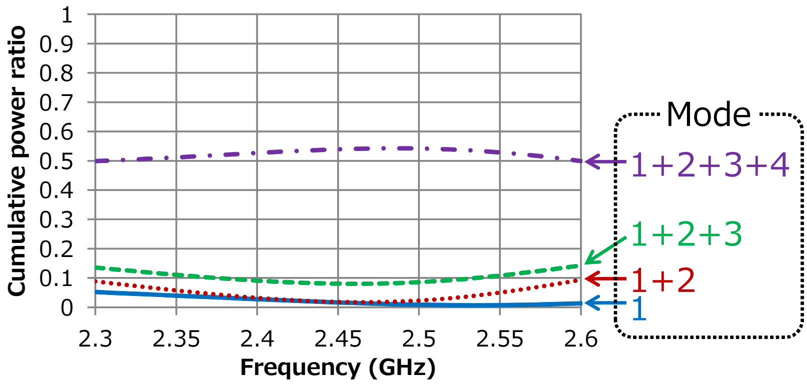

(b) Port 2 excitation

Figure 6.2: The cumulative power distribution by mode current when each port is excited and the switch is open

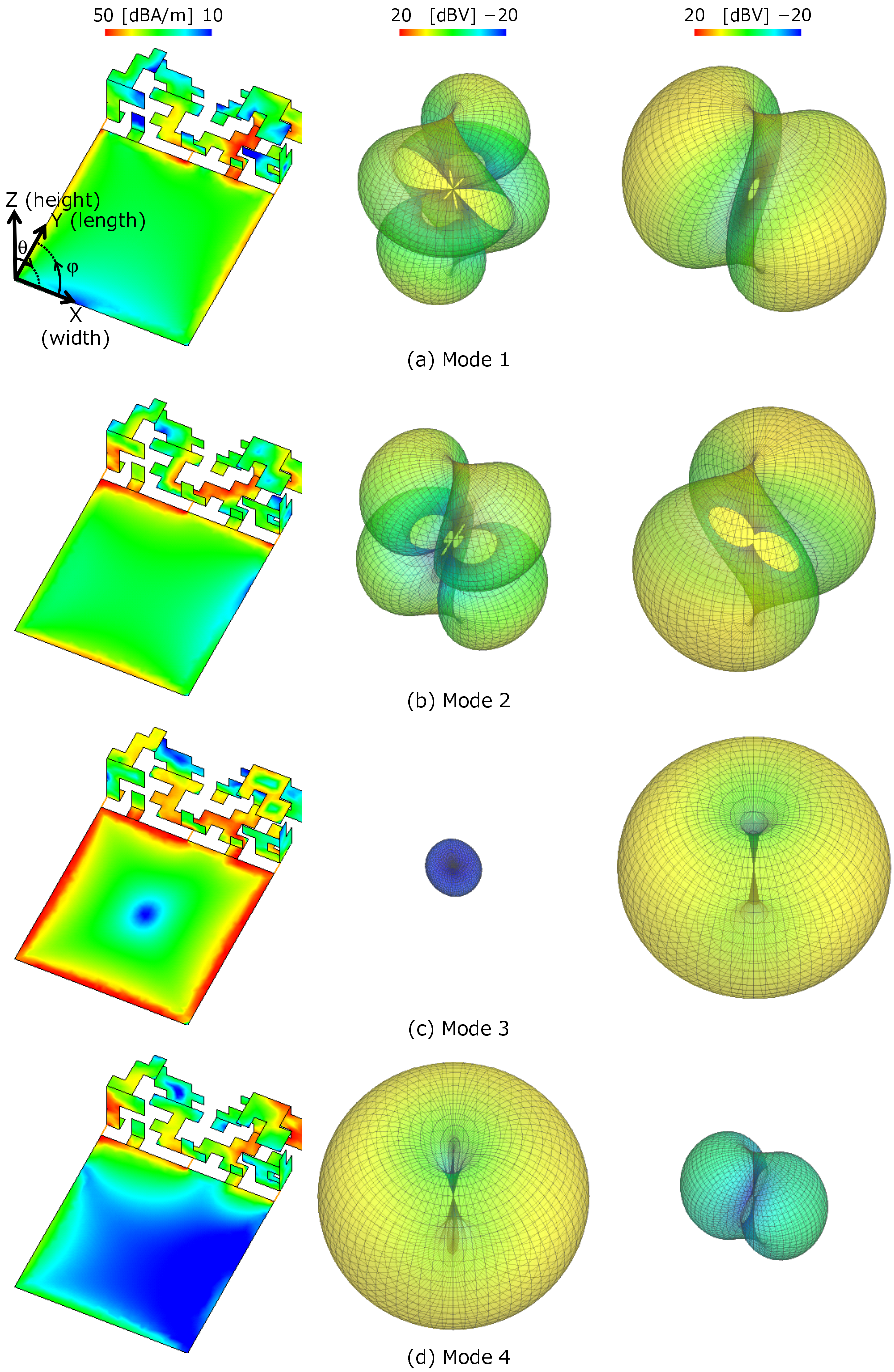

Figure 6.3: The current distribution and radiation pattern of four modes when the switch is short

how the proposed antenna realize low correlations of directivity is not based on the change in modes themselves but on the power distribution ratio of modes changed by the coupled modes at each port caused by the state of the switch, and between ports, it depends almost all on the spatial correlation.

The power distribution of other modes which are not shown in Fig. 6.2 and Fig. 6.4 is also confirmed that they are relatively small compared with that the total power of four modes discussed above reaches 50-80 percent.

6.3 Calculated results of MIMO channel capacity

In order to confirm the advantage of the steerability, the MIMO channel capacity of the proposed antenna in a propagation environment is discussed by comparing it with a MIMO system without the steerability, i.e. just the conventional MIMO system. Especially the proposed antenna including the ground plane has only the size of a quarter wavelength in each dimension, and that is substantially small as the antenna system of two branch. The radiation efficiency, however, deteriorate down to around 60 percent and also the correlation of directivity, 0.83 when the port 2 is excited between the state of the switch is not enough. Then, referring to some papers [57–59] that have analyzed MIMO channel capacity with a propagation model, the improvement of the MIMO channel capacity by the directivity switching of the proposed antenna is verified. Using a geometric-based 3-d channel model supposing a uniform Rayleigh distribution and randomly rotating polarization, the MIMO channel capacity between two dipole antennas as a transmitting end the proposed antenna or two dipole antennas as a receiving end were calculated. As an arrangement of the two dipoles, a parallel and perpendicular arrangement shown in Fig. 6.5 have been studied. The total length of all dipoles are 55 mm or 0.45 wavelength at 2.45 GHz for the best impedance matching at the test frequency, 2.45 GHz. The distance between antennas is 30 mm or a quarter wavelength for the parallel arrangement and a small gap of 2 mm for the perpendicular arrangement. $S_1 1$ is -14.2 dB, so there is almost no reflection loss and the S_{21} corresponding to the coupling loss is -9 dB.

Figure Fig. 6.6 shows the cumulative distribution of channel capacity with the parallel dipole antennas. About the receiving end, a dotted line, solid line, and broken line indicate the value when the state of the switch is open, short, adaptively selected, respectively. And a dot-and-dash line indicates the value of the two parallel dipole antennas. The transmitting end is the two parallel dipole antennas for all variations of the receiving end.

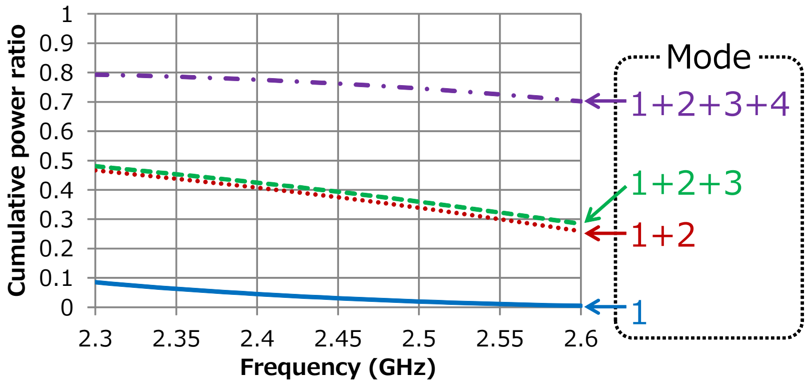

(a) Port 1 excitation

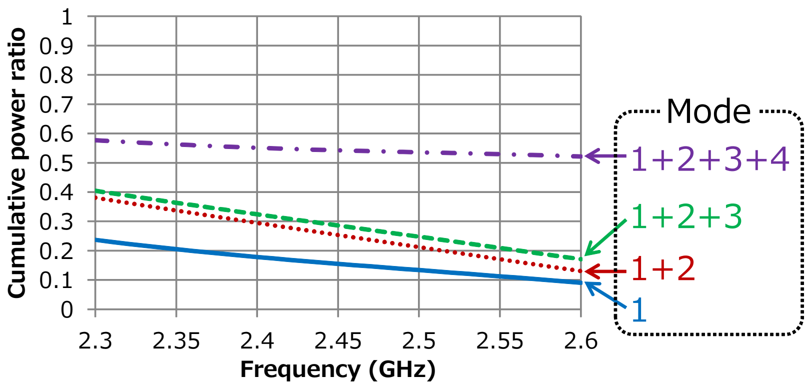

(b) Port 2 excitation

Figure 6.4: The cumulative power distribution by mode current when each port is excited and the switch is short

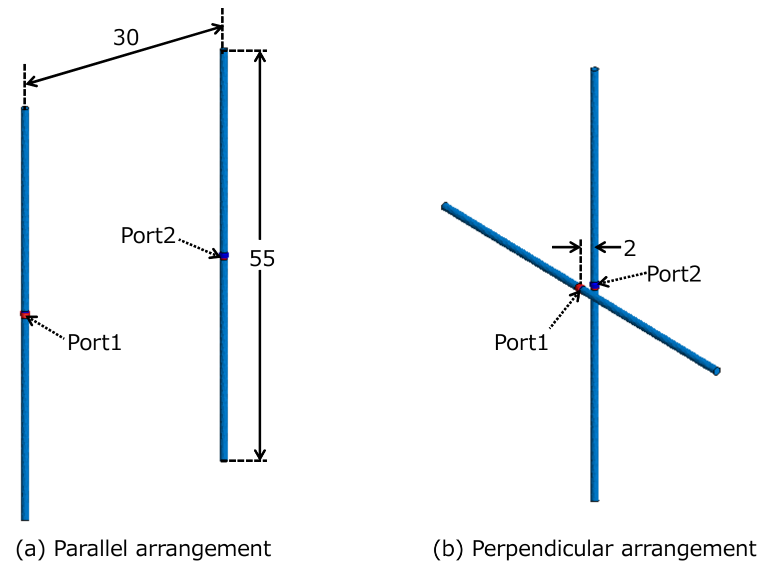

Figure 6.5: The two arrangements of dipole antennas for calculating channel capacities

The channel capacities when the state of the switch is open and short are less than that of the parallel dipole antennas by around 1 bit. It is supposed that this is because the total efficiency of the proposed antenna deteriorates down to around 60 percent. However, the channel capacity when the state of the switch is adaptively selected is greater than the parallel dipole antennas within the range where the CDF is less than 65 percent. This means that the switching adapt the propagation environment in real time and compensate more than the deterioration caused by the downsizing of the antenna, for example. Although the necessary area for the parallel dipole antennas is $55 \times 30 = 1650$ (mm^2), it is just $40 \times 28 = 1280$ (mm^2) for the proposed antenna even including the ground plane, two thirds the area for the parallel dipole antennas. In addition, the net area for the antenna in the proposed antenna is yet small.

The reason why the proposed antenna realize the greater channel capacity than the parallel dipole antennas can be clearly understood by the investigation in the eigenvalue. Figure 6.7 shows the cumulative distribution of eigenvalues with the parallel dipole antennas. The explanation of the legend is the same as that for Fig. 6.6. The graph shows that the 1st eigenvalue of the proposed antenna is approximately 1 dB less than that of

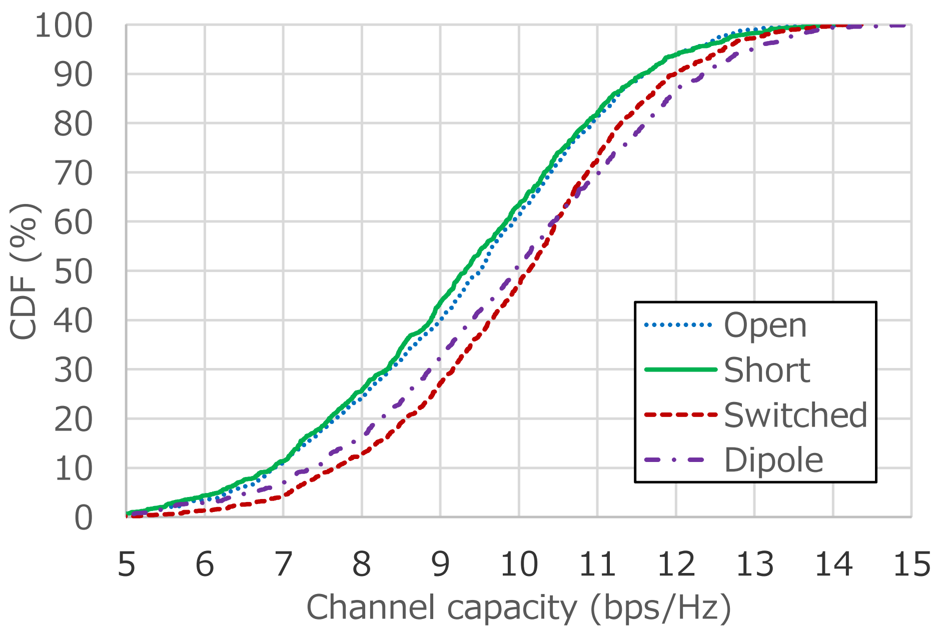

Figure 6.6: The cumulative distribution of channel capacity with the parallel dipole antennas

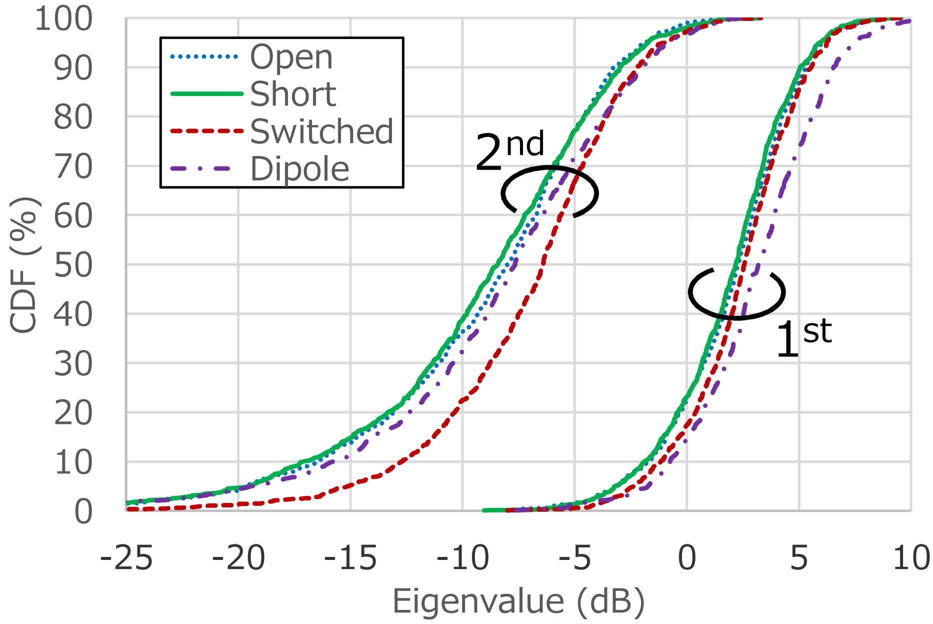

Figure 6.7: The cumulative distribution of eigenvalues with the parallel dipole antennas

the parallel dipole antennas on average caused by the deterioration in total efficiency. Since also the parallel dipole antennas have some loss caused by the mismatch and the coupling between ports, the difference becomes 1 dB. However, the 2nd eigenvalue of the proposed antenna is greater than that of the parallel dipole antennas within the range where the CDF is less than 80 percent. Therefore, as a result of the merge of the inferiority in the 1st eigenvalue and superiority in the 2nd eigenvalue, the channel capacity becomes greater than the parallel dipole antenna within the range where the CDF is less than 65 percent as shown in Fig. 6.6. In other words, although the proposed antenna is inferior to the parallel dipole antennas when concentrating on just one propagation channel, the proposed antenna is superior to the parallel dipole antennas when plural propagation channels are available. Then, taking into account various propagation environments, the proposed antenna is more likely to have an advantage over the parallel dipole antennas.

Similarly, the cumulative distribution of eigenvalues with the vertically crossed dipole antenna is shown in Fig. 6.8. The explanation of the legend is

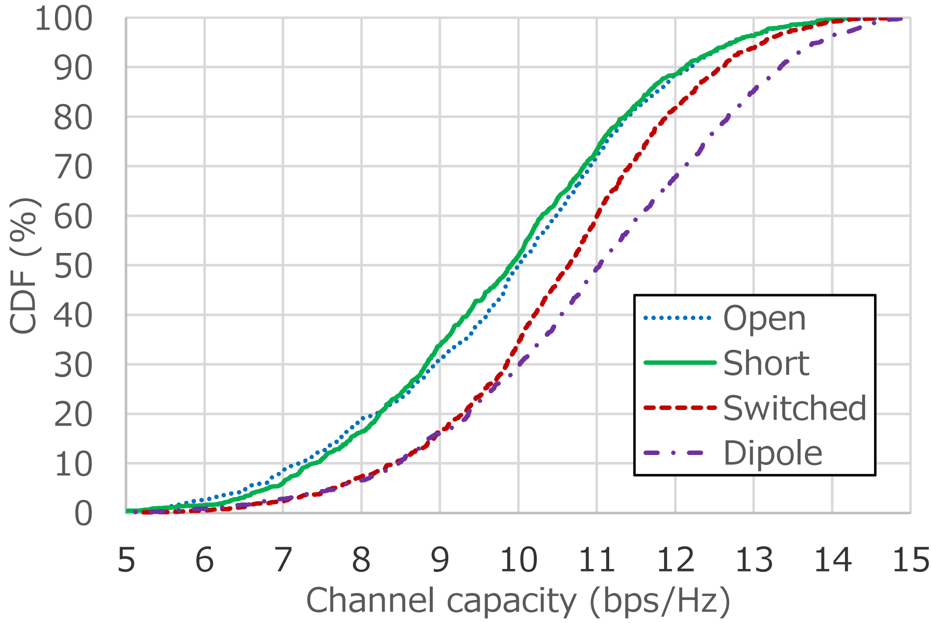

Figure 6.8: The cumulative distribution of channel capacity with the vertically crossed dipole antennas

the same as that for Fig. 6.6. In this case, although the improvement of the channel capacity from one state of the switch to the adaptive switching can be seen, the improved channel capacity is yet inferior to that of the vertically crossed dipole antennas. However, the dipole antennas have maintain their orthogonality and the occupied area of $55 \times 55 = 3025$ (mm^2) is too large to install to a small device.

Nevertheless, similar to Fig. 6.7, the diversity effect of the proposed antenna can be found from the eigenvalue. Figure 6.9 shows the cumulative distribution of eigenvalues with the vertically crossed dipole antennas. Although the 1st eigenvalue of the proposed antenna is 2 dB less than that of the vertically crossed dipole antennas similar to the situation of the parallel dipole antennas, the 2nd eigenvalue of the proposed antenna is greater than than of the vertically crossed dipole antennas within the range where the CDF is less than 45 percent. However, the total performance of the proposed antenna in the propagation environment applied this time come short of that of the vertically crossed dipole antennas.

As discussed above, although the proposed antenna does not have suf-

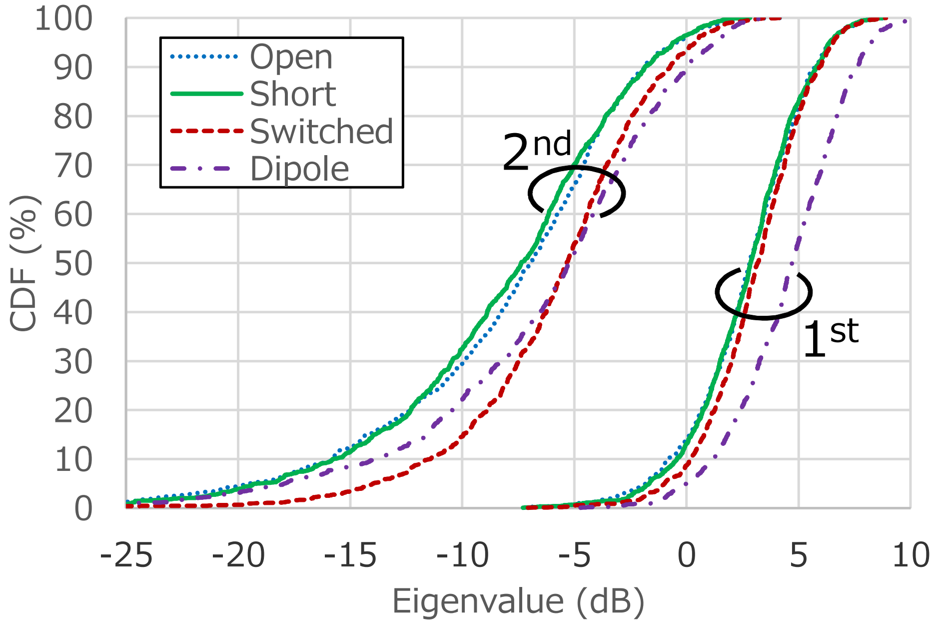

Figure 6.9: The cumulative distribution of eigenvalues with the vertically crossed dipole antennas

ficient characteristics, e.g. the total efficiency, the correlation of directivity between the state of the switch at port 2, nevertheless, the calculation of the channel capacity results that of the proposed antenna is superior to that of the parallel dipole antennas with a probability of 65 percent.

6.4 Summary

The proposed antenna has low correlations of directivity between ports for each state of the switch depending almost all on the spatial diversity, and also that between the state of the switch for each port caused by the change in the power distribution of modes. In other words, the correlation between the state of the switch is not based on the change in modes themselves but on the power distribution ratio of modes. This low correlation gives an advantage over the MIMO system without steerability in each branch. It is confirmed that the channel capacity calculated with Rayleigh distribution of the proposed antenna is higher than that of lossless two dipoles with a probability of 65 percent.

Chapter 7

Conclusion

7.1 Summary of preceding chapters

Tunable/Steerable antennas have been studied in order to overcome the physical limitations on electrically small antennas.

- Tunable antenna has been designed for cellular systems.
  - The advantage is confirmed in terms of operation bandwidth and efficiency by comparing with physical limitations and some conventional studies. The operation bandwidth is 3 times wider than the physical limitation and the benchmark with the conventional studies is shown again in Table 7.1.
  - Novel multiband automatic tunable antenna using a probe was proposed, demonstrated, and the frequency-independent operation has been confirmed.
- Compact two-branch directivity-switching antenna using a single switch for 2.4 GHz band has been proposed.
  - The low correlation of directivity has been explained in terms of the power distribution of modes
  - The enhancement of MIMO channel capacity has been confirmed. For example, the channel capacity calculated with Rayleigh distribution of the proposed antenna is higher than that of lossless two dipoles with a probability of 65 percent.

Table 7.1: Benchmark of tunable antenna

		Tunability					
Wireless System		LTE700 EGSM	DCS PCS UMTS	LTE2600	Size (W × L × T) [mm]		Radiation Efficiency (%)
Band (MHz)	f_{min}	704	1710	2500	Antenna	Ground	
	f_{max}	960	2170	2690			
This work		✓ 749 MHz—	✓	✓	60 × 10 × 1	60 × 90 × 1	> 40
Takemura[14]		✓		✓	50 × 10 × 1	50 × 90 × 1	> 40
Liu[15]		823 MHz—	✓		38 × 10 × 6	40 × 90 × 1	—
Chen[16]		✓	✓	✓	64 × 11 × 6	64 × 129 × 1.5	> 30
Xia[17]		✓	✓	✓	45 × 6 × 6	45 × 110 × 1	> 50
Ramachandran[18]		✓		✓	45 × 12 × 6	66 × 110 × 1	> 35

7.2 Remarks for future studies

This dissertation has mainly focused on

- verifying the fundamental function and performance of tunable/steerable antennas, and
- benchmarking the absolute performance by comparing with some conventional ones or physical limitations,

and their beneficial functionality and advantage over the antennas without tunability or steerability have been cleared up. On the other hand, that seems to be in a primary phase, and some advanced studies seems to remain for the design of these antennas.

For example, although the proposed tunable antenna designed in this dissertation is confirmed to be on the frontier as shown in Fig. 7.1, not all the terms are satisfied from a viewpoint of general requirements. And also the steerable antennas for MIMO system does not have all sufficiently low correlations between ports and the state of the switch. Designing these antennas with all terms of performances and compromised condition of the design area should be studied in the future.

Similarly, it is also interesting topic that how much additive conditions– such as, the size of the antenna, an increase in the number of switches or variable lumped elements, etc.– enhance the operation bandwidth, MIMO channel capacity of a tunable/steerable antenna, and also the combination of tunability and steerability. From the viewpoint of a communication system, the advantage should be confirmed again with the control time, in other words the transition time for the tunable/steerable antenna.

Although some of the above-mentioned issues are a little touched on at the last part of each chapter, the quantitative discussions are expected to follow this dissertation.

Bibliography

[1] L. J. Chu, "Physical Limitations on Omni-Directional Antennas," *Journal of Applied Physics*, vol. 9, pp. 1163–1175, 1948.

[2] M. Gustafsson, C. Sohl, and G. Kristensson, "Physical limitations on antennas of arbitrary shape," *Proceedings of the Royal Society A,* 463, pp. 2589–2607, 2007.

[3] M. Cismasu, and M. Gustafsson, "Antenna Bandwidth Optimization with Single Frequency Simulation," *IEEE Transactions on Antennas and Propagation*, vol. 62, no. 3, pp. 1304–1311, Mar. 2014.

[4] K. Fujimoto, A. Henderson, A. Hirasawa, and J. R. James, "Small Antennas," John Wiley & Sons, Jan. 1987, ISBN-10:0471914134.

[5] W. C. Y. Lee, "Mobile Communication Engineering," McGraw

[6] W. C. Jakes, "*Microwave Mobile Communications*," *IEEE Press*, 1974.

[7] M. A. Jensen, and Y. Rahmat-Samii, "Performance Analysis of Antennas for Hand-Held Transceivers Using FDTD," *IEEE Transactions on Antennas and Propagation*, vol. 42, no. 8, pp. 1106–1113, 1994.

[8] T. Taga, and K. Tsunekawa, "A Built-in Antenna for 800 MHz Band Portable Radio Units," Proc. of ISAP 1985, no. 121-1, pp. 425–428, 1985.

[9] R. Yamaguchi, K. Sawaya, and S. Adachi, "Effect of dimension of conducting box on radiation pattern of a monopole antenna for portable telephone," *IEICE Transaction on Communication*, vol. E-76B, no. 12, pp. 1526–1531, 1993.

[10] K. Fujimoto, and J. R. James, "*Mobile Antenna Systems Handbook*," Artech House, 1994

[11] J. Toftgard, S. N. Hornsleth, and J.B. Andersen, “Effects on Portable Antennas of the Presence of a Person,” *IEEE Transaction on Antennas and Propagation*, vol. 41, no. 6, pp. 739–746, June 1993.

[12] M. A. Jensen, and Y. Rahmat-Samii, “EM Interaction of Handset Antennas and a Human in Personal Cummunications,” *Proceedings of the IEEE*, vol. 83, no. 1, Jan. 1995

[13] V. Hombach, K. Meier, M. Burkhardt, E. Kuhn, and N. Kuster, “The Dependence of EM Energy Absorption Upon Human Head Modeling at 900 MHz,” *IEEE Transaction on Microwave Theory and Techniques*, vol. 44, no. 10, pp. 1865–1873, Oct. 1996.

[14] N. Takemura, “Tunable inverted-L antenna with split-ring resonator structure for mobile phones,” *IEEE Transactions on Antennas and Propagation*, vol. 61, 1891-1897, Apr. 2013.

[15] Liu, and R. Langley, “Frequency-Tunable Mobile Phone Antennas with Matching Circuits,” *EuCAP 2007, The 2nd European Conference on Antennas and Propagation*, Nov. 2007.

[16] Y. Chen, R. Martens, R. Valkonen, and D. Manteuffel, “A Varactor-Based Tunable Matching Network for a Non-Resonant Mobile Terminal Antenna,” *EuCAP 2014, The 8th European Conference on Antennas and Propagation*, Nov. 2014.

[17] Xia, et al, “A Compact Multi-band Tunable LTE Antenna for Mobile Applications,” *IEEE AP-S, Antennas and Propagation Society International Symposium Digest*, Jul. 2015.

[18] Ramachandran, “Reconfigurable Small Antenna for Mobile Phone using MEMS Tunable Capacitor,” *Loughborough Antennas and Propagation Conference*, Nov. 2013.

[19] A. Cardona, “Tunable BaSrTiO3 Applications for the RF Front End,” *IEEE MTT-S, International, Microwave Symposium Digest*, 2011

[20] R. Whatley, et al, “CMOS Based Tunable Matching Networks for Cellular Handset Applications,” *IEEE MTT-S, International, Microwave Symposium Digest* (2011)

[21] A. S. Morris III, Q. Gu, M. Ozkar, and S. P. Natarajan, “High Performance Tuners for Handsets,” *IEEE MTT-S, International, Microwave Symposium Digest*, 2011

[22] M. A. de Jongh, A. van Bezooijen, K.R. Boyle, and T. Bakker, "Mobile Phone Performance Improvements using an Adaptively Controlled Antenna Tuner," *IEEE -S, International, Microwave Symposium Digest*, 2011

[23] P. Turalchuk, I. Munina, P. Kapitanova, D. Kholodnyak, D. Stoepel, S. Humbla, J. Mueller, M. A. Hein, and I. Vendik, "Broadband Small-Size LTCC Directional Couplers," in Proc. 40th European Microwave Conf., 2010, pp. 1162–1165

[24] C. Wang, and K. Chang, "A 3-D Broadband Dual-Layer Multiaperture Microstrip Directional Coupler," *IEEE Microwave Wireless Components Letter,* vol. 12, no. 5, pp. 160–162, May 2002

[25] Kashiwagi, M. Nishio, S. Obayashi, H. Shoki, and T. Morooka, B-1-174, 2010 IEICE Society Conf.

[26] S. Gabriel, et al, "The dielectric properties of biological tissues: I. Literature survey," *Physics in Medicine and Biology*, vol. 41, no. 11, pp. 2231–2249, 1996.

[27] M. Higaki, S. Obayashi, and H. Shoki, "Multiband Automatic Tunable Antenna System Based on the Received Power of a Probe," *IEICE Transactions on Communications*, vol. E99-B, no. 11, Nov. 2016.

[28] M. Higaki, S. Obayashi, and H. Shoki, "Novel Multiband Autonomous Impedance Restoration Antenna System by Using a Probe," *IEEE AP-S, Antennas and Propagation Society International Symposium Digest*, Jul. 2012.

[29] M. Higaki, S. Obayashi, H. Shoki, "Automatic Tunable Antenna Controlling Varactors Based on the Received Power of a Probe," *IEEE AP-S, Antennas and Propagation Society International Symposium Digest*, Jul. 2013.

[30] M. Higaki, S. Obayashi, and H. Shoki, "The study of multiband autonomous impedance regulation antenna system with using a probe," *IEICE Technical Report*, AP2011-114, vol. 111, no. 288, pp. 141–144, Nov. 2011.

[31] M. Higaki, S. Obayashi, and H. Shoki, "The mechanism of multiband autonomous impedance regulation antenna system with using a probe," *IEICE Proceedings of General Conference*, B-1-226, Mar. 2012.

[32] M. Higaki, S. Obayashi, and H. Shoki, "The performance of autonomous impedance regulation antenna system that uses a probe," *IEICE Proceedings of Society Conference*, B-1-161, Sep. 2012.

[33] M. Higaki, S. Obayashi, and H. Shoki, "The performance of automatic impedance matching antenna system using a probe and two varicaps," *IEICE Proceedings of General Conference*, B-1-187, Mar. 2013.

[34] R. F. Harrington, "Reactively controlled directive arrays," *IEEE Transactions on Antennas and Propagation*, vol.26, no.3, pp. 390–395, May 1978.

[35] T. Ohira, and K. Inagaki, "Electric Means for Antenna Beamforming: Adaptive Array Antenna Architectures from a Viewpoint of RF Hardware Design Engineers," IEICE Journal, vol. 83, no. 12, pp. 920–926, Dec. 2000

[36] T. Ohira, and J. Cheng, "Analog smart antennas," Adaptive Antenna Arrays, pp. 184–204, ISBN3-540-20199-8, Berlin: Springer Verlag, June 2004.

[37] T. Ohira, and K. Iigusa, "Electronically steerable parasitic array radiator antenna," Electronics and Communications in Japan (Part 2: Electronics), ECJB, 87, 10, pp. 25–45, 2004, Wiley Periodicals.

[38] K. Gyoda and T. Ohira, "Design of Electronically Steerable Passive Array Radiator (ESPAR) Antennas," *IEEE AP-S, Antennas and Propagation Society International Symposium Digest*, pp. 922–925, Jul., 2000

[39] T. Ohira and K. Gyoda, "Electronically steerable parasitic array radiator antennas for low-cost analog adaptive beamforming," *Proceedings 2000 IEEE International Conference on Phased Array Systems and Technology* (Cat. No.00TH8510), Dana Point, CA, 2000, pp. 101–104. Dec. 1997.

[40] H. Kawakami, and T. Ohira "Electronically steerable passive array radiator (ESPAR) antennas," *IEEE Antennas and Propagation Magazine*, vol. 47, no. 2, April 2005.

[41] A. Akiyama, K. Ito, T. Ohira and M. Ando, "Variable Beamforming Performance Analysis for Electronically Steerable Parasitic Array Radiator Antennas," *IEEE APMC, Proceedings of Asia-Pacific Microwave Conference*, vol. 2, pp. 1103–1106, Nov. 2002.

[42] K. Ito, A. Akiyama, and M. Ando, "Numerical Simulations on Beam/Null Forming Performance of ESPAR Antennas," *IEICE Transactions on Communications*, vol. E86-B, no. 9, pp. 2844–2847, Sep. 2003.

[43] C. Y. Chiu, and R. D. Murch, "Recon

gurable Slot Antenna using Switched Stub Technique," it IEEE/iWAT, International Workshop on Antenna Technology Digest, pp. 922–925, Mar. 2009.

[44] C. Y. Chiu, and R. D. Murch, "Recon

gurable Multi-slot Multi-port Antennas using RF-MEMS Switches for Handheld Devices," *IEEE APMC, Proceedings of Asia-Pacific Microwave Conference*, pp. 999–1002, Dec. 2010.

[45] H. Uno, Y. Saito, G. Ohta, Y. Koyanagi, and K. Egawa, "Switched-Beam Slot Sector Antenna for WLAN applications," *IEEE AP-S, Antennas and Propagation Society International Symposium Digest*, pp. 922–925, Jul., 2005.

[46] M. I. Lai, T. Y.Wu, J. C. Hsieh, C. H.Wang, and S. K. Jeng, "A Miniature, Planar, and Switched-Beam Smart Antenna Employing a Four-Element Slot Antenna Array for Digital Home Applications," *IEEE AP-S, Antennas and Propagation Society International Symposium Digest*, pp. 922–925, Jul., 2007.

[47] N. Honma, T. Seki, K. Nishikawa, K. Tsunekawa, and K. Sawaya, "Compact Six-Sector Antenna Employing Three Intersecting Dual-Beam Microstrip Yagi-Uda Arrays With Common Director," *IEEE Transactions on Antennas Propagation*, vol. 54, no. 11, pp. 3055–3062, Nov. 2006.

[48] W. C. Y. Lee and Y. S. Yeh, "Polarization diversity system for mobile radio," *IEEE Transactions on Communications*, vol.COM-20, no.5, pp. 912–923, Nov. 1972.

[49] K. Meksamoot, M Krairiksh, and J. Takada, "A Polarization Diversity PIFA on Portable Telephone and the Human Body Effects on Its Performance," *IEICE Transactions on Communications*, vol. E84-B, no. 9, Sep. 2001.

[50] S. Ghosh, T.-N. Tran, and T. Le-Ngoc, "Miniaturized MIMO-PIFA with Pattern and Polarization Diversity," *2012 IEEE VTC Spring*, 2012, pp. 1–5.

[51] Y. Yao, X. Wang, X. Chen, J. Yu, and S. Liu, "Novel Diversity/MIMO PIFA Antenna With Broadband Circular Polarization for Multimode Satellite Navigation," *IEEE Antennas Wireless Propag. Lett.*, vol. 11, pp. 65–68, 2012.

[52] H. Sato, Y. Zhu, Q. Chen, T. Sudo, T. Ohishi, and T. Suzuki, "Indoor Experiment of Polarization Switching Diversity Antennas for On-Body Use," *IEICE General Conference*, BS-1-9, Mar. 2016.

[53] K. Ogawa, and T. Uwano, "A Diversity Antenna for Very Small 800-MHz Band Portable Telephones," *IEEE Transactions on Antennas and Propagation*, AP-42, no. 9, pp. 1342–1345, Sep. 1994.

[54] W. C. Y. Lee, and Y. S. Yeh, "Polarization Diversity System for Mobile Radio," *IEEE Transaction on Communication*, vol. 20, no. 5, pp. 912–923, Nov. 1972.

[55] Y. Yamada, K. Kagoshima, and K. Tsunekawa, "Diversity Antennas for Base and Mobile Stations in Land Mobile Communication Systems," *IEICE Transaction on Communications*, vol. E47-B, no. 10, pp. 3202–3209, Oct. 1991.

[56] K. Meksamoot, M. Krairiksh, and J. Takada, "Performance of Polarization Diversity PIFA on a Portable Telephone in Multipath Environment," *IEICE Technical Report*, MW99-105, vol. 99, no. 325, pp. 69–76, Sep. 1999.

[57] P. Almers, et al, "Survey of Channel and Radio Propagation Models for Wireless MIMO Systems," *EURASIP Journal onWireless Communications and Networking*, Feb. 2007.

[58] F. M. Andreas, "A Generic Model for MIMO Wireless Propagation Channels in Macro- and Microcells," *IEEE Transactions on Signal Processing,* vol.52, no.1, Jan. 2004.

[59] M. Shafi, et al, "Polarized MIMO Channels in 3-D: Models, Measurements and Mutual Information," *IEEE Journal on Selected Areas in Commun.*, vol.24, no.3, Mar. 2006.

[60] N. Ito, H. Arai, T. Maruyama, K. Cho, "Effect of the Characteristic of MIMO Transmission of Using Unti-Uniform Directivity for switched MIMO transmission antenna," *IEICE Technical Report, Antennas and Propagation*, vol. 105, no. 561, pp. 21–24, 2006, Jan. AP2005-134.

[61] S. Blanch, et al, "Exact representation of antenna system diversity performance from input parameter description," *IET Electronics Letters*, vol.39, no.9, May, 2003.

[62] J. B. Andersen, and H. H. R amussen, "Decoupling and descattering networks for antennas," *IEEE Transactions on Antennas and Propagation*, vol. AP-24, no. 6, pp. 841–846, Nov. 1976.

[63] S. Li, and N. Honma, "Decoupling Network Comprising Transmission Lines and Bridge Resistance for Two-Element Array Antenna," *IEICE Transactions on Communications*, vol. E97-B, no. 7, pp. 1395–1402, July 2014.

[64] K. Kagoshima, S. Obote, A. Kagaya, K. Nishimura and N. Endo, "An array antenna for MIMO systems with a decoupling network using bridge susceptances," *2011 Wireless VITAE*, pp. 1–4, 2011.

[65] M. Higaki, M. Sano, S. Kishimoto, "Two-Branch Directivity-Switching Electrically Small Antenna Using a Single Switch for 2.4 GHz band," *IEICE Transactions on Communications*, vol. J100-B, no. 9, Sep. 2017 (to be published)

[66] M. Higaki, M. Sano, and S. Kishimoto, "Characteristic Mode Analysis for Two-Branch Directivity-Switching Antenna Using a Single Switch," *IEICE Technical Report*, AP2016-161, vol. 116, no. 454, pp. 27–32, Feb. 2017.

[67] M. Higaki, M. Sano, S. Kishimoto, and K. Murata, "The Analysis of a 2-Branch Directivity-Switching Antenna Using a Single Switch," *IEICE Proceedings of General Conference*, B-1-3, Mar. 2017.

[68] R.F. Harrington and J.R. Mautz, "The theory of characteristic modes for conducting bodies," IEEE Transactions on Antennas and Propagation, vol.19, no.5, pp. 622–628, Sep. 1971.

[69] IEEE Std 145-2013: IEEE Standard for Definitions of Terms for Antennas

[70] Y. Rahmat-Samii and E. Michielssen, "Electromagnetic Optimization by Genetic Algorithms," *Wiley*, ISBN: 978-0-471-29545-7, July 1999 (Book).

[71] M. Ohira, H. Deguchi, M. Tsuji, H. Shigesawa, "Multiband single-layer frequency selective surface optimized by genetic algorithm with geometry-refinement technique," *IEEE/AP-S Antennas and Propagation Society International Symposium Digest*, 2, pp. 833–836 (2003-6).

[72] T. Maruyama and K. Cho, "Novel multi-band scroll configured thin-monopole antenna designed using genetic algorithm employing maze-generating algorithm for chromosome," *ISAP* 2005, FB1-3, pp. 1005–1008, August 2005.

[73] R. F. Harrington, "Field Computation by Moment Methods," New York, NY: McMillan, 1968.

[74] R. F. Harrington, "Matrix methods for field problems," *Proc. IEEE*, vol. 55, pp. 136–149, Feb. 1967.

[75] J. H. Richmond, "Digital computer solutions of the rigorous equations for scattering problmems," *Proc. IEEE*, vol. 53, pp. 796–804, Aug. 1964.

[76] T. Hirano, J. Hirokawa, M. Ando, T. Ide, A. Sasaki, K. Azuma, and Y. Nakata, "Method of Moments / Transmission Line Modeling, for Plasma Excitation Single-layer Slotted Waveguide Arrays with Complicated Outer Baffles," *IEEE/AP-S Antennas and Propagation Society International Symposium Digest*, vol. 3, pp. 2372–2375, June, 2004.

[77] K. Kurokawa, "Power Waves and the Scattering Matrix", *IEEE Transactions on Microwave Theory and Techniques*, Mar. 1965, pp. 194–202

[78] M. Higaki, J. Hirokawa, and M. Ando, "Mechanical Phase Shifting in the Power Divider for Single-Layer Slotted Waveguide Arrays," *IEICE Transactions on Communications*, vol. E87-B, no. 2, Feb. 2004.

Appendix A

Matchable impedance

An impedance matching circuit with passive element(s) operates as a bilinear transform for the input impedance of an antenna. Therefore, a disc indicating the area where VSWR is less than a certain value on the Γ-plane is inverse-transformed to another circle indicating the matchable impedance for the antenna. If any 2×2 parameter of a matching circuit is known, the F parameter can be calculated, e.g.,

$$F = Z_{21}^{-1} \begin{bmatrix} Z_{11} & |Z| \\ 1 & Z_{22} \end{bmatrix}, \tag{A.1}$$

and we can obtain the matchable impedance Z_a:

$$Z_a = F^{-1} \begin{bmatrix} Z_{in} \\ 1 \end{bmatrix}, \tag{A.2}$$

where Z_{in} is the input impedance of the antenna and a matching circuit. To obtain the boundary circle of the matchable impedance, we calculated the three transformed points from the three points on the circle indicating VSWR$= 3$, and the equation for the transformed circle by the formula.

Appendix B

Method to trim discarded patch cells

To accelerate the iterative electromagnetic simulations in the optimization with genetic algorithm, and to avoid configuration error, here the method to eliminate floating or corner-touching patches is noted. A floating patch is defined as the one with no connection with any ports or ground plane. Since basically floating patches require a half wavelength to resonate, it will occupy too large area when designing electrically small antennas. A corner-touching patch named in this paper is the two patches touching only at the corner each other. Although there is no current through that touching corner in many types of electromagnetic simulations, in the actual fabrication it is impossible to layout. Then the process enumerated below has been coded and executed every individual modeling in genetic algorithm to eliminate these discarded patches.

1. Numbering every patch and construct adjacent matrix and corner-touching matrix to refer and judge adjacent or corner-touching
2. After a modeling, check every patch whether connected to ports or ground plane.
3. Confirm the commonly adjacent patches for existing pair of corner-touching patches. $\rightarrow$ If no, eliminate the patch.

Acknowledgement

At the end of this dissertation, I would like to express my gratitude to some people. I could not have done any of this study unless I had a strong support behind me. First of all, I am greatly indebted to Professor Hirokawa and would like to show my greatest appreciation to Professor. Professor advised me not only on this dissertation, but also on the related papers as my supervisor. Especially I have had support and a discussion on summarizing technological issues into a consistent dissertation. I would like to offer my special thanks also to Former Professor Ando. By my postponed doctoral course I could not convey my gratitude with my graduation to Professor. Professor have given me constructive and encouraging comments at the beginning and in the course of my study. Needless to say, I owe a very important debt to some researchers in Toshiba. Dr. Shoki and Mr. Obayashi are my senior researcher and coauthors in my some papers who advised me and revised the papers. I would like to deeply appreciate the support. I would like to offer my special thanks to the former laboratory leader Dr. Matsuoka. He gave me important comments on and proofreading in my papers so that the papers would have been accepted in spite of his busyness as a manager. Also I would like to appreciate my coworkers. They are Mr. Sasaki, Dr. Ono, Dr. Inoue, Dr. Ohishi, Mr. Yamada, Dr. Hashimoto, Dr. Sano, and Dr. Murata. They have supported me a lot at work while I paralleled my assignment as a program leader in Toshiba R&D Center and my doctoral course.

List of publications

Works concerning the dissertation

Papers

[1] M. Higaki, S. Obayashi, and H. Shoki, “Multiband Automatic Tunable Antenna System Based on the Received Power of a Probe,” *IEICE Transactions on Communications*, vol. E99-B, no. 11, Nov. 2016.

[2] M. Higaki, M. Sano, S. Kishimoto, “Two-Branch Directivity-Switching Electrically Small Antenna Using a Single Switch for 2.4 GHz band,” *IEICE Transactions on Communications*, vol. J100-B, no. 9, Sep. 2017. (to be published)

International conferences

[1] M. Higaki, S. Obayashi, and H. Shoki, “Novel Multiband Autonomous Impedance Restoration Antenna System by Using a Probe,” *IEEE AP-S, Antennas and Propagation Society International Symposium Digest*, Jul. 2012.

[2] M. Higaki, S. Obayashi, H. Shoki, “Automatic Tunable Antenna Controlling Varactors Based on the Received Power of a Probe,” *IEEE AP-S, Antennas and Propagation Society International Symposium Digest*, Jul. 2013.

[3] M. Higaki, K. Hashimoto, “Automatic Tunable Multiband Antenna Using RF-MEMS Capacitors Supporting Transmission Power Control,” *IEICE AWAP, Proceedings of Asian Workshop on Antennas and Propagation*, 2014

IEICE Technical Reports on Antennas and Propagation

[1] M. Higaki, S. Obayashi, and H. Shoki, "The study of multiband autonomous impedance regulation antenna system with using a probe," *IEICE Technical Report*, AP2011-114, vol. 111, no. 288, pp. 141–144, Nov. 2011.

[2] M. Higaki, M. Sano, and S. Kishimoto, "Characteristic Mode Analysis for Two-Branch Directivity-Switching Antenna Using a Single Switch," *IEICE Technical Report*, AP2016-161, vol. 116, no. 454, pp. 27–32, Feb. 2017. (in Japanese)

Domestic conferences

[1] M. Higaki, S. Obayashi, and H. Shoki, "The mechanism of multiband autonomous impedance regulation antenna system with using a probe," *IEICE Proceedings of General Conference*, B-1-226, Mar. 2012.

[2] M. Higaki, S. Obayashi, and H. Shoki, "The performance of autonomous impedance regulation antenna system that uses a probe," *IEICE Proceedings of Society Conference*, B-1-161, Sep. 2012.

[3] M. Higaki, S. Obayashi, and H. Shoki, "The performance of automatic impedance matching antenna system using a probe and two varicaps," *IEICE Proceedings of General Conference*, B-1-187, Mar. 2013.

[4] M. Higaki, "The study on the combination of matching circuit and antenna for high-efficiency and broadband performance," *IEICE Proceedings of Society Conference*, B-1-43, Sep. 2015.

[5] M. Higaki, "The study on the high-efficiency and broadband tunable antenna with taking the loss of inductors into account," *IEICE Proceedings of General Conference*, B-1-154, Mar. 2016.

[6] M. Higaki, M. Sano, S. Kishimoto, "Study on two-branch radiation pattern switching array antenna with single switch," *IEICE Proceedings of Society Conference*, B-1-3, Sep. 2016.

[7] M. Higaki, M. Sano, S. Kishimoto, and K. Murata, "The Analysis of a 2-Branch Directivity-Switching Antenna Using a Single Switch," *IEICE Proceedings of General Conference*, B-1-3, Mar. 2017.

Other works

Paper

[1] M. Higaki, J. Hirokawa, and M. Ando, "Mechanical Phase Shifting in the Power Divider for Single-Layer Slotted Waveguide Arrays," *IEICE Transactions on Communications*, vol. E87-B, no. 2, Feb. 2004.

International conferences

[1] M. Higaki, N. Odachi, S. Sekine, and H. Shoki, "A study on the variable radiation pattern antenna using a parasitic slot," *IEEE AP-S, Antennas and Propagation Society International Symposium Digest*, Jun. 2004.

[2] M. Higaki, N. Odachi, S. Sekine, H. Shoki, and T. Morooka, "Built-in antenna with switchable radiation pattern for portable phone," *IEICE ISAP, Proceedings of International Symposium on Antennas and Propagation*, 4A1-2, 2007.

[3] M. Higaki, A. Yamada, and K. Inoue, "Novel Small Structure for Low Profile Antenna by Analogy with EBG Structure," *IEEE AP-S, Antennas and Propagation Society International Symposium Digest*, Jun. 2008.

[4] M. Higaki, A. Yamada, K. Inoue, N. Odachi, S. Obayashi, H. Shoki, and T. Morooka, "Small Artificial Structure for Low Profile Antenna by Analogy with EBG Structure," it IEEE iWAT, Proceedings of International Workshop on Small Antennas and Novel Metamaterials, 2008.

Domestic conferences

[1] M. Higaki, S. Obayashi, and H. Shoki, "A study on the variable radiation pattern antenna using a parasitic slot," *IEICE Proceedings of Society Conference*, B-1-179, Sep. 2003.

[2] M. Higaki, N. Odachi, S. Sekine, and H. Shoki, "A study on the efficiency of the variable resonant frequency antenna," *IEICE Proceedings of General Conference*, B-1-144, Mar. 2005.

[3] M. Higaki, N. Odachi, S. Sekine, and H. Shoki, “Variable radiation pattern antenna with a parasitic element on the reverse side,” *IEICE Proceedings of General Conference*, B-1-134, Mar. 2006.

[4] M. Higaki, N. Odachi, S. Sekine, and H. Shoki, “Improvement of the antenna radiation efficiency near lossy medium by using a small piece of metal,” *IEICE Proceedings of General Conference*, B-1-136, Mar. 2007.

[5] M. Higaki, A. Yamada, K. Inoue, N. Odachi, S. Obayashi, H. Shoki, and T. Morooka, “Small Metamaterial Structure for Low Profile Antenna,” *IEICE Proceedings of General Conference*, B-1-163, Mar. 2008.

[6] M. Higaki, A. Yamada, K. Inoue, N. Odachi, S. Obayashi, H. Shoki, and T. Morooka, “Low Profile Antenna Comprising Directly Fed Metamaterial Structure,” *IEICE Proceedings of Society Conference*, BS-1-2, Sep. 2009.